الجمهورية الجزائرية الديموقراطية الشعبية
People's Democratic Republic of Algeria
وزارة التعليم العالي والبحث العلمي
Ministry of High Education and Scientific Research
جامعة قاصدي مرباح – ورقلة
Kasdi Merbah University – Ouargla
كلية العلوم التطبيقية
Faculty of Applied Sciences
قسم الهندسة الميكانيكية
Department of Mechanical Engineering

Order number:

Serial number:

Thesis presented in Partial Fulfilment of the Requirements of Doctorate Degree in

"Thermo-énergétique"

Presented by: Tarik HADIBI

Entitled:

Experimental study of a solar drying process with improved thermal performances

Etude expérimentale d'un procédé de séchage solaire à performances thermiques améliorées

Discussed publicly on: …/…/2021
Before the jury composed of:

Pr. Noureddine SETTOU	Kasdi Merbah University Ouargla	Chairman
Pr. Hamza BOUGUETTAIA	Kasdi Merbah University Ouargla	Examiner
Dr. Boubekkeur DOKKAR	Kasdi Merbah University Ouargla	Examiner
Pr. Noureddine GHERRAF	Larbi Ben M'hidi University Oum el Bouagui	Examiner
Pr. Abdelghani BOUBEKRI	Kasdi Merbah University Ouargla	Supervisor
Dr. Djamel MENNOUCHE	Kasdi Merbah University Ouargla	Co-supervisor

Academic Year : 2020/2021

Table of Contents

Thesis Acknowledgement

Foremost, I would like to express my sincere gratitude to my supervisor **Prof. Abdelghani BOUBEKRI** for the continuous support of my Ph. D study and research, for his patience, motivation, enthusiasm, and immense knowledge. His guidance and helps all the time of research.

Besides my advisor, I would like to thank my co-supervisor **Dr. Djamel MENNOUCHE** for his guidance through this process; his discussion, ideas, and feedback have been absolutely invaluable.

I would like to thank my fellow graduate students, research technicians, collaborators, and the multitude of undergraduates who contributed to this research. I am very grateful to all of you.

I would like to thank **Prof. Abdul Karim Salim ALLAF** mentor of research team of intensification of eco-process for industry, laboratory of engineering science for environment LaSIE - UMR-CNRS 7356 (University of La Rochelle, France) for his acceptance to welcome me in his laboratory, I am deeply grateful for his confidence, his patience, his sympathy and for his dedication. I would like to express my gratitude and warm thanks to the member of research team **Dr. Colette Besombes** for her help throughout my stay in LaSIE laboratory.

I would like to thank **Prof. Soufiene AZZOUZ** from "Laboratoire d'Energétique et des Transferts Thermique et Massique, Département de Physique, Faculté des sciences de Tunis, Manar II Tunis, Tunisia'' for his for agreeing to welcome me to his laboratory, I am deeply grateful for his confidence, his patience, his sympathy and for his dedication.

I would like to thank **Prof. Naji ABDENOURI** member of research team of "Control and Computing for Intelligent Systems and Green Energy, Cadi Ayyad University, Marrakesh, Morocco'' for his agreeing to welcome me to his laboratory, I am deeply grateful for his confidence, his patience, his sympathy and for his dedication.

Finally, I would especially like to thank my amazing family for the love, support, and constant encouragement I have received over the years. In particular, I would like to thank **my parents**, my brothers and daughters. You are the salt of the earth, and I undoubtedly could not have done this without you.

List of Figures

List of Tables

Nomenclature

Symbol	***Signification (unit)***
a, k, k_1, n, b, c, g	Constants of mathematical models
D_0	The pre-exponential factor of the Arrhenius equation ($m^2\ s^{-1}$)
D_{eff}	Effective moisture diffusivity ($m^2\ s^{-1}$)
DR	Drying rate
E_a	The energy of activation ($kJ\ mol^{-1}$)
f	Dimensionless drying rate
L	Half thickness (m)
M	Moisture content (kg water/kg dry matter, d.b)
MBE	Mean bias error
m_d	Mass of dry matter (g)
MR	Moisture ratio
m_t	Mass of the product at the time t (g)
M_t	The moisture content at the time t (kg water/kg dry matter, d.b)
N	Number of observations
P	Number of constants
Phase I	Combined of warming up of the product and surface-air interaction stage
Phase II	The falling rate period or diffusional stage
r	Correlation coefficient
R	Universal gas constant ($8.3143\ J\ mol^{-1}\ K^{-1}$)
t	Time (h), (s)
T	Temperature (°C)
Subscription	
0	Environmental, initial
abs	Absolute
acc	Annualized capital cost
b	Batch
bdp	Branded dried product
C	Collector
c	Chemical
ccd	Capita cost of the dryer
d	Day, drying day
dry	Dried
e	Equilibrium
ee	Electric energy
exp,i	Experimental, observed
fre	Fresh
h	Hour
i	Inlet/index, inflow
IF	Impact factor
k	Kinetic

kg	Kilogram
l	Loss
mc	Maintenance cost
out,o	Outlet, outflow
p	Potential
ph	Physical
pre,i	Predicted
rec	Running electricity
rfc	Running fuel
tot	Total
Greek symbol	
χ^2	Chi-square
α, β	Constants of mathematical models
η	Efficiency
λ	The latent heat of evaporation

ملخــص

تهدف هذه الأطروحة إلى التحقيق تجريبيًا ومن خلال نمذجة التجفيف الشمسي لمنتجين زراعيين ذوي تأثير وطني كبير إلى جانب خسارة موسمية كبيرة وقيمة غذائية عالية هما الطماطم في شكل معجون والثوم.استعملت تقنيات مختلفة للتجفيف بالحمل الحراري وأنظمة التجفيف الشمسي الهجين المدمجة مع التسخين الإضافي مثل مبادل حراري يعمل بالمياه الجوفية والمقاومة الكهربائية ، من ناحية ، أو مقترنة بعملية التجفيف المبتكرة مثل التجفيف باستعمال التحرير اللحظي للضغط (DIC) ، من ناحية أخرى.

سمح التجفيف الحراري المتحكم فيه تحت درجة حرارة في حدود 45-60 درجة مئوية بتقليل مدة التجفيف بمقدار 5.6 ساعة و 4.3 ساعة ، لسرعات هواء تبلغ 1.5 و 2.5 م/ثا على التوالي. يسمح التجفيف الهجين باستخدام المبادل الحراري للمياه الجوفية (GWHE) بتجفيف معجون الطماطم خلال 18 ساعة متتالية ، بمتوسط درجة حرارة تجفيف 38 درجة مئوية في الليل. لوحظ أن النظام الهجين أكثر ملاءمة وجاذبية من حيث الجودة ومن الناحية الاقتصادية مع فترة استرداد رأس المال المدفوع مقدرة بـ 2.21 سنة مقارنة بـ 8.44 سنة للمجفف العادي. من بين ثمانية نماذج رياضية ، وجد أن النموذج المقترح ذو أعلى معامل ارتباط R^2=0.9996 أكثر ملاءمة لوصف وتتبع سلوك التجفيف باستخدام أربع تقنيات تجفيف لمعجون الطماطم. عينات من معجون الطماطم مجففة مسبقًا إلى 0.6 (d.b) باستخدام النظام الهجين المزود بـ GWHE و معالجة بتقنية (DIC). سمحت تقنية التحرير اللحظي للضغط DIC مع (t = 30 s ، P = 0.3 MPa) بتقليل مدة التجفيف مقارنة بالتجفيف الشمسي الهجين من 7 ساعات إلى 1.5 ساعة. تم تحسين انتشار الرطوبة بنسبة 386 و 162 و 157٪ لتقنية DIC مقارنة بالعينات الشاهدة، بدرجة حرارة تجفيف تبلغ 39 و 50 و 70 درجة مئوية على التوالي. علاوة على ذلك ، فإن استخدام تقنية DIC يعزز الجودة المرئية لمعجون الطماطم المجفف مع استهلاك منخفض للطاقة مقارنة بأنظمة التجفيف التقليدية. تم إجراء تحليل الطاقة للتجفيف الهجين بالطاقة الشمسية والكهربائية (HSED) للثوم في حالة التجفيف العادي والنشط. مع الطاقة المجسدة البالغة 919.62 كيلوواط ساعة ، تراوح وقت استرداد الطاقة لـ HSED بين 0.32 و 0.62 سنة مع تفاوت كفاءة الطاقة من 69.61٪ إلى 89.86٪. بلغت قيمة التحسن في حدود 0.036-1.693 كيلوواط ، على التوالي ، وتم تحقيق أعلى معامل تأثير بيئي بنسبة 40.35٪ بأقصى كفاءة طاقوية.

الكلمات المفتاحية: *التجفيف الشمسي؛ معجون الطماطم؛ ثوم؛ مبادل حراري؛ المياه الجوفية؛ فترة استرداد رأس المال؛ التحرير اللحظي للضغط DIC؛ إستهلاك الطاقة؛ النوعية*

Abstract

This thesis aims to investigate, experimentally and by modelling, the solar drying of two agro-products with high national impact, large seasonal loss and high nutritional values which are tomato in paste form and garlic. Various techniques were investigated, using convective drying and hybrid solar drying systems integrated with auxiliary heating such as geothermal water heat exchanger and electric resistance, on one hand, or coupled to innovative drying process as swell drying (Instant Controlled Pressure Drop (DIC) followed by Hot Air Drying (HAD)), on the other hand.

Controlled convective drying with temperature in the range of 45-60 °C reduced drying time by 5.6 h and 4.3 h, for air velocities of 1.5 and 2.5 m s^{-1}, respectively. Hybrid drying using geothermal water heat exchanger (GWHE) allowed to dry tomato paste in 18 consecutive hours, with average drying temperature of 38 °C at night. The hybrid system was found to be more suitable and attractive in both visual quality and economically with a payback period of 2.21 years compared with 8. 44 years for basic dryer. Among eight mathematical models, the proposed model with highest correlation coefficient R^2 =0.9996 was found to be more suitable to describe the drying behavior using four drying techniques of tomato paste. Samples of tomato paste were pre-dried to 0.6 (d.b) using the hybrid system provided with GWHE and then treated by instant controlled pressure drop (DIC) technology. DIC technology with (P =0.3 MPa, t =30 s) reduced systematically the drying time compared with hybrid solar drying from 7 h to 1.5 h. Effective moisture diffusivity improved by 386, 162, and 157% for DIC technology compared with controlled samples, for drying temperature of 39, 50 and 70 °C, respectively. Moreover, using DIC technology enhanced the visual quality of dried tomato paste with low energy consumption compared to conventional drying systems. Energy and exergy analysis of Hybrid Solar-Electric Drying (HSED) of garlic has been carried out under passive and active mode. With embodied energy of 919.62 kWh, the energy payback time for the HSED varied between 0.32 and 0.62 years with exergy efficiency in the range of 69.61%-89.86%. In addition, improvement potential was in the range of 0.036-1.693 kW, respectively, and the highest environmental impact factor of 40.35% was achieved at the maximum exergy efficiency.

Keywords: *Solar Drying; Tomato Paste; Garlic; Heat Exchanger; Geothermal Water; Payback Period; Instant Controlled Pressure Drop DIC; Energy Consumption; Quality*

Résumé

Cette thèse vise à étudier, expérimentalement et par modélisation, le séchage solaire de deux agro-produits à fort impact national, à forte perte saisonnière et à haute valeur nutritionnelle que sont la tomate en pâte et l'ail. Diverses techniques ont été étudiées, utilisant des systèmes de séchage par convection et de séchage solaire hybride intégré à un chauffage auxiliaire tel que l'échangeur de chaleur à eau géothermique (GWHE) et une résistance électrique, d'une part, ou couplés à un processus de séchage innovant comme le séchage par expansion (Détente Instantanée Contrôlée (DIC) suivie de Séchage à Air Chaud (HAD)), d'autre part.

Le séchage par convection contrôlée avec une température comprise entre 45 et 60 °C a réduit le temps de séchage de 5,6 h et 4,3 h, pour des vitesses d'air de 1,5 et 2,5 m s^{-1}, respectivement. Le séchage hybride à l'aide d'un échangeur de chaleur à eau géothermique (GWHE) a permis de sécher la pâte de tomate en 18 heures consécutives, avec une température de séchage moyenne de 38 °C la nuit. Le système hybride s'est avéré plus approprié et plus attrayant en termes de qualité visuelle et économique avec un retour d'investisement de 2,21 ans contre 8,44 ans pour le séchoir basique. Parmi huit modèles mathématiques, le modèle proposé avec un coefficient de corrélation le plus élevé R^2 = 0,9996 s'est avéré plus approprié pour décrire le comportement de séchage en utilisant quatre techniques de séchage de la pâte de tomate. Les échantillons de pâte de tomate ont été pré-séchés à 0,6 (g/g, d.b) en utilisant le système hybride intégré à un échangeur GWHE ensuite traités par la technologie de détente instantanée contrôlée (DIC). La technologie DIC avec (P = 0,3 MPa, t = 30 s) a réduit systématiquement le temps de séchage par rapport au séchage solaire hybride de 7 h à 1,5 h. La diffusivité a été améliorée de 386, 162 et 157% pour la technologie DIC par rapport aux échantillons de contrôle, pour des températures de séchage de 39, 50 et 70 °C, respectivement. De plus, l'utilisation de la technologie DIC a amélioré la qualité visuelle de la pâte de tomate séchée avec une faible consommation d'énergie par rapport aux systèmes de séchage conventionnels. L'analyse énergétique et exergétique du Séchage Hybride Solaire-Electrique (HSED) de l'ail a été réalisée en mode passif et actif. Avec une énergie de fabrication de 919,62 kWh, le temps de récupération énergétique du HSED variait entre 0,32 et 0,62 an avec un rendement exergétique compris entre 69,61%-89,86%. De plus, le potentiel d'amélioration était de l'ordre de 0,036 à 1,693 kW, respectivement, et le facteur d'impact environnemental le plus élevé de 40,35% a été atteint au rendement exergétique maximal.

Mots clés: *séchage solaire; Pate de Tomate; Ail; Echangeur de Chaleur; Eau Geothermique; Retour d'Investisement; Détente Instantanée Controllée DIC;Consommation d'Energie; Qualité*

Scientific Works

Published paper

Hadibi, T., Boubekri, A., Mennouche, D., Benhamza, A., Abdenouri, N., 2021. 3E analysis and mathematical modelling of garlic drying process in a hybrid solar-electric dryer. *Renewable Energy* 170, 1052–1069. https://doi.org/https://doi.org/10.1016/j.renene.2021.02.029.

Tarik, H., Abdelghani, B., Djamel, M., Soufien, A., Abderrahim, B., Abdelmadjid, H., 2020. EXPERIMENTAL INVESTIGATION AND MATHEMATICAL MODELING OF HOT AIR CONVECTIVE DRYING OF TOMATO PASTE UNDER NEAR SOLAR DRYING OPERATING CONDITIONS. *Algerian Journal of Arid Environment* "*AJAE*" 10.

Benhamza, A., Boubekri, A., Atia, A., El Ferouali, H., **Hadibi, T**., Arıcı, M., Abdenouri, N., 2021. Multi-objective design optimization of solar air heater for food drying based on energy, exergy and improvement potential. *Renewable Energy*. https://doi.org/https://doi.org/10.1016/j.renene.2021.01.086.

International Symposium

Tarik Hadibi, Abdelghani Boubekri, Djamel Mennouche, Abderrahmane Benhamza: Experimental study and mathematical modeling of tomatoes thin layer drying using basic indirect solar dryer. 6th SMSTS, Tunisia on March, 19-21, 2018.

Tarik Hadibi, Abdelghani Boubekri, Djamel Mennouche, Abderrahmane Benhamzam: Experimental comparison and mathematical modeling of tomato paste direct solar drying under passive and active mode. 7th SMSTS, November, 14-16, 2019, Morocco.

Tarik Hadibi, Abdelghani Boubekri, Djamel Mennouche, Abderrahmane Benhamza, Colette Besombes, Karim Allaf: Effect of instant controlled pressure drop process coupled to solar drying on tomato paste drying kinetics. 7th SMSTS, November, 14-16, 2019, Morocco.

Tarik Hadibi, Abdelghani Boubekri, Djamel Mennouche, Abderrahmane Benhamzam: Hot air convective drying of tomato paste as optimized by the experimental design method. ISTSID, 24-25-26/02/2019, El Oued, Algeria.

General Introduction

Nowadays, with the ever-growing world population in the world, 7.594 billion in 2019, with an average annual population growth of 1.2% since 2000 (http://wdi.worldbank.org/table/2.1); the major problem facing the world, especially developing and third world is the lack of food and somewhere the famine, in another word, food insecurity. The population has grown rapidly in the 21st century accompanied by a significant increase in demand for food and agricultural products on one hand and high losses on the other hand.

Losing food is generally viewed as undesirable and something to be avoided. There are probably few issues in the international policy debate around which there is a stronger consensus. Reducing food loss and waste is seen as a way to lower production costs, improve food security and nutrition, and contribute towards environmental sustainability, notably by easing the pressure on natural resources and decreasing greenhouse gas (GHG) emissions. In the context of the challenge of sustainably feeding a world population projected to reach almost 10 billion in 2050, minimizing food loss and waste and making the most of resources underpinning the food system are considered particularly important.

Reducing food loss and waste seems a simple and reasonable goal. Obviously, it is unacceptable to allow food to spoil due to neglect or improper handling or to throw away food that could be consumed by humans. Drying is the traditional method of preserving food loss and waste.

Basically, drying is a key industrial process of great practical importance in chemical and pharmaceutical industries, agriculture and food processing, pulp and paper, wood and minerals processing, solid fuel preparation (e.g., biomass or coal drying). It consists of a mass transfer process aimed at removing a solvent – in general water (or moisture) – from a solid, liquid, or a semisolid (a highly viscous liquid). Hence, drying is a thermal separation process and usually occurs by evaporation of moisture or by sublimation or by a supercritical process which avoids the solid-liquid boundary, or by reverse osmosis.

Drying is an exceptional way to overcome spoilage problems in foods such as fruits, vegetables and grains. It is a powerful process of relatively high energy consumption where it accounts for around 10-15% of the overall global industrial energy consumption.

The drying process is recognized as one of the most energy intensive processes among separation technologies.

Solar radiation in the form of solar thermal energy is an alternative source of energy for drying especially to dry fruits, vegetables, agricultural grains, and other kinds of material, such as wood. This procedure is especially applicable in the so-called “sunny belt” world-wide, i.e. in the regions where the intensity of solar radiation is high and sunshine duration is long (Algeria). It is estimated that in developing countries there are significant postharvest losses of agricultural products, due to lack of other preservation means. Solar energy drying is a fairly economical procedure for agricultural products, especially for medium to small quantities of products. It is always used from domestic up to small commercial size drying of crops, agricultural products, and foodstuffs, such as fruits, vegetables, aromatic herbs, wood, etc. contributing thus significantly to the economy of small agricultural communities and farms.

In general, compared to conventional and traditional drying methods, solar drying has several benefits as follow:

- Significant improvement in product quality (color, texture, flavor, and taste).
- Prevention from contamination by insects, microorganisms, dust..etc.
- Reduction in drying time up to 50% compared to open sun drying.
- Reduction of drying and storage losses.
- A considerable increase in the shelf life of dried products allows us to preserve and transport the product in a safe case.
- Reducing energy consumption.

Despite all these advantages, researchers are working on innovative methods to improve the solar drying process rather than reducing drying time, energy consumption and improving the sensory and nutritional quality of the dried product. Assisted solar dryers and methods of pre-treating the product are widely proposed and used.

Based on the above, as a first step, the current work aims to determine the best way to solar drying using various adjustments and techniques available to improve the thermal performances of the solar drying process means reducing drying time and improve product quality. The work is divided into several chapters; every chapter treats a specific technique for enhancing direct solar drying under the prevailing climatic conditions. As well as, according to the huge production with a high loss level, the product to be dried is tomato paste.

The first chapter contains a detailed study of solar dryer kinds in one hand. A deep classification and development of solar dryers are determined (direct, indirect, mixed-mode, and hybrid dryers) under both passive and active mode, with a specification of solar drying with energy

storage. “DIC” instant controlled pressure drop is presented and detailed in this chapter as an innovative process for drying, in the second hand.

The second chapter investigated the drying kinetics and activation energy of dried tomato paste using a controlled convective dryer working under near solar drying operating conditions (T = 45, 50, and 60 °C) and (V = 1.5 and 2.5 m s^{-1}). Nine conventional mathematical models are fitted to the characteristic curves.

The third chapter investigated experimentally and compares the solar drying of tomato paste using both of a basic direct solar dryer and a modified one provided with a geothermal water heat exchanger (GWHE) with 67 °C. Unlike the basic dryer, the modified one was carried out to ensure the continuous drying process at night and cloudy days. The techno-economic analysis of the hybrid solar dryer has been carried out.

In the fourth chapter, improved direct solar drying of tomato paste using four drying techniques was conducted: (i) basic direct solar drying, (ii) direct solar drying provided with geothermal heat exchanger, (iii) direct solar drying with accelerated air drying using two electric DC fans generated by a P-V module, and (iv) combined direct solar drying between ventilated and heat exchanger mode. Drying time and kinetics of tomato paste by using four drying techniques were investigated. Additionally, mathematical modeling and characteristic drying curve of tomato paste have been determined.

The innovative drying process is reported in the fifth chapter. Pre-solar drying of tomato paste followed by DIC treatment (*in French:* “Détente Instantanée Contrôlée”) is considered as a novel drying process to reduce drying time, improve effective diffusivity, and better visual and sensorial quality. An optimal couple of absolute steam pressure thermal holding time (P,t) was determined using the method of design experiments. The optimal (P = 0.3 MPa, t = 30 s) was then applied to the pre-solar dried samples. Starting accessibility was considered to determine the effective moisture diffusivities and activation energies.

In the sixth chapter, garlic as an important product to dry was investigated by using a hybrid solar-electric dryer. The experiments have been carried out under forced and natural convection at drying temperatures of 50, 60, and 70°C. Drying kinetics, characteristic drying curve, modeling, diffusion process, the energy analysis, and techno-economic analysis were determined.

The main results of the above-mentioned chapters are briefly presented at the end of this thesis as a general conclusion. In addition; the general conclusion followed by a perspective part includes three points that we were unable to do, either because of time or instruments.

1 Solar Drying Systems and Innovative Drying Process (Swell Drying)

1.1 Introduction

The present chapter aims to investigate in the literature review the classification of solar drying systems used recently for agro-products and another materials preservation on one hand. Four types of solar dryers are discussed. Otherwise, innovative drying process namely swell drying is investigated.

1.2 Advanced in solar drying systems

Solar drying is a technological process works on the principle of greenhouse effect. This system which needs a simple technology allow to be adapted to the rural regions for drying applications (Perea-Moreno et al., 2016), also in the most developing countries where supplies of non-renewable sources of energy are either unavailable, unreliable or, for many farmers, too expensive this technology can be used (Hernandez-Escobedo et al., 2015). The produce is dried using solar thermal energy in a cleaner and healthier fashion. In broad terms, solar drying system can be classified into two major groups, namely: (1) Passive dryer (conventionally termed natural circulation). Active dryer (most types of which are often called forced convection solar dryers). Otherwise, according to the solar dryer types, there are four types of solar dryers (Pardhi and Bhagoria, 2013). The main categories of solar dryers are presented in Figure (1.1) and detailed with their advantages and limitations in Table (1-1).

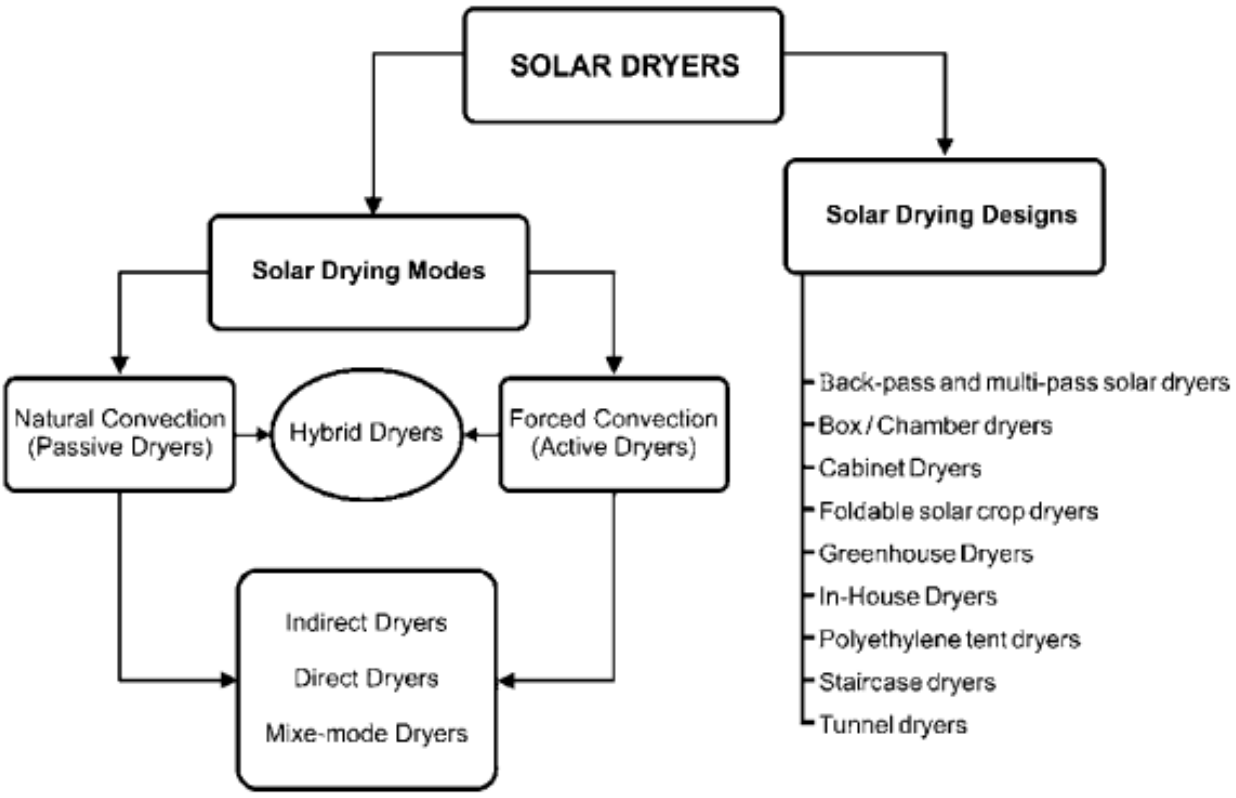

***Figure 1-1**: Classification of solar drying systems* (Banout, 2017)

***Table 1-1**: presents the main advantages and limitations of various solar dryer types*

Type	*Advantages*	*Limitations*
Direct type	- Least expensive - Simple	- UV can damage the product - Small capacity - Required long drying time - Low efficiency - The product to be dried itself acts as an absorber
Indirect type	- Less damage from high temperature - Products protected from UV - High efficiency	- More complex and expensive than direct type
Mixed-mode	- High efficiency - Less damage from high temperature	UV radiation may cause damage to the product - More complex and inexpensive than direct sun
Hybrid system	- The ability to work without the sun reduces - Loss of product is minimized - Allows better control of drying - High efficiency - Required short drying time - Good quality	- Expensive - May cause fuel dependence

1.2.1 Direct solar dryers

Solar energy is specifically used for dehydration crops in the direct-type solar dryer. In direct solar dryer, the researches and structure of direct solar dying is quick and operational and cost of maintenance are often lower and limited amount of the food product can be dried (Banout, 2017). A direct-type solar dryer is commonly used in areas that receive direct sunlight for longer periods during the day (Mustayen et al., 2014). In these dryers, the material to be dried is placed in an enclosure, with transparent covers or side panels. Heat is generated by absorption of solar radiation on the product itself as well as the internal surfaces of the drying chamber. This heat evaporates the moisture from the drying product and promotes the natural circulation of drying air (El-Sebaii and Shalaby, 2012). A direct solar dryer also is known as a solar cabinet dryer.

1.2.2 Indirect solar dryers

In indirect solar dryers, the drying process depends mainly on the drying conditions (air mass flow rate, and airflow temperature and relative humidity) in the drying chamber and on the drying kinetics of the product at those conditions. The drying conditions at the inlet of the drying chamber depend on the air heating process in the solar collector (Banout, 2017), and thus the

drying process is highly dependent on the ambient conditions and the solar irradiance. While the solar drying process is characterized by variable drying conditions, the drying kinetics is generally studied at constant drying conditions (Blanco-Cano et al., 2016). The indirect solar drying system is more efficient as compared to the direct solar drying system, since the air is heated by the operation of a solar air heater and the heated air flow in the room where the crop is stored.

1.2.3 Mixed-mode solar dryers

The combination of direct and indirect solar dryer is called mixed mode solar dryer; the product is dehydrated by this process, either by indirect solar radiation or when ambient air is first heated. It passes through the room where the crop is kept at that time (Banout, 2017).

1.2.4 Hybrid solar dryers

Hybrid solar drying systems are dryers where the solar energy is just one of more sources of energy used for heating the drying air. They employ solar energy with additional electric or fossil fuel-based heating systems and ventilators to ensure air circulation (Banout, 2017). Commonly the hybrid solar dryers operate under forced convection mode. If they are warm enough, the drying air heated by solar energy could be used directly for the drying process; otherwise, the dehydrator operated by fossil fuel is used to achieve required values of drying temperatures (e.g., during nights or during the time with low insolation like rainy seasons) (Ekechukwu, 1999). Furthermore, Fudholi et al., (2010) described in their work different hybrid dryer designs such as shown in Figure (1.2):

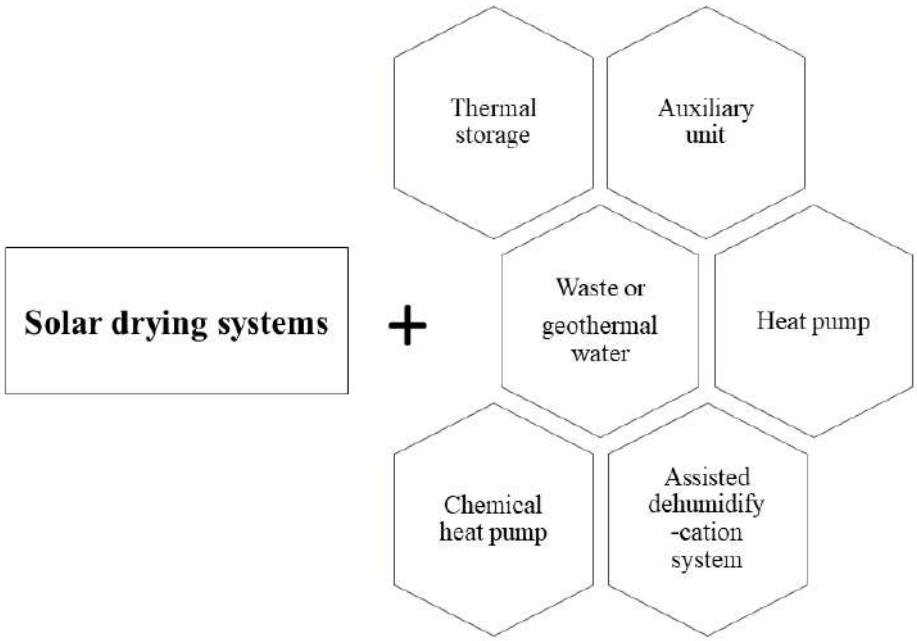

Figure 1-2: *Solar drying systems with various heating systems*

Dryers with thermal energy storage

In order to avoid the intermittent effects in solar dryers, some of the researchers integrated it with thermal energy storage to store excess heat energy in the sunshine time and utilize it in the off-sunshine time. The surplus solar energy can be stored in solids or well-insulated fluids in the form of sensible heat or latent heat or thermos-chemical. Among these methods, latent heat storage provides higher storage with small temperature difference between storing and releasing energy (Kaviti and Deep, 2017). Figure (1.3) shows some of the major techniques involved in thermal energy storage.

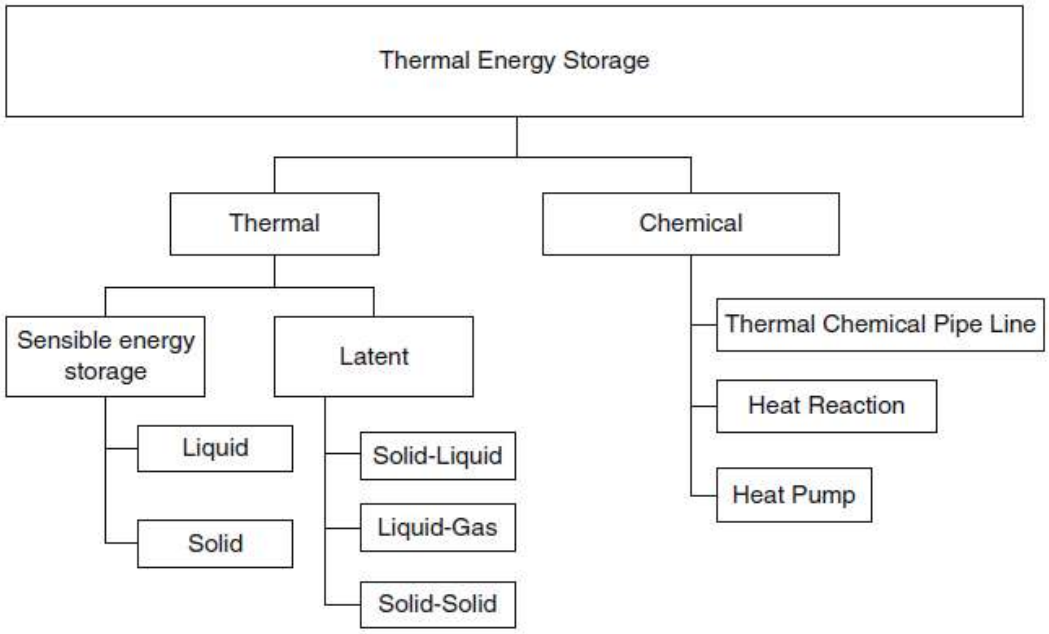

***Figure 1-3**: Various types of thermal energy storage* (Bal et al., 2010)

1.3 Swell-drying (DIC + Hot Air Drying)

Conventional airflow drying, sun drying, solar drying, vacuum drying, etc., are known to be easy to use, they can be tightly controlled, and are widely used. Sun and solar drying can be employed to directly process fruit and vegetables near the harvesting area, which is suitable for many products. In addition, there is the advantage of using a free and renewable energy, often significantly reducing the energy cost of the operation. However, Alternative to conventional processes, many innovative techniques have been studied to preserve the nutritional quality and to protect food from deterioration on one hand and to enhance the drying kinetics on the other hand. The principles and the applications of the swell-drying process in food drying and decontamination are presented in the next part.

Swell-drying involves coupling airflow drying with instant controlled pressure drop (DIC) texturing process. This process has been used mainly with plants, fruit, vegetables, seaweeds and

microalgae, seafood, meat and pharmaceutical products. The reduction in processing time leads to a significant improvement in product quality. However, the industrial application of these technologies is still limited.

The innovative process called instant controlled pressure drop (*Détente instantannée contrôlée* in French, DIC) was invented as a drying and decontamination food process. This process is based on the thermomechanical effect induced by a rapid pressure drop leading to instant evaporation of water and inactivation of vegetative bacteria and spores. DIC technology is distinguished by its ability to handle a wide range of solid food products. In addition, this process results in volume expansion and positive texture modification. Preservation of sensory aspects and nutriment compounds of food products was also reported using this technology. Based on the DIC technology, many industrial projects were realized and several patents were filed (Allaf and Allaf, 2014). The DIC technology as a food drying and microbial decontamination process is reviewed in this chapter.

1.3.1 Instant controlled pressure drops (DIC) technology

1.3.1.1 Theoretical principles

Instant controlled pressure drop (French acronym: DIC, for "*Détente Instantané Contrôlée*") was invented by Allaf and Vidal as, practically, a high temperature short time (HTST) type process followed by an abrupt pressure drop toward a vacuum (Allaf and Vidal, 1988). The different steps of a typical DIC treatment are presented in detail in Figure (1.4). This process consists of, in the first place, a short heating step (10–60 s) including a saturated steam injection under high-pressure (up to 1 MPa) applied to product put initially under vacuum. This step involves vapour condensation and product heating, in which the moisture content of the product increases by 0.1 g H_2O/g dry basis. The initial vacuum ensures rapid contact between the steam and the sample and consequently improves the heat transfer. Sometimes, the compressed air could be used as a pressurized agent as for the multicycle DIC treatment. Following the first heating step, the abrupt dropping of pressure (0.5 MPa.s^{-1}) toward a vacuum (3–5 kPa) over only 10–60 ms results in an auto evaporation of water within the product, which produces an amount of vapor and a significant mechanical stress enabling the product to be expanded. Furthermore, the auto evaporation of water ensures rapid cooling, which prevents the thermal degradation of the sensitive compounds and thus ensures the high quality of treated products. The cooling rate can reach exceptional levels of 1500–2000 kW m^{-2} (Allaf et al., 2013). Moreover, the extension stress within the product creates a new expanded and porous structure (Al Haddad et al., 2008). The new structure increases the specific surface area and the mass transfer diffusivity as well as the stating

accessibility of the product, thus improving the drying process, solvent extraction, and many other functional properties of foods (Haddad et al., 2001). The energy costs can also be reduced.

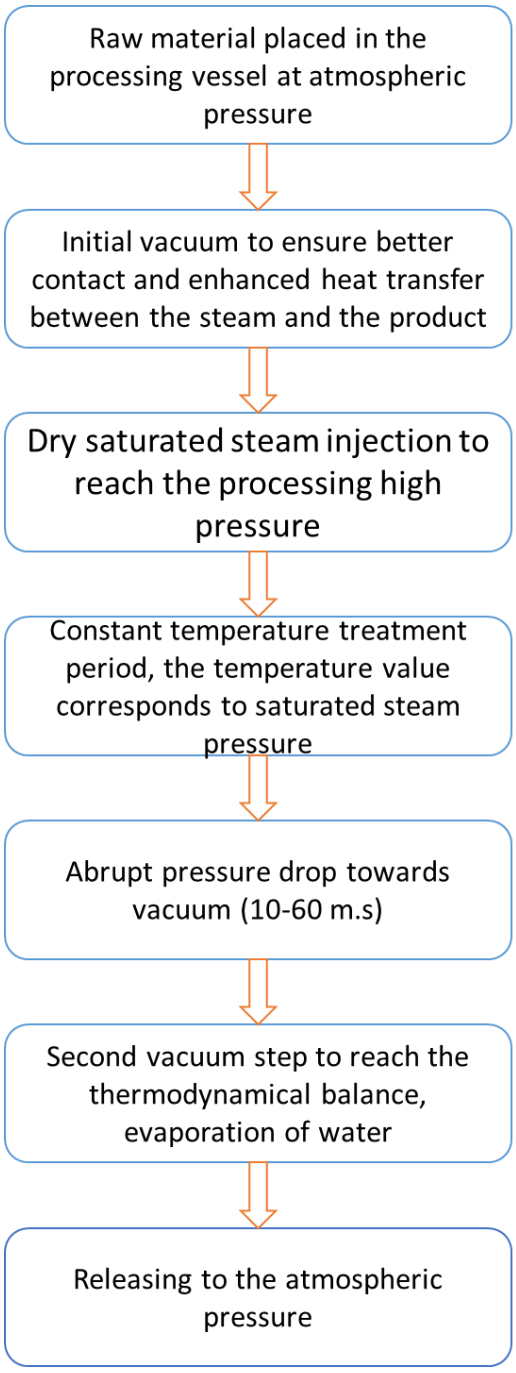

***Figure 1-4**: DIC treatment steps*

DIC equipment is mainly composed of four components (Mounir and Allaf, 2008); as presented in Figure (1.5):

- A processing vessel, which is an autoclave with a heating jacket where the product to be treated is placed.

- A pneumatic valve, which ensures a nearly instant liberation of steam pressure contained in the treatment vessel to the vacuum tank.
- A vacuum system composed of a vacuum pump and a tank with a cooling jacket. The tank volume is usually 100–130 times higher than the volume of the processing vessel. A water ring pump maintains the tank pressure at about 2.5–5 kPa.
- An extract collection trap used to recover condensates.

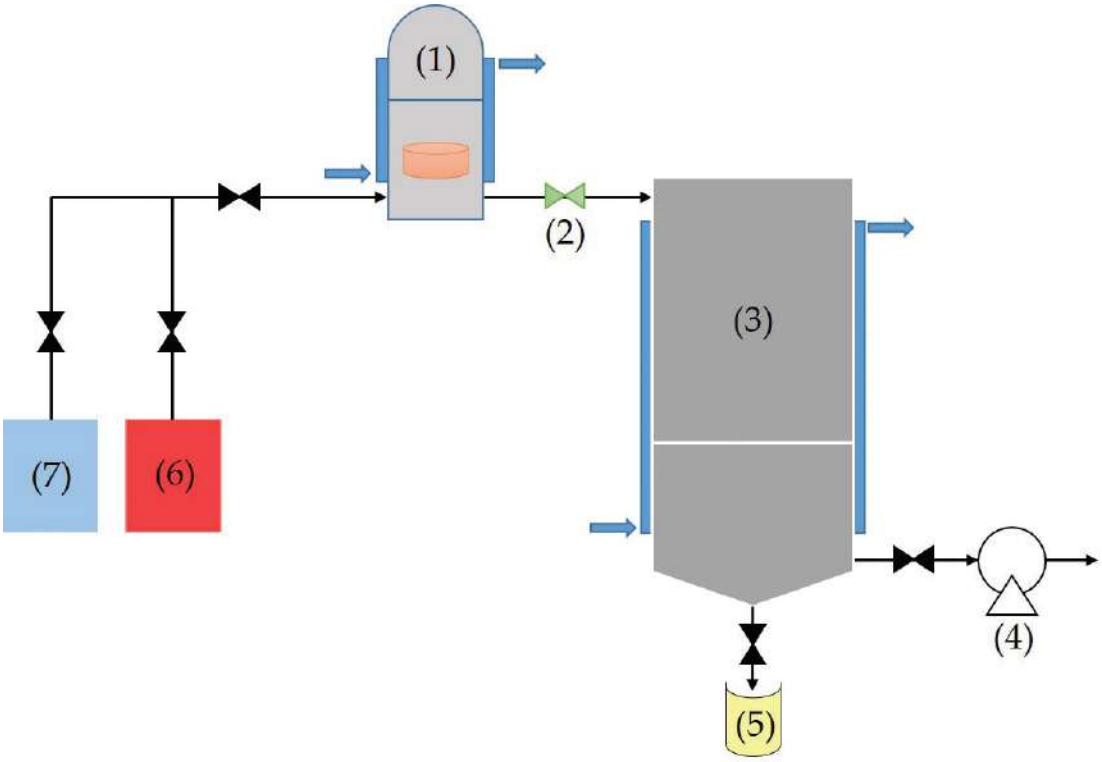

Figure 1-5: *Schematic presentation of a typical DIC reactor: (1) treatment vessel, controlled instant pressure drop valve, (3) vacuum tank with cooling jacket, vacuum pump, (5) extract collection trap, (6) steam generator, and (7) air compressor*

The operating pressure and temperature profiles during a DIC cycle are presented in Figure (1.6).

- Initial vacuum,
- Injection of saturated dry steam during the cycle thermal treatment time,
- Abrupt pressure-drop towards the vacuum
- Releasing to atmospheric pressure.

The initial vacuum stage deals with greatly increasing the next interaction between steam and exchange surface. The use of saturated dry steam allowed heating by condensation, the rate of which is thousands of times higher than conventional convection.

During this heating stage, both high pressure and high temperature were maintained for a period defined to practically homogenize the temperature and the water content in the matrix. The abrupt pressure-drop towards the vacuum following the heat treatment led to an auto-vaporization coupled to an "instantaneous" cooling towards the equilibrium temperature (here, for 4-5 kPa, it is about 30°C) and eventually to a controlled expansion of the solid material.

Besides, DIC treatment can be performed through multi-cycles. The number of cycles is the number of various pressure drops towards a vacuum and the processing time is computed for the total cycles (Allaf and Allaf, 2014).

DIC cycle can be summarized as follow:

(A): establishment of the vacuum within the processing reactor; (B): injection of steam at the selected pressure; (C) maintain of treatment pressure during selected time; (D): instant controlled pressure drop towards vacuum and (E): establishment of the atmospheric pressure within the processing reactor

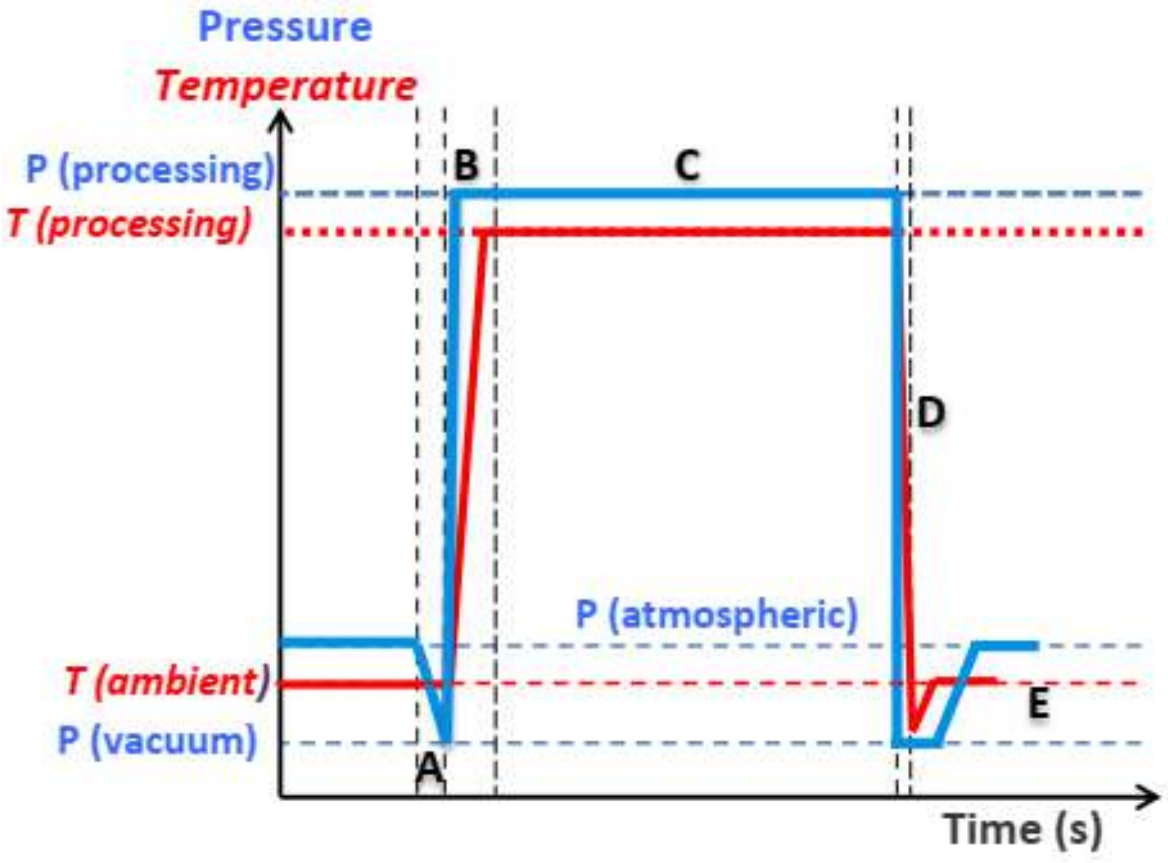

***Figure 1-6**: Pressure and temperature profiles of a typical DIC treatment during a DIC treatment*

1.3.1.2 DIC drying treatment in drying applications

The DIC treatment combined with classical hot air drying may be considered as an innovative and alternative intensifying drying process. This combination is very flexible and easy to be realized. Several protocols were proposed in the literature. In general, swell drying is defined as an operation that combines optimized hot air-drying step with a DIC texturing operation. In this method, instant pressure drop (DIC) step is inserted generally after a hot air drying treatment or, often, between two steps of conventional hot air drying. The first drying step allows the product to reach an elastic state with a water content of 20–30 g H_2O/100 g dry basis, which is an essential condition before application of DIC treatment.

Swell drying reduces the drying shrinkage phenomenon, which takes place during the first hot-air drying step, via a controlled expansion. Mounir et al. (2012) presented the effect of swell-drying on cheese compared to hot air drying only, Figure (1.7). The instant controlled pressure drops (DIC) technology has been proposed and successfully tested as a texturing process for partially dried materials. It improves also the drying kinetics by increasing water diffusivity (2–10 times) and initial accessibility (about two times).

The reduction in processing time (often reduced by more than 50%) leads to a significant improvement in product quality and energy consumption, at selected conditions of the DIC treatment (0.35 MPa and 5 s). Téllez-Pérez et al. (2015) noticed an improvement in drying kinetics of Moroccan Pepper, while the total hot air drying (THD) samples needed around 120 min to achieve a moisture content of 4% d.b, swell drying samples needed less than half of this time (48 min); Figure (1.8).

Furthermore, the swell drying process ensures effective microbiological decontamination of the end products (Albitar et al., 2011).

***Figure 1-7**: Cheese: snacks made with DIC-textured pure cheese (right) and with HAD (left)*

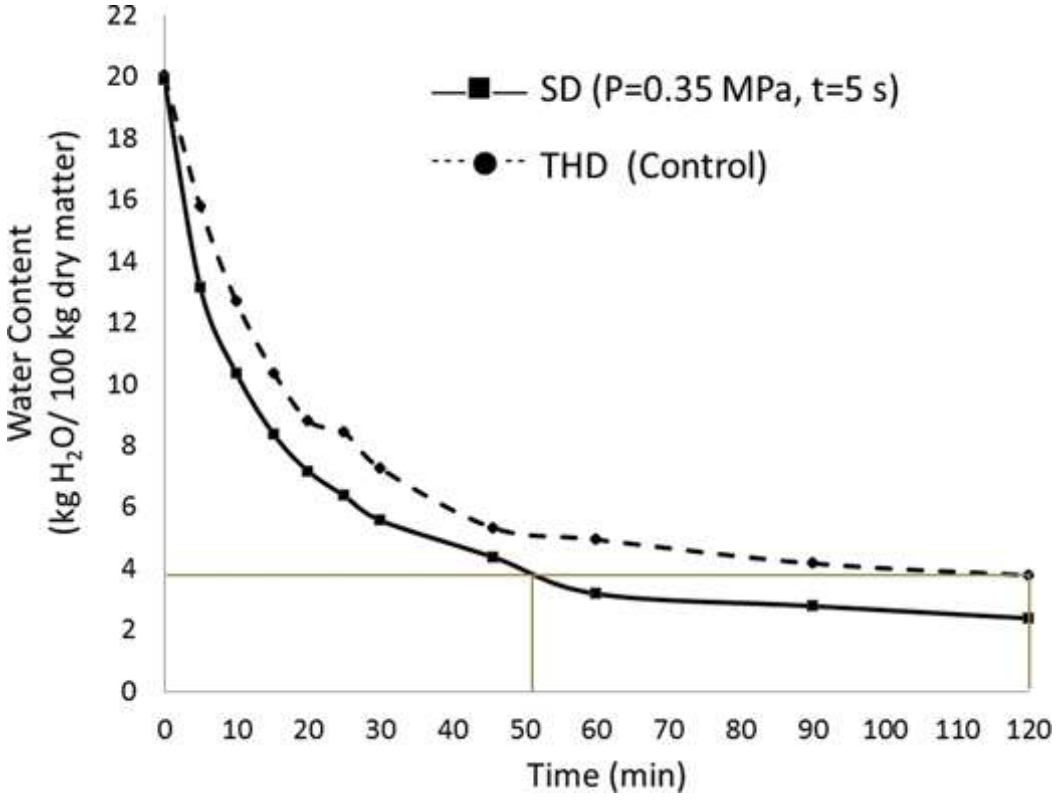

***Figure 1-8**: Drying kinetics of green Moroccan peppers: THD (Control) and SD (P = 0.35MPa, t = 5)*

1.3.1.3 Instant controlled pressure drops (DIC) decontamination of food

DIC treatment can be used as a decontamination process with a large variety of food, animal feed, powders, baby foods, intermediate ingredients, etc. It can also serve as a superficial

decontamination for fresh cut fruit and vegetables. DIC often combines swell-drying with a perfect decontamination.

To better understand how DIC works as a decontamination process, studies were carried out to evaluate the impact of multiple cycles of pressure drops towards a vacuum on vegetative forms and spores. We observed that, for conventional thermal treatments, including ultrahigh temperature (UHT), temperature and treatment time were the only operating parameters. For DIC the number of pressures drop cycles is an additional effective parameter, acting on both vegetative flora and spores. The high destruction rate of vegetative flora and spores with DIC is probably due to the various stresses resulting in irreversible changes in the cells of microorganisms such as:

- Protein denaturation.
- Shrinkage of the cellular membrane.
- Denaturation of protein enzymes.
- Breakdown of the cell structure and/or.
- Instant thermal and mechanical stress.

These changes are mainly due to the heat shock to which microorganisms are exposed as the temperature increases; indeed, this shock increases after several cycles of pressure drops that induce successive cycles of heating-instant cooling. Moreover, they may be due to the stress and strains exerted on the cell after steam expansion inside the cell followed by an instant pressure drop towards a vacuum, resulting in the breakdown of cell structure.

1.3.1.4 Other applications of instant controlled pressure drop (DIC) in food processing

In addition to its application as a decontamination and intensifying drying process, DIC technology can be used in other various operations in food processing (Allaf and Allaf, 2014), such as, blanching-steaming of vegetables. Furthermore, the DIC process has been used to enhance or assist the conventional edible oil extraction from various vegetal materials (Allaf et al., 2013). Multi-DIC cycles allow the extraction of essential oils of aromatic plants with low energy and low water consumption. The structure expansion by DIC increases the porosity and the specific surface area of the treated plants and improves, as a result, the solvent extraction. DIC texturing is considered, thus, as a solvent extraction pre-treatment, which decreases the extraction time.

1.3.1.5 Quality of instant controlled pressure drop (DIC)-treated products

The nutritive quality of processed food is effectively influenced by the operating conditions. High temperature and long heating times result in important degradation of vitamins and bioactive molecules (Lešková et al., 2006). The nutritive values of DIC-treated products were

evaluated (Alonzo-Macías et al., 2013; Téllez-Pérez et al., 2015). Thanks to its effective heating and rapid cooling, DIC-dried products are characterized by higher content and availability of bioactive compounds. The open porous structure, because of DIC texturing, allows increasing the availability of these compounds.

Sensory characteristics are crucial quality attributes and normally influence the consumer preferences (Asioli et al., 2019). DIC dried, or treated products in general, are distinguished by preserved and even improved sensory properties such as flavour, color, and texture. In addition, the expansion ratio of DIC swell dried vegetables is an important product quality; Figure (1.9). The expansion phenomenon results in increasing the specific surface area, which was for example two times higher for swell dried apples compared to hot air-dried samples. Relative expansion ratio is defined as a volumetric ratio between DIC and conventional hot air-dried products, which allows evaluating the macro-structural changes caused by DIC texturing; Figure (1.10).

***Figure 1-9**: Swell-dried fruits and vegetable*

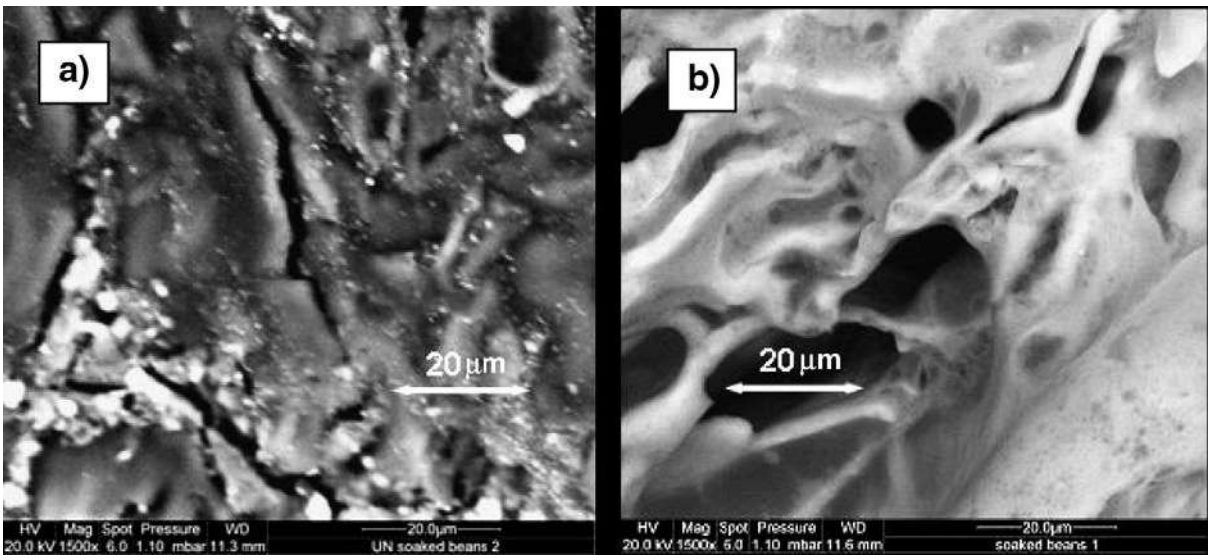

***Figure 1-10**: Micrographs of cross-sections of Ethiopian coffee beans. a) raw bean; b) bean treated with steam DIC, m =28% d.b., p =0.5 MPa, t= 35 s* (Kamal et al., 2008)

1.4 Conclusion

This section presents a review of various kinds of solar dryers available today, under load, and no-load conditions. The kinds examined are the direct, indirect, mixed-mode and hybrid solar dryers. Among the different types of solar dryers, the indirect solar dryer with an electric heater is superior in the speed and quality of drying. A backup heating system is necessary for products that require continuous drying. Solar drying systems provided with sensible and/or latent heat storage media accelerate the drying operation during the night time and low-intensity solar

radiation periods and exclude the need for using auxiliary heat sources during low solar radiation seasons. Solar dryers with forced convection have been selected to be more suitable for dry products with high moisture content. As compared with open sun drying, solar drying is more effectively, economically, and environmentally. Despite the high cost, researchers trend to develop solar drying systems under the hybrid mode, especially with thermal energy storage medium according to their speed and producing product in good quality

The technology using instant controlled pressure drop (DIC) as a post-harvesting treatment for fruits and vegetables, pharmaceutical products, marine products, etc., followed by conventional airflow drying, is one of the most efficient drying processes. This drying strategy enables the user to increase drying performance, reduce costs, and optimize product quality.

2 Hot Air Convective Drying of Tomato Paste Under Near Solar Drying Operating Conditions

2.1 Introduction

Tomatoes (Lycopersicon esculentum. var) are one of the most important grown vegetable crops, mostly in the world. The cultivation of tomato is widespread throughout the world. According to (FAO, 2014) , the universal production of tomato on 2014 was 170.750.767 million tons, whereas Algeria produced 1.065.609 million tons with a world rank of 18 and a world share of 0.6%. In particular, 90% of world output is produced in the northern hemisphere (Mediterranean area, California and China).

The industrial processing of tomato, which is considered a highly deformable material, leads to a great variety of derived products from which: concentrated tomato products, pizza sauce, tomato powder, peeled tomato, tomato sauce seasoned (Celma et al., 2009).

Tomato drying has been investigated to a great extent, and a lot of data are available in literature. Sahin et al. (2011) investigated experimentally the effects of several drying methods, such as hot-air drying at 65, 75 and 85 °C drying temperatures. Krokida et al. (2003) studied the drying kinetics of some vegetables including tomato fruit and determined the equilibrium moisture content of each dried product. Bagheri et al. (2013) modeled the thin layer solar drying of tomatoes slices with thickness of 3, 5 and 7 mm at the air velocity of 0.5 and 1 m s^{-1} using a basic indirect solar dryer. Sacilik et al. (2006) studied experimentally solar drying curves of tomato cut in half dried under atmospheric conditions of Ankara (Turkey) and they compared them to the way drying in open air. Doymaz (2007) studied experimentally the effect of treatment on drying kinetics of tomatoes cut in half and distributed on shelves of a forced convection dryer at temperatures of 55, 60, 65 and 70 °C by using electric resistors passing perpendicularly through the grids. Belghith et al. (2016) investigated the modelling effect of drying parameters on the drying behavior of tomato quarters and halves along with the exchange surface with the surrounding environment with the hot air dryer used in the present work.

From that vast extensive literature review on the impact of changing in drying parameters during drying operation, very little information is available on thin layer drying behavior of tomato, particularly the tomato paste that is less investigated.

The available literature on the different drying techniques of tomatoes shows that the most suitable treatment temperatures are in the range of 40°C to 70°C which represents the order of magnitude commonly provided by the solar drying. Nevertheless, in the case of solar drying the process is constrained by the instability of the temperature along of the day, which could possibly affect the good prediction of the physical behavior and the quality of the final product.

Hence, this chapter was carried out to fulfill the existing research gaps on thin layer modelling of tomato paste. The main objectives of this study are to:

- Investigation by modelling the drying kinetics of dried tomato paste using a controlled convective dryer working under near solar drying operating conditions.
- Predict the most suitable drying models for describing the drying behavior of tomato paste with various drying conditions.
- Study the effect of drying conditions on effective moisture diffusivities and activation energy of tomato paste.

2.2 Experimental protocol

2.2.1 Sample preparation

Fresh local tomatoes (L. esculentum. var) were bought at a local market in Ouargla, southern of Algeria. They were singled out one by one using a visual criterion like color, size, absence of physical damage and uniform maturation degree. Forty kilograms of tomatoes were properly washed with running water to remove skin, dirt and then cut into halves or quarters. After that, it was grinded in a kitchen blender and separated in a whole series of sieves with different sizes to remove the skin and the seeds from the paste. Finally, the paste was drained in tissue bag to obtain 4 kilograms of tomato paste, and 15 liters of tomato juice. The tomato paste was sealed in plastic bags and stored at 4°C.

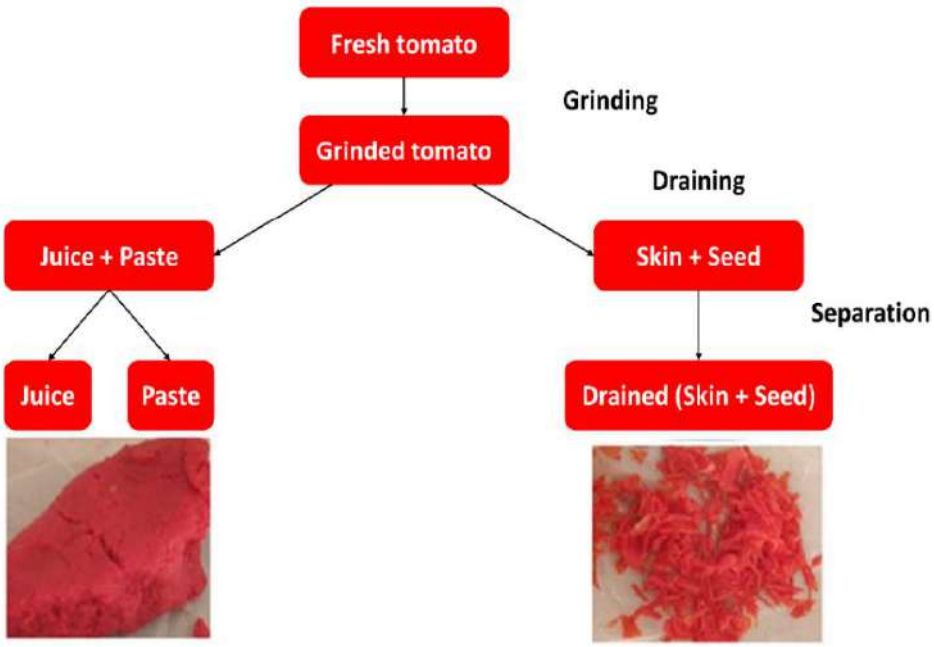

Figure 2-1: *Sample preparation*

2.2.2 Initial moisture content determination

The sample's initial moisture content was determined using a direct measurement method, which consists of placing a sample weight of 3g in a Laboratory Incubator at 105°C (±1) °C for 24 (h) until a constant weight is obtained.

2.2.3 Experimental procedure

Prior to start the drying experiments, the system was run for at least a quarter of an hour (15 min) to obtain steady state conditions. A batch of 50 g of fresh tomato paste has been taken out from the refrigerator to rest. Samples were spread in a perforated tray (dimensions in cm: 5×5 ± 0.1) in thin layer of about 1.5 cm thickness.

The tray loaded with tomato paste was suspended to a digital balance with a standard error of ± 0.001 g. Air parameters were adjusted and controlled continuously using an industrial programmable controller. In order to guarantee dried product quality, experiments were performed in the temperature range from 45 to 60°C, in a relative humidity of 16 % at two air velocities of 1.5 and 2.5 m s^{-1}. The mass of the product was continuously measured using an electronic balance (precision of 0.01g) and recorded by a microcomputer.

2.2.4 Drying equipment

Drying experiments were performed in a laboratory scale, convective and vertical downward flow dryer (designed and constructed in the LETTM laboratory, Sciences Faculty of Tunis). This dryer is designed to work in closed loop and was equipped with a programmable controlling system for drying air parameters. The layout of the dryer is given in Figure (2.2).

The dryer presented in Figure (2.2) is equipped with a controlling system for temperature, velocity and relative humidity of drying air and consists of a vertical airflow conducted through a tunnel to cross perpendicularly the tomato paste samples spread uniformly on a perforated tray, placed inside the drying chamber. Moisture loss was obtained through periodic measuring the samples weight during drying which was recorded at 30 min intervals by means of a digital balance interfaced with a PC to insure the data acquisition.

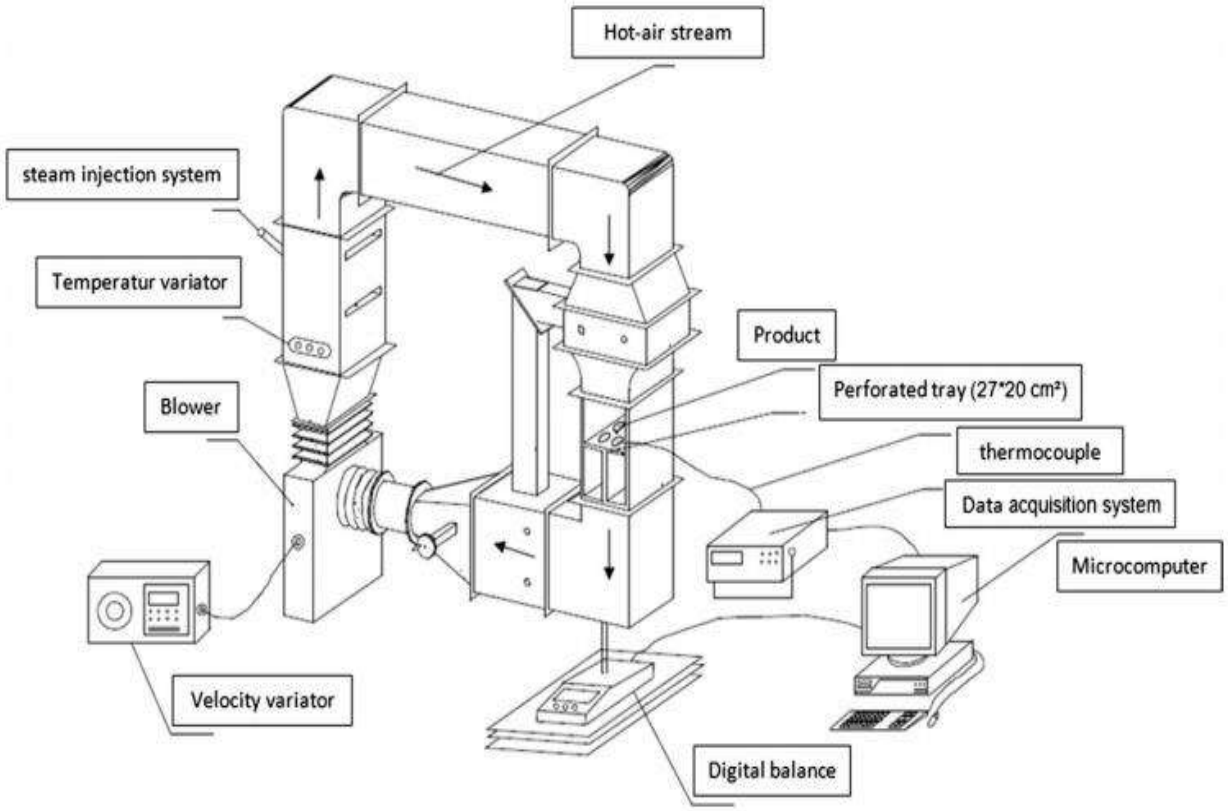

***Figure 2-2**: Schematic diagram of the drying loop* (Belghith et al., 2016)

2.2.5 Experimental uncertainty

Based on instruments selection, drying condition, calibration, observation, test planning, certain errors and uncertainties occur during measurements (Akpinar et al., 2003). During the drying experiment of tomato paste, the drying temperature, air velocity, relative humidity and weight losses were measured with appropriate instruments. The uncertainties of measurements are presented in Table (2-1).

***Table 2-1**: Uncertainties of the various parameters*

Parameters	*Expression*	*Unit*	*Value*
Drying chamber temperature	T	°C	±1
Drying chamber relative humidity	RH	%	±2
Weight loss of the sample	m	g	±0.01
Air velocity	V	m s^{-1}	±0.1
Samples dimensions	L	cm	±0.1

2.2.6 Modelling of thin layer drying curves – theoretical approach

The drying curves were fitted to nine different moisture ratio models to select a suitable model for describing the drying process of tomato paste in Table (2-2).

***Table 2-2**: Mathematical models widely used to describe drying kinetics*

Model	*Equation*	*References*
Newton	$MR = \exp(-kt)$	(O'callaghan et al., 1971)
Page	$MR = \exp(-kt^n)$	(Diamante and Munro, 1991)
Modified page	$MR = \exp\left(-(kt)^n\right)$	(Overhults et al., 1973)
Henderson and Pabis	$MR = a.\exp(-kt)$	(Zhang and Litchfield, 1991)
Logarithmic	$MR = a.\exp(-kt) + c$	(Yagcioglu, 1999)
Wangh and Singh	$MR = 1 + at + bt^2$	(Wang and Singh, 1978)
Diffusion approach	$MR = a.\exp(-kt) + (1-a)\exp(-kbt)$	(Kassem, 1998)
Demir et al.	$MR = a.\exp(-kt)^n + b$	(Demir et al., 2007)
Midili and Kucuk	$MR = a.\exp(-kt^n) + bt$	(Midilli et al., 2002)

Moisture ratio of the samples during convective drying was expressed by Eq (2.1):

$$MR = \frac{M_t - M_e}{M_0 - M_e} \qquad \text{(Eq. 2.1)}$$

The values of M_e are relatively small compared to M_t and M_0 where error implied in the simplification is negligible. Equation (2.1) becomes Equation (2.2):

$$MR = \frac{M_t}{M_0} \qquad \text{(Eq. 2.2)}$$

2.2.7 Statistical analysis

To validate the goodness of the fit, two statistical criteria, namely root of mean square error (RMSE), reduced and coefficient of determination (R^2) were calculated using Origin software program. The coefficient of determination (R^2) is one of the primary criteria in order to evaluate the fit quality of selected models. In addition to R^2, root mean square error (RMSE) is used to determine suitability of the fit (Ghatrehsamani et al., 2012; Rayaguru and Routray, 2012). For the best fit, the R^2 value should be high and RMSE values should be low. These can be calculated as follows:

$$R = \frac{\sum_{i=1}^{n}(MR_i - MR_{pre,i}).\sum_{i=1}^{n}(MR_i - MR_{exp,i})}{\sqrt{\left[\sum_{i=1}^{n}(MR_i - MR_{pre,i})^2\right].\left[\sum_{i=1}^{n}(MR_i - MR_{exp,i})^2\right]}} \quad \text{(Eq. 2.3)}$$

$$RMSE = \left[\frac{\sum_{i=1}^{n}(MR_{pre,i} - MR_{exp,i})^2}{N}\right]^{1/2} \quad \text{(Eq. 2.4)}$$

It has been accepted that the drying characteristics of biological products in falling rate period can be described by using Fick's diffusion equation (Bagheri et al., 2013). The solution of Fick's law for a slab was according to Equation (2.5) (Okos et al., 1992).

$$MR = \frac{8}{\pi^2}\sum_{n=1}^{\infty}\frac{1}{(2n+1)^2}\exp\left(-(2n+1)^2\pi^2\frac{D_{eff}.t}{4L^2}\right) \quad \text{(Eq. 2.5)}$$

For long drying time in hours, Equation (2.5) can be further simplified to only the first term of series (Tütüncü and Labuza, 1996). Thus, Equation (2.5) is written in logarithmic form according to Equation (2.6):

$$MR = \frac{8}{\pi^2}\exp\left(-\pi^2\frac{Deff.t}{4L^2}\right) \quad \text{(Eq. 2.6)}$$

The Fick's diffusion equation developed for solid objects with slab geometry reported by Crank (Crank, 1979) was applied to the experimental data. The assumption applied in using this equation was that there was uniform initial moisture distribution and negligible external resistance (Tunde-Akintunde, 2011). The equation is as indicated in Equation (2.7).

$$\ln MR = \ln\left(\frac{8}{\pi^2}\right) - \left(\pi^2\frac{D_{eff}.t}{4L^2}\right) \quad \text{(Eq. 2.7)}$$

Diffusivities are typically determined by plotting experimental drying data in terms of ln (*MR*) versus drying time t in Equation (2.7), because the plot gives a straight line with a slope according to Equation (2.8); (Akpinar and Bicer, 2008).

$$Slope = -\frac{\pi^2 D_{eff}.t}{4L^2} \quad \text{(Eq. 2.8)}$$

Or $k = \left[\ln(MR) - \ln\left(\frac{8}{\pi^2}\right) \right] / t$, which is the slope of the straight line which fits the experimental data of ln (*MR*) against drying time.

The activation energy in a drying process, E_a, is the minimum quantity of energy that must be overcome to make this process realizable. The E_a value is closely related to D_{eff} coefficient and its dependence on temperature can be expressed by Arrhenius model (da Silva et al., 2012).

The origin of the self-diffusion is the thermal agitation. The diffusion is thermally activated, and the diffusion coefficient is traditionally calculated by using the Arrhenius law determined with Equation (2.9):

$$D_{eff} = D_0 \exp\left(-\frac{E_a}{RT_{abs}}\right) \quad \text{(Eq. 2.9)}$$

From Equation (2.9), a plot of ln (D_{eff}) vs $\frac{1}{T}$ gives a straight line whose slope is $\left(-\frac{E_a}{R_g}\right)$ which allows obtaining the activation energy.

$$\ln(D_{eff}) = \ln(D_0) - \frac{E_a}{R}\frac{1}{T} \quad \text{(Eq. 2.10)}$$

2.3 Results and discussion

2.3.1 Effect of drying air temperature and air velocity on drying time

The experimental curves in Figures (2.3-4) shows that increasing air drying temperature from 45 to 60°C decreased significantly the drying time (11.16 h, 10.45 h, 5.73 h) to air temperature 45, 50, and 60°C respectively, for air velocity of 1.5 m s^{-1}. This influence is due to increasing in the partial vapor pressure of water in the product. Also, an increase in air velocity from 1.5 to 2.5 m s^{-1} decreases relatively the drying time as a result of increasing convective heat and mass transfer coefficient between the drying air and the product (for T = 45°C drying time is 11.16 h and 9.62 h, respectively, to 1.5 m s^{-1}, 2.5 m s^{-1} (air velocity). For T = 50°C it is 10.45, 9.08 hours respectively. Finally, for T = 60°C it fell down to 5.73 h and 5.32 h. Therefore, there is a strong function of temperature and relatively weak function of air velocity. Observing that air drying temperature has a higher effect on the moisture content reduction, which is similar to Coşkun et al., (2017) conclusion.

Otherwise, by observing the effect of air velocity on drying kinetics Figures (2.5-7), the results show a slight effect of air velocity at low temperatures compared with high ones. The effect of air velocity increases with increasing drying air temperature. Boughali et al., (2009) confirmed that the air velocity is not an influential parameter as compared with the drying air temperature

and the influence decreases with drying process increasing.

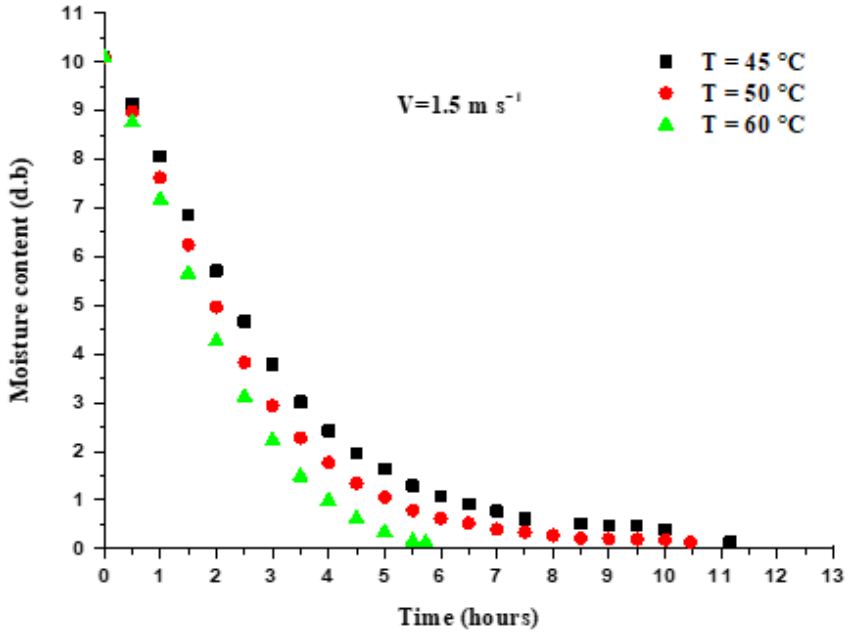

***Figure 2-3**: Effect of drying air temperature at V = 1.5 m s^{-1} on drying kinetics of tomato paste*

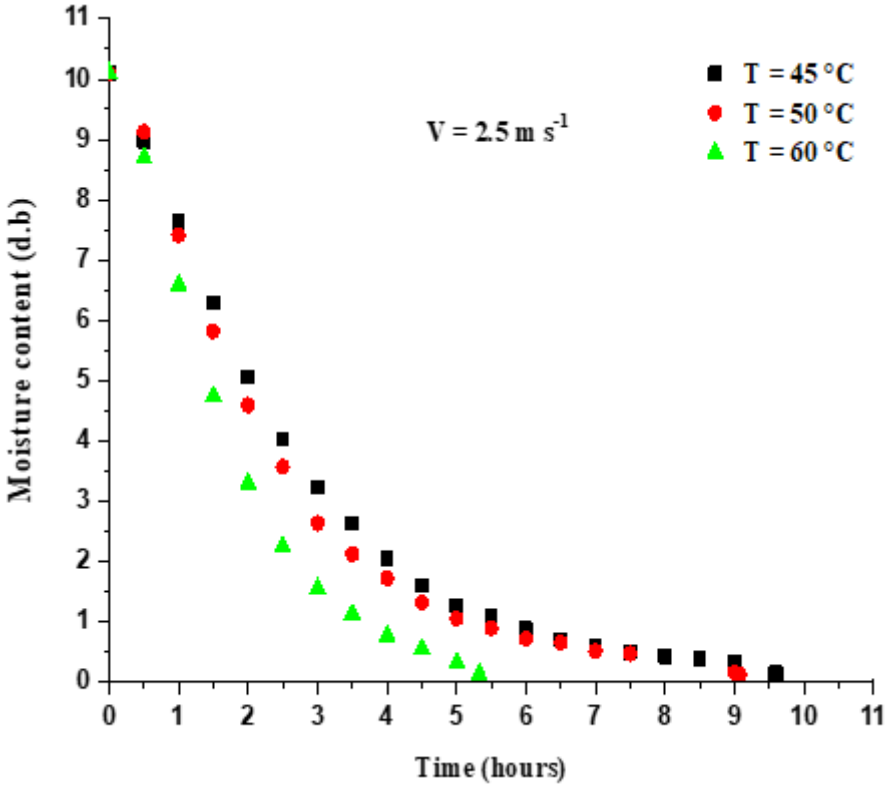

***Figure 2-4**: Effect of drying air temperature at V = 2.5 m s^{-1} on drying kinetics of tomato paste*

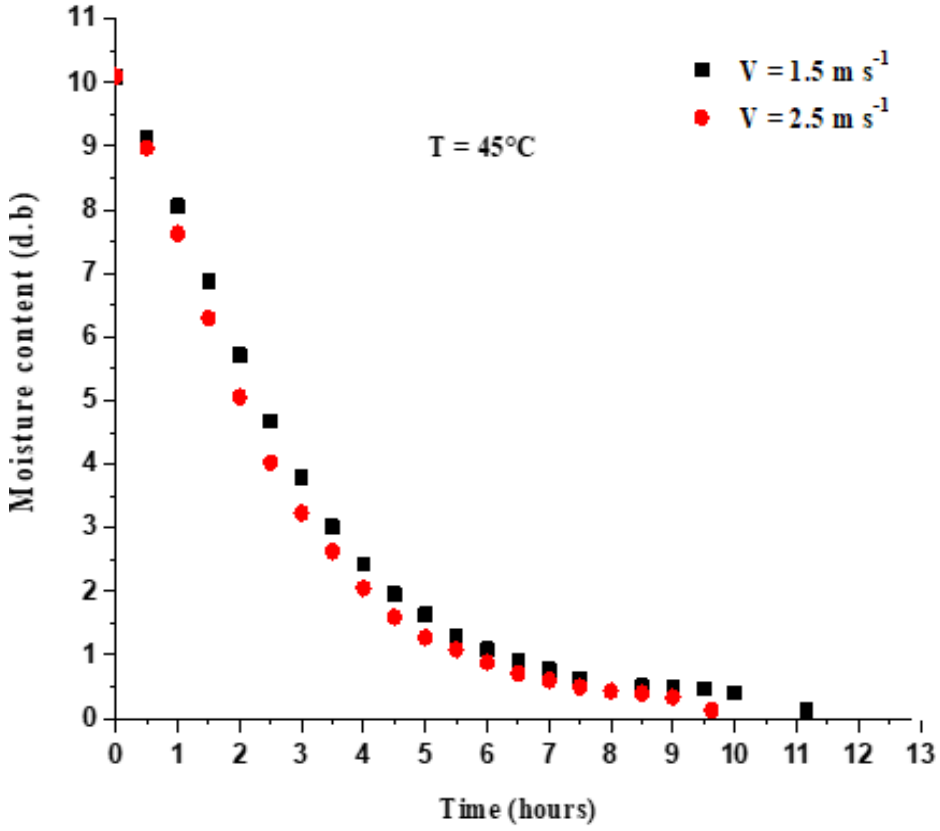

***Figure 2-5**: Effect of air velocity at T = 45 °C on drying kinetics of tomato paste*

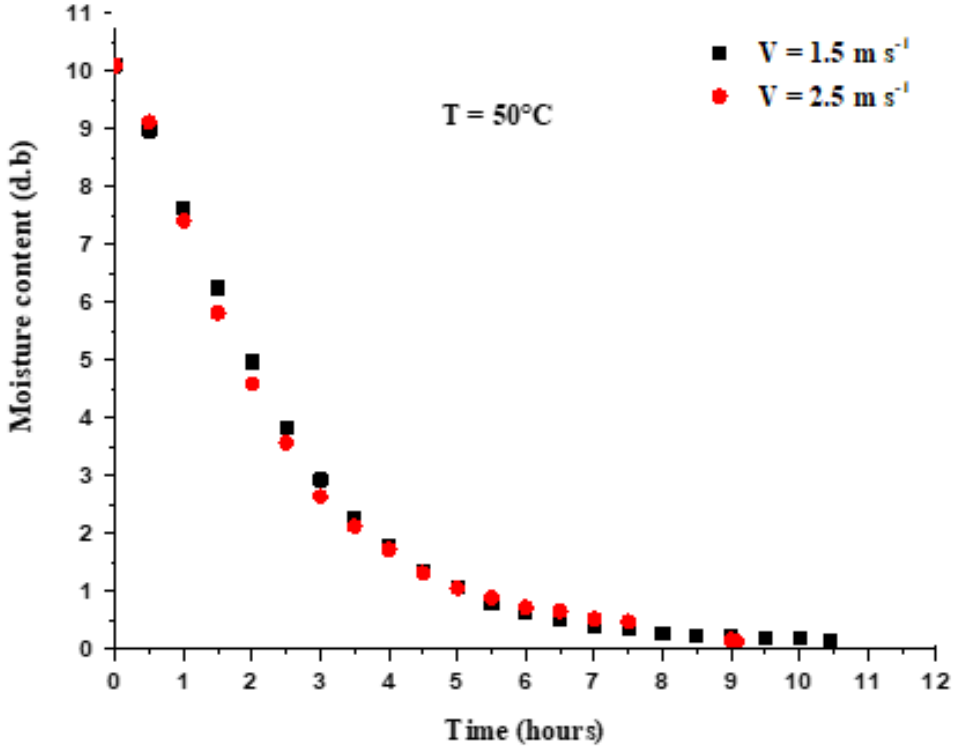

***Figure 2-6**: Effect of air velocity at T = 50 °C on drying kinetics of tomato paste*

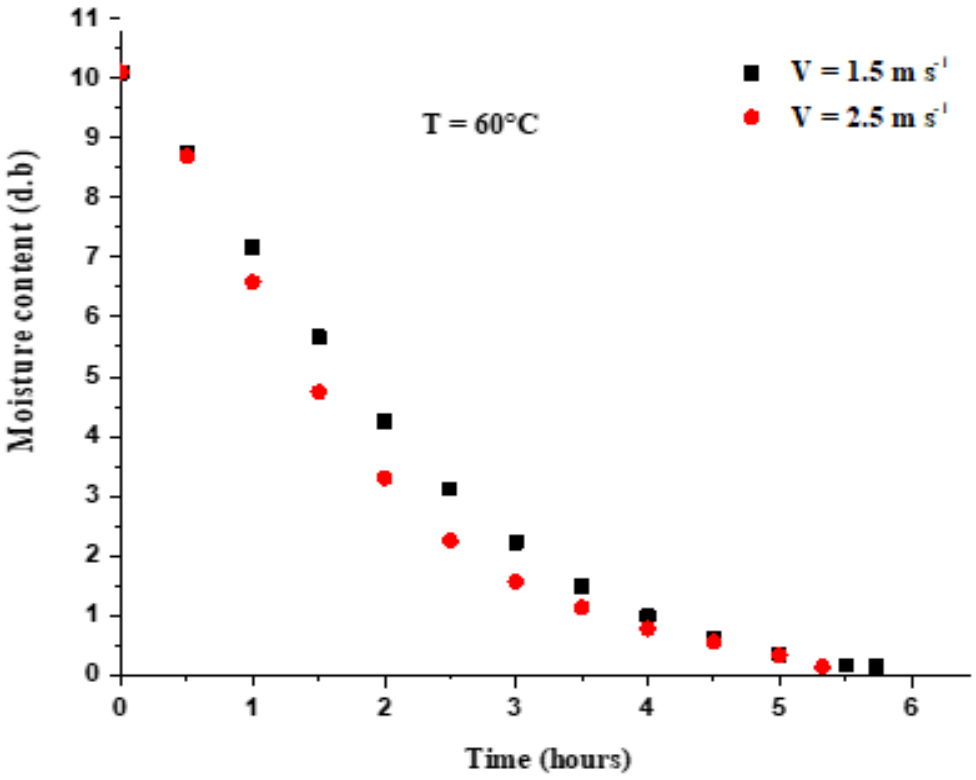

***Figure 2-7**: Effect of air velocity at T = 60 °C on drying kinetics of tomato paste*

2.3.2 Statistical results of thin layer drying models for convective drying

The moisture content of tomato paste is transformed into dimensionless moisture ratio to perform modelling studies easily. The values of the moisture ratio of tomato paste samples are calculated using Equation (2.6). The moisture ratio values are fitted to nine theoretical drying models listed in Table (2-3). The acceptability of the model is based on correlation coefficient, mean squared deviation and root mean square error. To observe the accuracy of the models, coefficient of determination (R^2) and the root mean square error (*RMSE*) values are calculated and given in Figures (3.8-9).

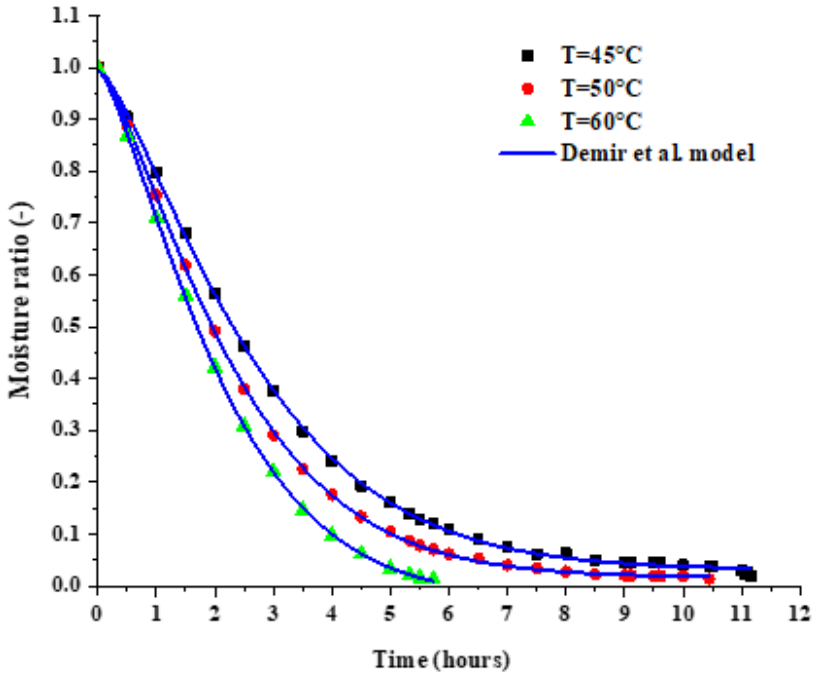

***Figure 2-8**: Moisture ratio versus drying time with V = 1.5 m s^{-1}*

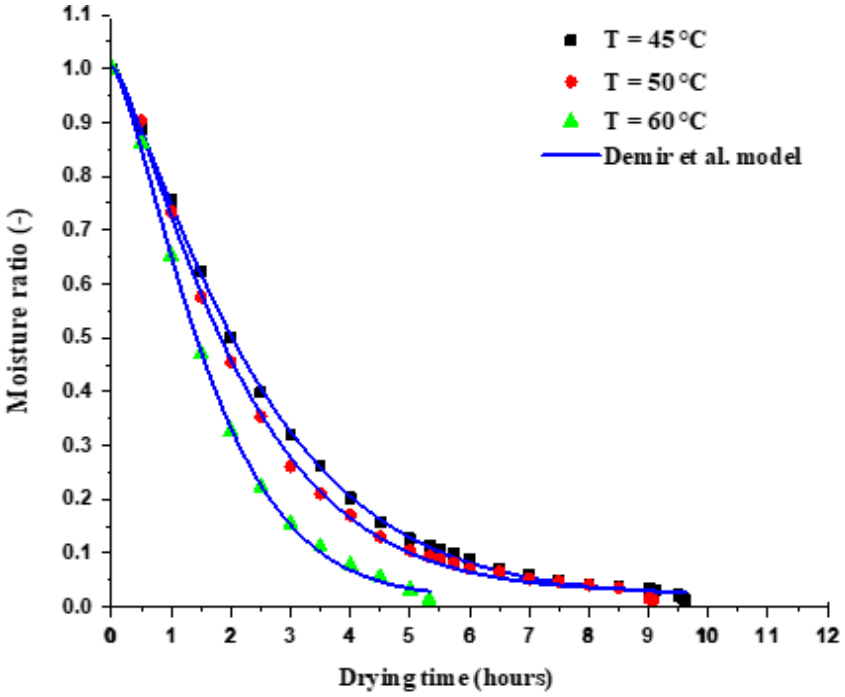

***Figure 2-9**: Moisture ratio versus drying time with V = 2.5 m s^{-1}*

The experimental moisture content data were determined on the dry basis and used for modelling. The moisture content data at each time of drying process, obtained at different drying temperatures 45, 50 and 60°C and for two levels of air velocity of 1.5 and 2.5 m s^{-1}, were converted to the moisture ratio values and fitted versus drying time.

By using regression analysis for, the value of correlation coefficient (R^2) and Root Mean Square Errors (*RMSE*) and their constant models are determined and listed in Tables (2.3-4).

***Table 2-3**: Statistical results of the nine selected thin layer drying models at different drying temperatures with 1.5 m s^{-1} air velocity, a) T = 45 °C, b) T = 50 °C, c) T = 60 °C*

Model	*R^2*	*RMSE*	*(χ^2)*	*Model coefficients*
Drying temperature =45°C				
Lewis	0.98932	0.02765	0.00076	k=0.33323
Page	0.99623	0.01668	0.00028	k=0.25971, n=1.18276
Modified page	0.99623	0.01668	0.00028	k=0.31989, n=1.18194
Henderson and Pabis	0.99331	0.02221	0.00049	a=1.06849, k=0.35292
Logarithmic	0.99335	0.02248	0.00051	a=1.06962, c=0.34884, k=-0.00338
Wangh and Singh	0.98001	0.03839	0.00147	a=-0.22723, b=0.01297
Diffusion approach	0.99101	0.02613	0.00068	a=8.842e12, b=1, k=0.25371
Demir *et al.*	0.99946	0.00649	0.000042	a=0.96882, b=0.03132, k= 0.24058, n=1.322
Midilli *et al.*	0.99927	0.00755	0.000057	a=1.00295, b=0.00276, k=0.2416, n=1.28765
Drying temperature =50°C				
Lewis	0.98787	0.03076	0.00094	k=0.40179
Page	0.99877	0.00998	0.000099	k=0.29965, n=1.25298
Modified page	0.99877	0.00998	0.000099	k=0.38223, n=1.25227
Henderson and Pabis	0.99235	0.02487	0.00062	a=1.07326, k=0.42697
Logarithmic	0.9932	0.02388	0.00057	a=1.07966, c=-0.01517, k=0.40639
Wangh and Singh	0.98075	0.03943	0.00156	a=-0.26288, b=0.01689
Diffusion approach	0.98787	0.03187	0.00102	a=1, b=1, k=0.40175
Demir *et al.*	0.99988	0.0032	0.00001	a=0.98401, b=0.01671, k=0.29334, n=1.32038
Midilli *et al.*	0.99983	0.00381	0.000014	a=1.00209, b=0.00167, k=0.29307, n=1.30165
Drying temperature =60°C				
Lewis	0.9727	0.05604	0.00314	k=0.48116
Page	0.99946	0.00824	0.000068	k=0.33256, n=1.39904
Modified page	0.99946	0.00824	0.000068	k=0.45523, n=1.39943
Henderson and Pabis	0.97976	0.05022	0.00252	a=1.07955, k=0.515
Logarithmic	0.99516	0.02564	0.00066	a=1.20271, c=-0.16299, k=0.36219
Wangh and Singh	0.99829	0.01462	0.00021	a=-0.34783, b=0.03069
Diffusion approach	0.9727	0.06092	0.00371	a=1, b=1, k=0.48127
Demir *et al.*	0.99993	0.00331	0.000011	a=1.02164, b=-0.02481, k=0.32827, n=1.34031
Midilli *et al.*	0.99991	0.00358	0.000013	a=0.99645, b=-0.00366, k=0.332, n= 1.35146

Table 2-4: *Statistical results of the nine selected thin layer drying models at different drying temperatures with 2.5 m s^{-1} air velocity, a) T = 45 °C, b) T = 50 °C, c) T = 60 °C*

Model	*R^2*	*RMSE*	*(χ^2)*	*Model coefficients*
Drying temperature =45°C				
Lewis	0.99231	0.02471	0.000610	k=0.3762
Page	0.99871	0.01031	0.00011	k=0.30376, n=1.17337
Modified page	0.99871	0.01031	0.00011	k=0.36227, n=1.17282
Henderson and Pabis	0.99545	0.01936	0.00037	a=1.05881, k=0.3957
Logarithmic	0.996	0.01853	0.00034	a=1.06497, c=-0.01413, k=0.37813
Wangh and Singh	0.98537	0.03474	0.00121	a=-0.25704, b=0.01653, k=0.3762
Diffusion approach	0.99231	0.02568	0.00066	a=1, b=1, k=0.3762
Demir *et al.*	0.99959	0.00602	0.000036	a=0.9861, b=0.01873, k=0.30171, n= 1.23192
Midilli *et al.*	0.99952	0.00653	0.000043	a=1.00609, b=0.00176, k=0.30046, n=1.21507
Drying temperature =50°C				
Lewis	0.98991	0.02957	0.00087	k=0.41348
Page	0.99682	0.017	0.00029	k=0.33804, n=1.1824
Modified page	0.99682	0.017	0.00029	k=0.39967, n=1.18171
Henderson and Pabis	0.99388	0.02358	0.00055	a=1.0647, k=0.43761
Logarithmic	0.99412	0.02366	0.00056	a=1.06978, c=-0.01017, k=0.4242
Wangh and Singh	0.97629	0.04639	0.00215	a=-0.27867, b=0.01938
Diffusion approach	0.98991	0.03101	0.00096	a=1, b=1, k=0.41347
Demir *et al.*	0.99867	0.01154	0.00013	a=0.98733, b=0.02725, k=0.34553, n=1.25496
Midilli *et al.*	0.99841	0.01264	0.00016	a=1.01679, b=0.0027, k=0.34376, n=1.22346
Drying temperature =60°C				
Lewis	0.98031	0.04774	0.00228	k=0.5523
Page	0.99913	0.01054	0.00011	k=0.43185, n=0.43185
Modified page	0.99913	0.01054	0.00011	k=0.53197, n=1.33002
Henderson and Pabis	0.98604	0.04216	0.00178	a=1.06939, k=0.5875
Logarithmic	0.99245	0.03267	0.00107	a=1.13575, c=-0.08892, k=0.47854
Wangh and Singh	0.99443	0.02663	0.00071	a=-0.40722, b=0.04262
Diffusion approach	0.98031	0.05278	0.00279	a=1, b=1, k=0.5523
Demir *et al.*	0.99944	0.00947	0.000089	a=0.98974, b=0.01607, k=0.44204, n=1.36656
Midilli *et al.*	0.99939	0.00986	0.000097	a=1.00639, b=0.00251, k=0.43837, n=1.3528

Based on the range and average values of the statistical parameters for each model, it can be concluded that Demir *et al.* model, followed by Midilli *et al.* model, gives the best representation of the experimental data and was applied successfully to describe and predict the behavior of this variety of tomato paste in these conditions.

Generally, the coefficient of determination (R^2) and Root Mean Square Errors (RMSE) values of Demir *et al.* model varied from 0.99988 to 0.99993, and 0.0032 to 0.00649, respectively for dried tomato paste with 1.5 m s^{-1} air velocity, and from 0.999440 to 0.99959, and 0.00602 to 0.01154, respectively with 2.5 m s^{-1} air velocity, Tables (2.5-6).

***Table 2-5**: Statistical results of Demir et al. model with V = 1.5 m s^{-1}*

T (°C)	*a*	*b*	*k*	*n*	*R^2*	*RMSE*
45	0.96882	0.03132	0.24058	1.322	0.99946	0.00649
50	0.98401	0.01671	0.29334	1.32038	0.99988	0.0032
60	1.02164	0.02481	0.32827	1.34031	0.99993	0.00331

***Table 2-6**: Statistical results of Demir et al. model with V = 2.5 m s^{-1}*

T (°C)	*a*	*b*	*k*	*n*	*R^2*	*RMSE*
45	0.9861	0.01873	0.30171	1.23192	0.99959	0.00602
50	0.98733	0.02725	0.34553	1.25496	0.99867	0.01154
60	0.98974	0.01607	0.44204	1.36656	0.99944	0.00947

The constant values of Demir *et al*. model for different conditions were regressed against. Regression analysis for these parameters yielded the following relationships:

$$a = 0.99532 - 0.00008\,T + 0.0095533\,V - 0.008435\,T^2 - 0.00174\,T.V$$

$$b = 0.028065 + 0.0033\,T + 0.0026117\,V - 0.008357\,T^2 - 0.00197\,T.V$$

$$k = 0.284425 - 0.022035\,T + 0.032095\,V + 0.06123\,T^2 - 0.04813\,T.V$$

$$n = 1.33115 - 0.050015\,T + 0.0069083\,V - 0.0377\,T^2 - 0.017305\,T.V$$

2.3.3 Determination of effective moisture diffusivities

The ln (*MR*) versus time (h) for different level of air velocity and drying temperature is shown in Figures (2.10-11). For drying temperature of 45, 50, and 60°C, respectively. All the figures show that the drying of tomato paste occurred in falling rate period, in other words, the liquid diffusion is by the dry win force controlling the drying process (Samimi-Akhijahani and Arabhosseini, 2018). The plotted curves show that the increase in temperature and air velocity increases the slope of straight line, in other words the effective moisture diffusivity increases.

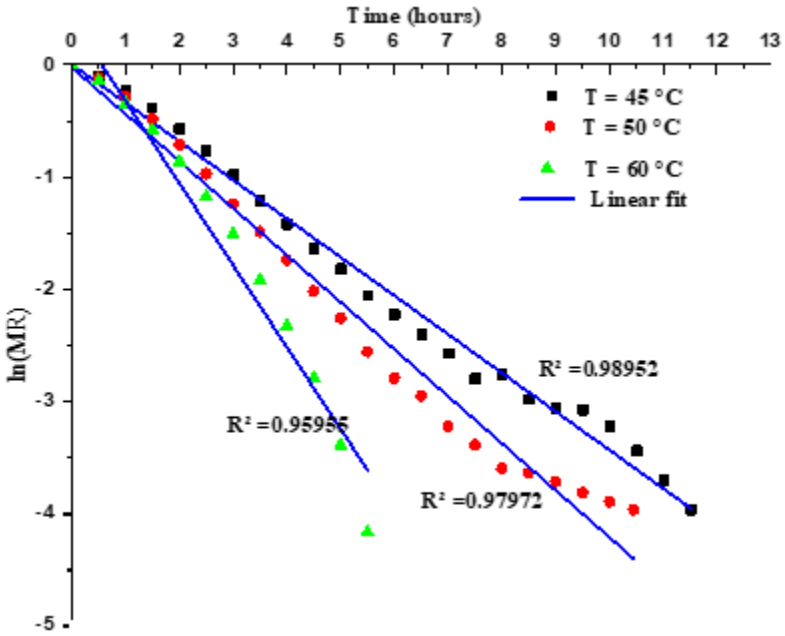

***Figure 2-10**: Effect of drying temperature on moisture diffusivity with V = 1.5 m s^{-1}*

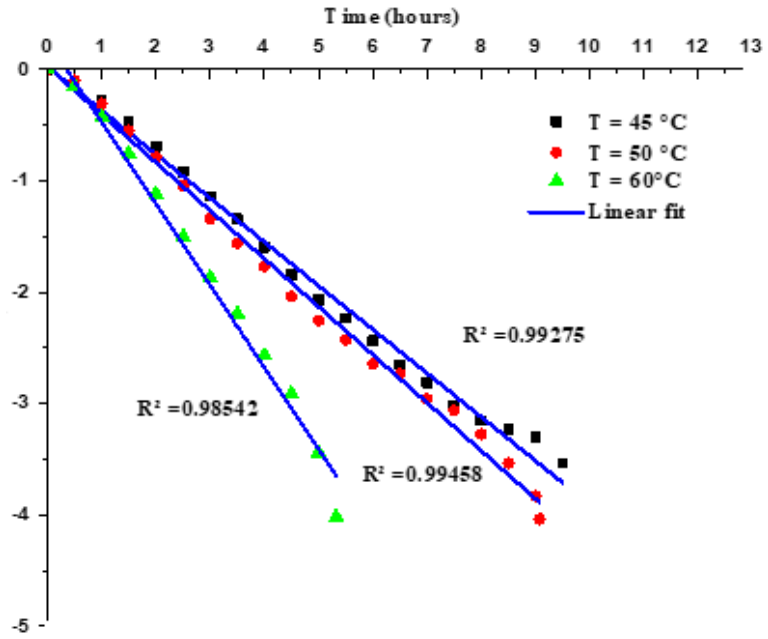

***Figure 2-11**: Effect of drying temperature on moisture diffusivity with V = 2.5 m s^{-1}*

Figure (2.12) presents the values of effective moisture diffusivities versus drying time for drying temperatures of 45, 50 and 60°C. Effective moisture diffusivities were found to be 2.18341 10^{-9}, 2.65319 10^{-9} and 4.62449 10^{-9} m² s^{-1}, respectively, for 1.5 m s^{-1} air velocity, and 2.49135 10^{-9}, 2.7334 10^{-9} and 4.65409 10^{-9} m² s^{-1}, respectively, for 2.5 m s^{-1} air velocity. It should be noticed that the drying air temperature has a higher effect on the moisture diffusivity. Lot of recent studies confirmed this result such us (Kipcak, 2018; Wang et al., 2018).

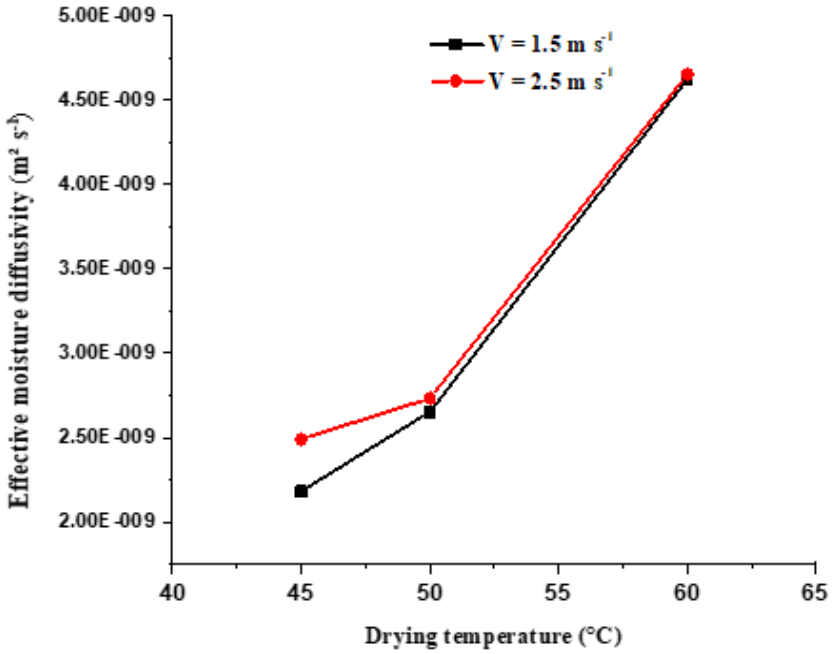

***Figure 2-12**: Effective moisture diffusivity at different drying temperatures*

2.3.4 Determination of activation energy

Figure (2.13) displays the ln D_{eff} vs 1/T for T = 45, 50 and 60 °C, respectively for air drying velocities 1.5 and 2.5 m s^{-1} respectively. According to the curves. It observed that increasing of air-drying velocity and drying temperature affect directly on the slope value, in other word, the activation energy. According the slopes of Figure (2.13), activation energies were found to be 44.836 and 38.159 kj/mol for air velocities 1.5 and 2.5 m s^{-1} respectively

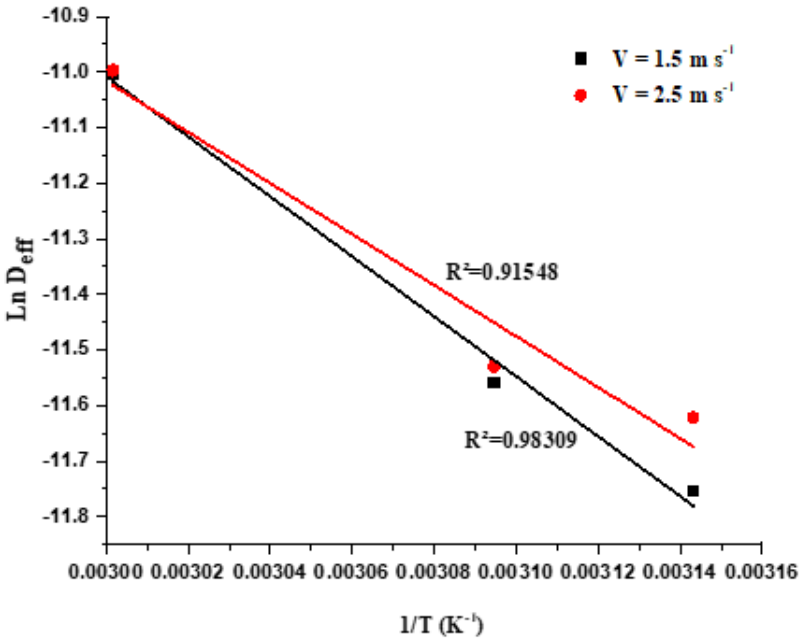

***Figure 2-13**: Effect of drying temperatures and air velocity on the activation energy*

Tables (2.7-8) show the activation energy and the pre-exponential factors of the Arrhenius equation for both drying temperatures with air drying velocities.

Observing that the activation energies decrease with the increasing of air-drying velocity. Increasing air-drying velocity reduces the external resistance at the surface which allows to increase the internal diffusion, decreases the internal resistance and interaction between the moistures inside the matrix.

***Table 2-7**: Activation energy and effective diffusivity coefficient of tomato paste à V = 1.5 m s^{-1}*

T °C	*Equation*	*E_a (KJ/mol)*
45	$D_{eff} = 0.0502 \exp\left(\frac{-5392}{T + 273.15}\right)$	44.839
50	$D_{eff} = 0.0469 \exp\left(\frac{-5392}{T + 273.15}\right)$	
60	$D_{eff} = 0.0496 \exp\left(\frac{-5392}{T + 273.15}\right)$	

***Table 2-8**: Activation energy and effective diffusivity coefficient of tomato paste à V = 2.5 m s^{-1}*

T °C	*Equation*	*E_a (KJ/mol)*
45	$D_{eff} = 0.046 \exp\left(\frac{-4598}{T + 273.15}\right)$	38.195
50	$D_{eff} = 0.004 \exp\left(\frac{-4589}{T + 273.15}\right)$	
60	$D_{eff} = 0.0045 \exp\left(\frac{-4589}{T + 273.15}\right)$	

2.4 Conclusion

The present chapter was carried out with the aim of valuing the surplus of local tomato production using hot air-drying methods. The tomato paste in the form of organic matter was invested. The drying tomato paste was then established using an automated laboratory drying loop (LETTM, El-Manar University of Tunis).

The effects of two drying parameters (air temperature, air velocity) on drying time and drying kinetics of dried tomato paste were investigated. They were conducted under air conditions as constant relative humidity of 16%, temperatures 45°C, 50°C, 60°C with airflow velocity of 1.5 and 2.5m s^{-1}. Obtained drying kinetics showed only falling periods and led to drying time ranged between 11.16 and 5.32 hours.

Evaluation of the suitable mathematical models, describing thin-layer drying behavior of

tomato paste with several drying conditions revealed that Demir *et al*. model was found the best fitted among nine investigated models, followed by Midilli *et al*. model.

The highest moisture diffusivities were 4.62449. 10^{-9} m^2 s^{-1} and 4.65409. 10^{-9} m^2 s^{-1} for the highest air-drying temperature 60°C, for both air velocities, respectively.

Finally, the activation energies were found to be 44.836 and 38.159 kJ/mol for air velocities 1.5 and 2.5 m s^{-1} respectively.

This chapter is valorised as a research paper entitled “Experimental investigation and mathematical modeling of hot air convective drying of tomato paste under near solar drying operating conditions”, (Tarik et al., 2020).

3 Kinetics and Economic Analysis of Hybrid Solar Drying of Tomato Paste

3.1 Introduction

Several experimental investigations have been performed in the past to evaluate the performances and economic analysis of numerous hybrid-drying systems such as studied by (Agarwal and Sarviya, 2016; Amer et al., 2010; Azaizia et al., 2020; Baniasadi et al., 2017; Ghasemkhani et al., 2016; Nabnean et al., 2016; Nayak et al., 2012; Prakash and Kumar, 2014; Shalaby and Bek, 2014; Singh Chauhan et al., 2018; Singh et al., 2006).

As per the literature review, no research exists on the effectiveness and economic feasibility of using geothermal water as a supplementary heating system in the food drying sector. Tomato paste was used in these experiments. The drying time, effective moisture diffusivity, and texture of the final dried tomato paste were compared using direct solar drying with and without geothermal water energy source. Additionally, the techno-economic feasibility of the drying systems was investigated using three methods, namely: (i) annualized cost method, (ii) life cycle saving method, and (iii) payback period method. The value of net present value and benefit-cost ratio was also determined.

3.2 Materials and methods

3.2.1 Experimental set-up

Drying experiments were performed simultaneously with two similar direct solar dryers with and without a geothermal water heat exchanger (GWHE). The systems were constructed at the Laboratory of New and Renewable Energy Development in Arid and Saharan Zones, LENERZA, Faculty of Mathematics and Material Sciences, University of Kasdi Merbah Ouargla, Ouargla 30000, Algeria. Experiments were conducted between January 3rd and 5th 2019 from 9:30 to 16:30. The dryer with GWHE is turned on even in the presence of sunlight, after sunset, and at night. Geothermal water of about 67°C temperature was pumped inside the heat exchanger using an electric pump. The dryer was insulated with polystyrene of 2 cm thickness to reduce the thermal losses to the outside during off sunshine hours started at 16:30 and whole night time. The experiments were stopped on the third day at 11:30 when the samples dried reached the desired moisture content level. A representative system of GWHE is replaced by a heat pump dryer in this thesis.

3.2.2 Description of the dryer

The conventional/basic dryer was designed by (Mennouche et al., 2014). It mainly consists of an inclined drying chamber at an angle of 31.9° (Latitude of Ouargla city) with a base painted in black to improve sunlight absorption and connected to a galvanized chimney to exhaust moist air. The lower sides of the drying chamber were made of galvanized sheets insulated with a

polystyrene medium. The schematic diagram of the drying system with geothermal water heat exchanger and the picture of dryers and GWHE are shown in Figures (3.1-2). The hybrid dryer was covered with an insulating material to reduce heat loss after sunset and at night. Ambient air enters the drying chamber and is heated when it comes in contact with GWHE and the absorbent. Hot air passes through the product, carries moisture on its surface, and is exhausted outside through the chimney. Moreover, the geometric dimensions of the basic solar dryer are given in Table 2.

***Figure 3-1**: Emplacement of the heat exchanger inside the drying chamber*

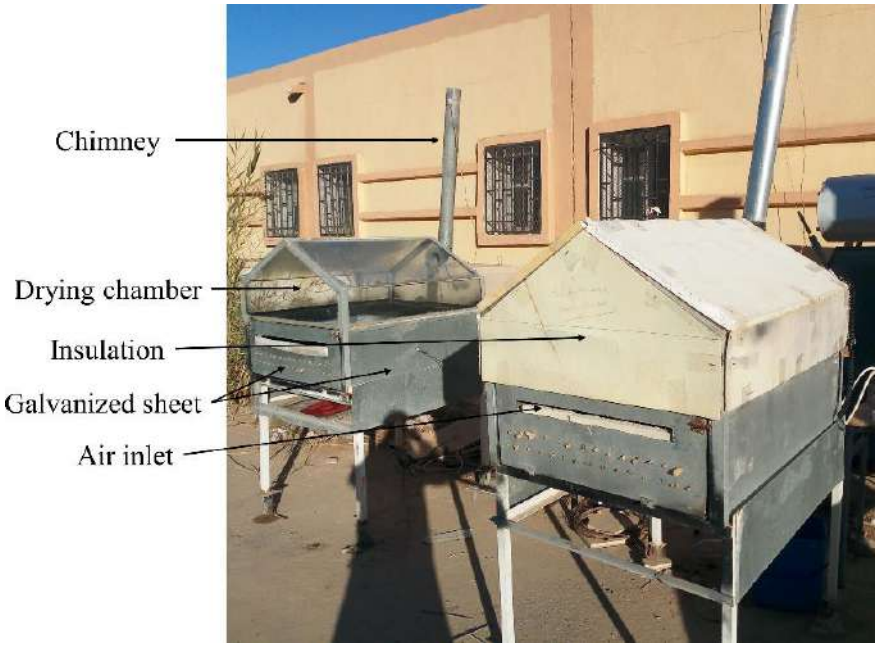

***Figure 3-2**: Picture of the direct solar dryers*

The geometric dimensions of the basic solar dryer are given in Table (3-1).

***Table 3-1**: Dimensions of the dryer components*

Signification	*Values (m)*
Length of the drying chamber	1.0
Width of the drying chamber	0.8
Galvanized metal sheets insulated thickness	0.05
Glass covers thickness	0.004
Absorber thickness	0.01
Air inlet	0.015
Chimney diameter	0.1
Chimney length	1.0

3.2.3 Heat exchanger

The geothermal water heat exchanger used in the experiments is designed and described as:

- Providing a copper tube of 25 m length and 12 mm of diameter;
- The copper tube was cut into 24 tube pieces with 85 cm of length;
- The 24 tube pieces were assembled in two floors with a distance of 5 cm between the floors, and each floor contains 12 parallel tube pieces;
- The tube pieces were arranged with 5 cm distance between each other;
- The whole of the tube pieces is welded with each other to have the shape of a tubular heat exchanger.

The geothermal water heat exchanger is placed inside the drying chamber, 5 cm above the base of the chamber. It covers the entire area of the drying chamber. Later, it was painted black and served the role of extra absorbent. The exchanger improved heat and mass transfer by increasing the drying temperature on the one hand and making the drying temperature suitable for drying of food during the night or cloudy days. Heat exchanger receives the hot water from the ground at a temperature of 67°C with flow rate of 0.05 L/s. Hot water supplies the heat through the heat exchanger to drying air inside drying chamber. The average outlet temperature of the heat exchanger was recorded at 63°C, and it can be used for recycling system or other thermal systems such as distillation. On the other hand, decreasing inlet dry air temperature led to increased heat exchange between the heat exchanger and drying air, so the outlet temperature decreased to an average value of 45 °C to maintain drying air temperature suitable for drying tomato paste at night.

3.2.4 Experimental measurement

Calibrated k-type sensors are used to record all temperatures every 15 minutes using the data acquisition system (NIcDAQ -9174). This acquisition displays the measurement results of the measurement by "LabVIEW NXG" software. Solar irradiation was recorded by a Solar Mac pyranometer in a range of 0-1000 W/m². Tomato paste mass was measured every 60 min using an electronic balance of 10 kg capacity with an accuracy of 0.01 kg.

3.2.5 Sample preparation

Twenty kilograms of fresh tomatoes (L. esculentum) were purchased from a local market in Ouargla city, southern Algeria. Tomatoes were washed properly with running water to remove dirt and cut into small pieces. These were ground in a kitchen mixer and separated into a whole series of sieves of different sizes to remove the skin and the seeds from the paste. Finally, the paste was drained in a tissue bag to obtain 2 kilograms of tomato paste and 15 liters of tomato juice. The tomato paste was wrapped in plastic bags and stored at 4°C.

3.2.6 Moisture content and Moisture ratio

The initial moisture content was measured by a moisture analyzer (IR 35, accuracy ± 0.001). A thin layer of tomato paste of 3g was placed inside the analyzer at temperature (105°C). The analyzer turns off automatically when the tomato paste sample weight becomes stable. Moisture content (*M*) dry basis (kg water/kg dry matter) is considered throughout this work. Moisture content and moisture ratio (*MR*) are calculated using the following mathematical relations (Midilli and Kucuk, 2003; Yaldiz et al., 2001):

$$M_t = \frac{m_t - m_d}{m_d} \qquad \text{(Eq. 3.1)}$$

$$MR = \frac{M_t - M_e}{M_0 - M_e} \qquad \text{(Eq. 3.2)}$$

However, *MR* is simplified to M_t/M_0 because M_e is very small compared to M_t and M_0 (Midilli and Kucuk, 2003; Yaldiz et al., 2001).

3.2.7 Effective moisture diffusivity

The effective moisture diffusivity (D_{eff}) is an essential transport characteristic of the food product. Determining D_{eff} is necessary to predict the mass of moisture transfers from the core of the product to its surface. It is defined by Fick's second law (Crank, 1979):

$$\frac{\partial}{\partial t}\left(\frac{M_t - M_e}{M_0 - M_e}\right) = \nabla\left[D_{eff}\nabla\left(\frac{M_t - M_e}{M_0 - M_e}\right)\right] = D_{eff}\nabla^2\left(\frac{M_t - M_e}{M_0 - M_e}\right) \quad \text{(Eq. 3.3)}$$

D_{eff} (in $m^2\ s^{-1}$) is affected by drying air temperature, moisture content, and the retraction of the product. Considering, the drying process occurred without external resistance, that neglected instant shrinkage, and constant drying temperature and diffusion coefficient (Koukouch et al., 2017), for an infinite plate. D_{eff} is developed and calculated by Crank (1979):

$$\frac{M_t - M_e}{M_0 - M_e} = \frac{8}{\pi^2}\sum_{n=1}^{\infty}\frac{\exp\left(-(2n+1)^2\pi^2\frac{D_{eff}.t}{4L^2}\right)}{(2n+1)^2} \quad \text{(Eq. 3.4)}$$

For a long drying period, Equation (3.4) becomes:

$$\frac{M_t - M_e}{M_0 - M_e} = \frac{8}{\pi^2}\exp\left(-\pi^2\frac{D_{eff}.t}{4L^2}\right) \quad \text{(Eq. 3.5)}$$

D_{eff} can be calculated using the slope method. Thus, Equation (3.5) becomes:

$$\ln\left(\frac{M_t - M_e}{M_0 - M_e}\right) = \ln\left(\frac{8}{\pi^2}\right) - \left(\pi^2\frac{D_{eff}.t}{4L^2}\right) \quad \text{(Eq. 3.6)}$$

D_{eff} can be deduced from the slope of natural logarithmic of moisture ratio against drying time by plotting the experimental points using Equation (3.6):

$$Slope = \frac{\pi^2 D_{eff}.t}{4L^2} \quad \text{(Eq. 3.7)}$$

Or, $k = \left[\ln(MR) - \ln\left(\frac{8}{\pi^2}\right)\right]/t$ which fits the experimental data $\ln(MR)$ against drying time.

3.2.8 Economic analysis

The following methods have performed the techno-economic analysis of the hybrid and basic dryers with 15 years of a lifetime:

- The annualized cost method;
- The life cycle savings;

- The payback period.

The net present value and benefit-cost ratio were also determined.

3.2.8.1 Annualized cost method

The total cost of drying the crop is calculated using traditional energy resources and comparing it to the cost of solar drying. The annual cost of the dryer is determined using the annual cost method. The annual cost is divided by the total annual quantity of dried product to calculate the drying cost per unit mass of the dried product (Singh et al., 2006).

3.2.8.1.1 Annualized cost

Annualized cost (*AC*) is the annual cost of maintaining, operating, and sustaining an asset throughout its life. The annual cost of the dryer is determined from Equation (3.8):

$$AC = C_{acc} + C_{mc} - S_a + C_{rfc} + C_{rec} \quad \text{(Eq. 3.8)}$$

Annualized capital cost (C_{acc}) and Annualized salvage (S_a) are determined as follow:

$$C_{acc} = C_{ccd} \times CRF \quad \text{(Eq. 3.9)}$$

$$S_a = S \times SFF \quad \text{(Eq. 3.10)}$$

Where CRF and SFF are capital recovery factor and salvage fund factor, respectively, and calculated from Equations (3.11-12):

$$CRF = \frac{i(1+i)^n}{(r+i)^n - 1} \quad \text{(Eq. 3.11)}$$

$$SFF = \frac{i}{(1+i)^n - 1} \quad \text{(Eq. 3.12)}$$

The cost of drying per kg of dried product is calculated by Equation (3.13):

$$CD_{kg} = \frac{AC}{M_{year}} \quad \text{(Eq. 3.13)}$$

For solar dryers, the annual dried amount of the product, M_{year} is calculated using Equation (3.14):

$$M_{year} = \frac{M_{dry} D_{year}}{D_b} \quad \text{(Eq. 3.14)}$$

Where: D_{year} and D_b are number of days of use of domestic dryer per year and number of drying days per batch, respectively.

3.2.8.2 Life cycle savings

First savings for each day of drying in the reference year are needed to calculate. Then, the current value of the annual savings is calculated over the solar dryer's life (Duffie and Beckman, 1991).

3.2.8.2.1 Saving per drying day

The cost of the primary product intended for solar drying per kilogram of dried product recovered from the dryer is determined using Equation (3.15).

$$C_{dry} = C_{fre} \times \frac{M_{fre}}{M_{dry}} \quad \text{(Eq. 3.15)}$$

The cost per kg of dried product for the solar dryer (C_{drys}) is defined as the sum of the cost of the product before drying (C_{dry}) and the cost of drying (CD_{kg}) per kilogram of the dried product (Singh et al., 2006):

$$C_{drys} = C_{dry} + CD_{kg} \quad \text{(Eq. 3.16)}$$

The saving per kilogram of the obtained dried product (B_{kg}) in the reference year when using the solar dryer is calculated from Equation (3.17). Savings per tray (B_b) and savings per drying day (B_d) are given in Equations (3.18-19), respectively (Singh et al., 2006):

$$B_{kg} = C_{bdp} - C_{drys} \quad \text{(Eq. 3.17)}$$

$$B_b = B_{kg} \times M_{dry} \quad \text{(Eq. 3.18)}$$

$$B_d = \frac{B_b}{D_b} \quad \text{(Eq. 3.19)}$$

3.2.8.2.2 The present worth of annual savings

Throughout the dryer life, the annual savings (B_j) are obtained to dry the product in a determined year (jth) by Equation (3.20). The present value (P_{was}) is obtained from annual savings values in a jth year using Equation (3.21), (Singh et al., 2006):

$$B_j = B_d \times D_{year} \times (1+r)^{j-1} \quad \text{(Eq. 3.20)}$$

$$P_{was} = F_{pwf} \times B_j \quad \text{(Eq. 3.21)}$$

The present worth factor for a determined year *j*th year is given by Equation (3.22), (Singh et al., 2006):

$$F_{pwf} = \frac{1}{(1+i)^j} \quad \text{(Eq. 3.22)}$$

Life cycle saving = The present worth of annual savings through the solar dryer's life.

3.2.8.3 Payback period (N)

The payback period (*N*) is the time corresponding to recover the primary investment for the drying system. *N* is calculated by dividing the primary investment by the annual cash cost. It is calculated from Equation (3.23):

$$N = \frac{\ln\left(1 - \frac{C_{ccd}}{B_1}(i-r)\right)}{\ln\left(\frac{1+r}{1+i}\right)} \quad \text{(Eq. 3.23)}$$

3.2.8.4 Net present value (NPV)

The purpose of the NPV calculation is to compare the value of future benefits with the initial investment cost and consider an appropriate rate of interest. When the initial investment cost is more than the present value of the benefits, the investment project study should be ignored. Even if the theoretical life of the project is different, the effectiveness of the project by improving the life of those investments can be compared to the lifetime of other investment projects (Selvanayaki and Sampathkumar, 2017). The mathematical relationship can be determined by knowing the total present value of all cash profits as a result of the investment project as in Equation (3.24):

$$NPV = \sum_{t=1}^{t=n} \frac{B_t - C_t}{(1+i)^t} \quad \text{(Eq. 3.24)}$$

Where B_t: Annual benefit (DZD), C_t: salvage value or annual cost (DZD), = 1, 2,3... *n* and *i*= discount rate (%)

3.2.8.5 Benefit-Cost Ratio (BCR)

BCR is a prerequisite for accepting of the investment. It is calculated by determining the present value of the total benefit minus the related cost and then allocating it to the present value

of the cost of the investment project (Selvanayaki and Sampathkumar, 2017). The total cost of the investment project can be determined by calculating the costs of labour, ongoing maintenance, and site change costs. *BCR* can be found by using Equation (3.25):

$$BCR = \frac{\sum_{t=1}^{t=n} \frac{B_t}{(1+i)^t}}{\sum_{t=1}^{t=n} \frac{C_t}{(1+i)^t}} \quad \text{(Eq. 3.25)}$$

3.3 Result and discussion

3.3.1 Solar radiation

Solar radiation variation with time during experiments is shown in Figure (3.3). The solar radiation data were recorded every 60 min (1h). The highest solar radiation values recorded were 869 and 982 W/m^2 at 13:30 in the first and second day and 938 W/m^2 on the third day; respectively.

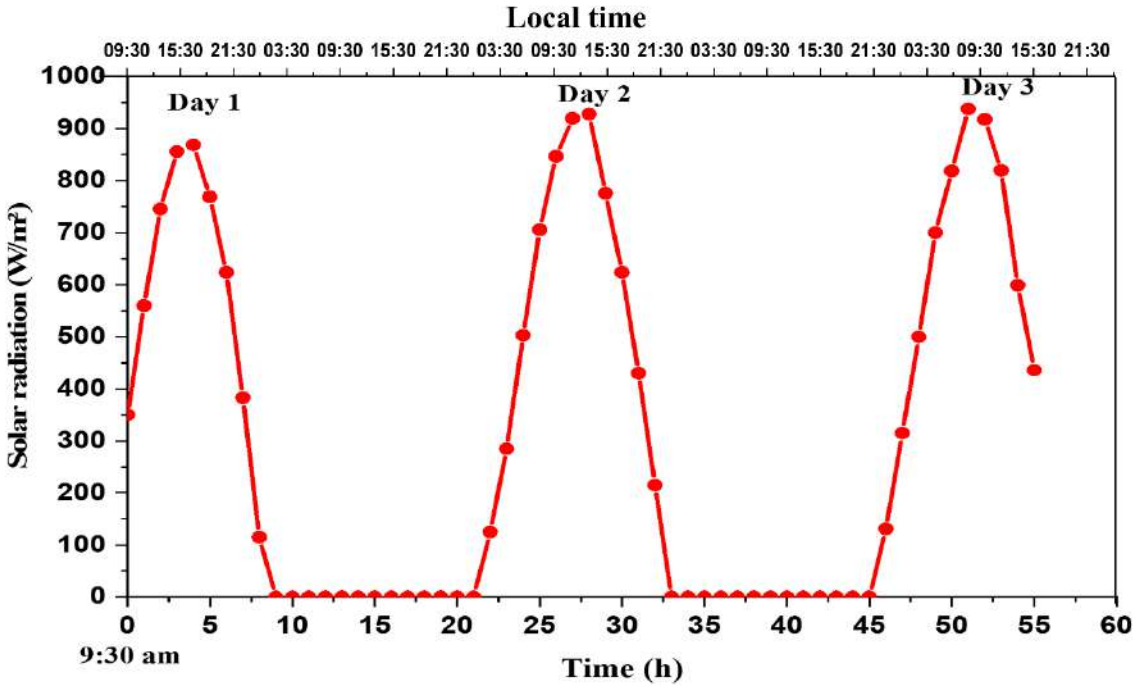

Figure 3-3 *Solar radiation versus local time*

3.3.2 Ambient and drying temperatures

Temperature measurement with respect to local time during three days of experiments is shown in Figure (3.4). The temperatures were recorded every 30 min. There was a clear fluctuation in ambient temperature on the first day, with a maximum value of 23.05°C after 3.5 h (at 13:00). Whereas, it was 20.15 and 18.08°C after 4 and 2 h (at 14:00 and 11:30) in the second and third day, respectively. The ambient temperature in the absence of solar radiation at the location of experiments started from 16:30, revealed a decreasing from 17.76 °C after 7.5 h (at 17:00) to

4.96°C after 21.5 h (at 07:00), whereas it was 5.87°C at the end of the continuous process after 22 h (at 07:30).

The drying air temperature in both solar dryers is also represented in Figure (3.4). The drying air temperature was 53.41°C after 4 h and 35.75°C after 22 h for the solar dryer provided with GWHE. Whereas, drying air temperature without GWHE increased every day with increasing of solar radiation and reached the maximum values of 41.07°C, 41.95°C, and 41.89°C after 4.5, 5, and 2 h (at 14:00; 14:30 and 11:30) in the first, second and third day respectively, from the experiments. The maximum drying air temperature difference 11.5°C recorded between solar dryer with GWHE and without GWHE during the daytime. The continuous drying process was observed in the solar dryer with GWHE because of covering it with polystyrene insulation from 17:00 to 07:30 which creates a significant difference in drying and ambient temperature (30.8° C). It is considered as an important finding. Results revealed an improvement in the performance of the solar dryer integrated GWHE. A similar result was found by Sandali et al., (2018) who improved the thermal performance of a direct solar dryer by integrating a sensible heat storage medium. However, only an increase of 4°C in drying temperature was noticed. The GWHE maintains the suitable drying air temperature for continuing the drying after sunset. 45°C of drying air temperature was recorded when using an air heater as a supplementary thermal energy source (Misha et al., 2015; Sharma and Sharma, 2012). It should be noted that the lowest drying temperature of 35.75°C is always suitable for drying tomato paste overnight.

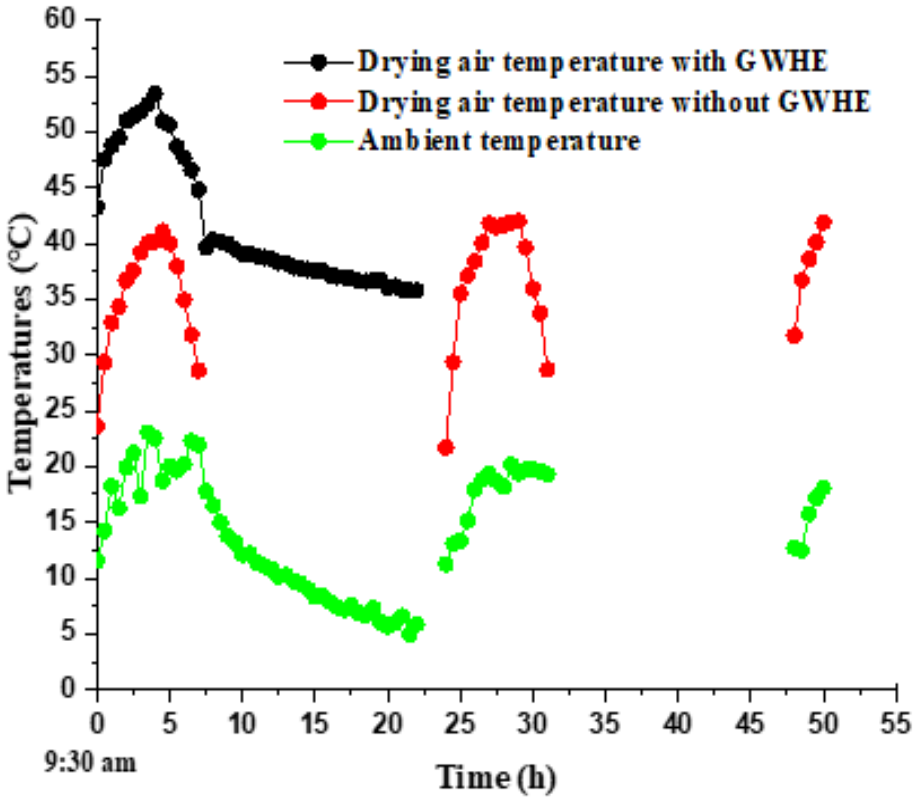

Figure 3-4 *Variation of temperatures with drying time*

3.3.3 Moisture content of tomato paste

Moisture removal is the ability of dry air to vaporize the water content of a substance. The initial moisture content of tomato paste was found to be 5.67% (d.b) as shown in Figure (3.5). Dried tomato paste reached the desired moisture level of 0.08 (d.b) in 22 consecutive hours using continuous solar dryer with GWHE, while it took 18 hours through three days from 09:30 to 16:30 using discontinuous solar dryer without GWHE. Samples dried without GWHE showed a slight variation in mass at the beginning of the second and third days of the experiment due to the absorption of moisture during off sunshine hours. The drying process occurred on the falling rate period for samples with a neglected air-surface interaction. The final moisture content 0.08% (d.b) was low enough to preserve the dried product from any losses such as microbial contamination...etc, with good appearance. On the other dried product obtained without GWHE was observed with the adverse smell. This was due to the long drying time. The hybrid system ensures that the drying process continues during the night and even during times when sunlight is reduced by clouds or flying desert sands caused by the light sandstorms. Otherwise, the effect of additional heating on the final texture of dried tomato paste is presented in Figure (3.6). The continuous drying process leads to a lower shrinkage of the final texture than the solar drying without GWHE. This result can be explained by the time the tomato paste was exposed to the solar radiation, while it was one and three days for drying with and without GWHE, respectively.

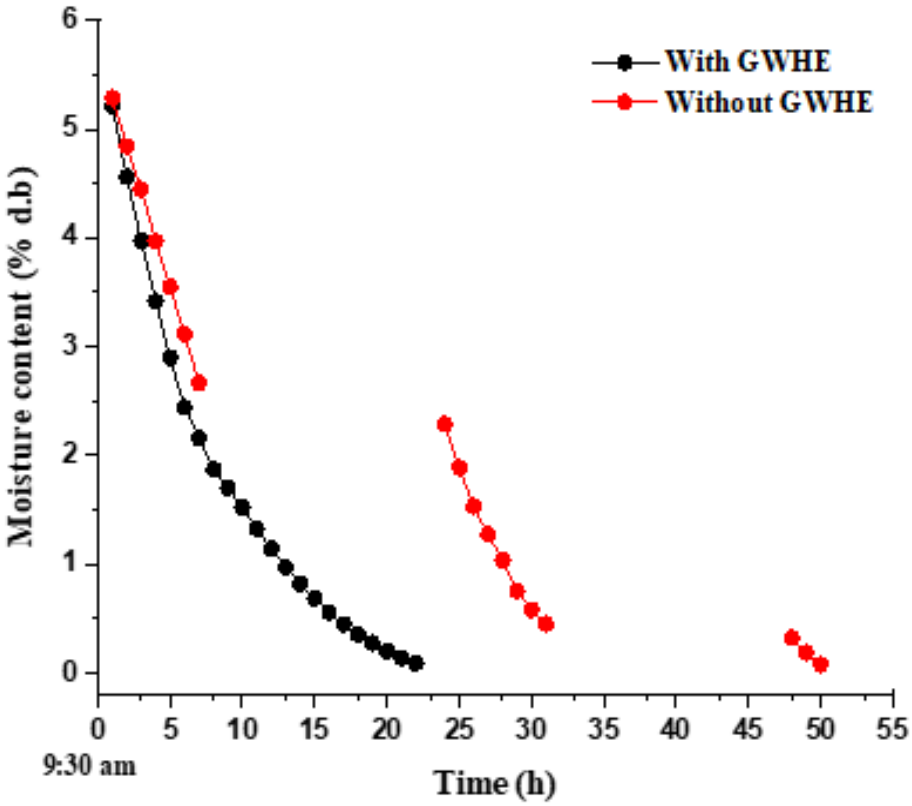

Figure 3-5 *Variation of moisture content with drying time with and without GWHE*

Figure 3-6*: Pictures of tomato paste: a) fresh tomato paste, b) tomato paste dried with GWHE and c) tomato paste dried without GWHE*

3.3.4 Drying rate

The evolution of drying rate in (kg water/kg dry matter; d.b. h) versus drying time is presented in Figure (3.7). The plot of drying rate against time allows predicting the drying periods of the process. In our case, it is clear the presence of two drying periods for drying without GWHE, the first phase took about one hour is considered as warming up of the product before starting the diffusion process, and the second phase is considered as diffusional. Otherwise, the curve of drying

with GWHE displays the presence of the second period only, so, the process is considered totally diffusional. As a result, the hybrid dryer provided with the heating system improved the drying process by eliminating the first drying period which takes about one hour for the basic dryer. The highest and lowest drying rate of tomato paste samples, respectively i.e. 1.46 gr/h after one hour and 1.03 gr/h after 5 hours, with an improvement of 30%. After 5 hours, the increase of solar radiation and decreasing of moisture inside the product affect directly on the drying rate. Similar results are obtained by (Kouchakzadeh, 2013), they found that the drying rate is enhanced by 50% using a hybrid system provided with an energy storage system.

Figure (3.8) displays the evolution of drying rate versus moisture content. The drying rate increase with the increase of moisture in the product, unlike the basic dryer, the drying rate in the hybrid system increased in regular form. Consequently, the heating system of the hybrid dryer leads to a rise in the drying temperature, as well as, accelerates the drying process by increase the diffusion rate of water from the core of the product to the surface.

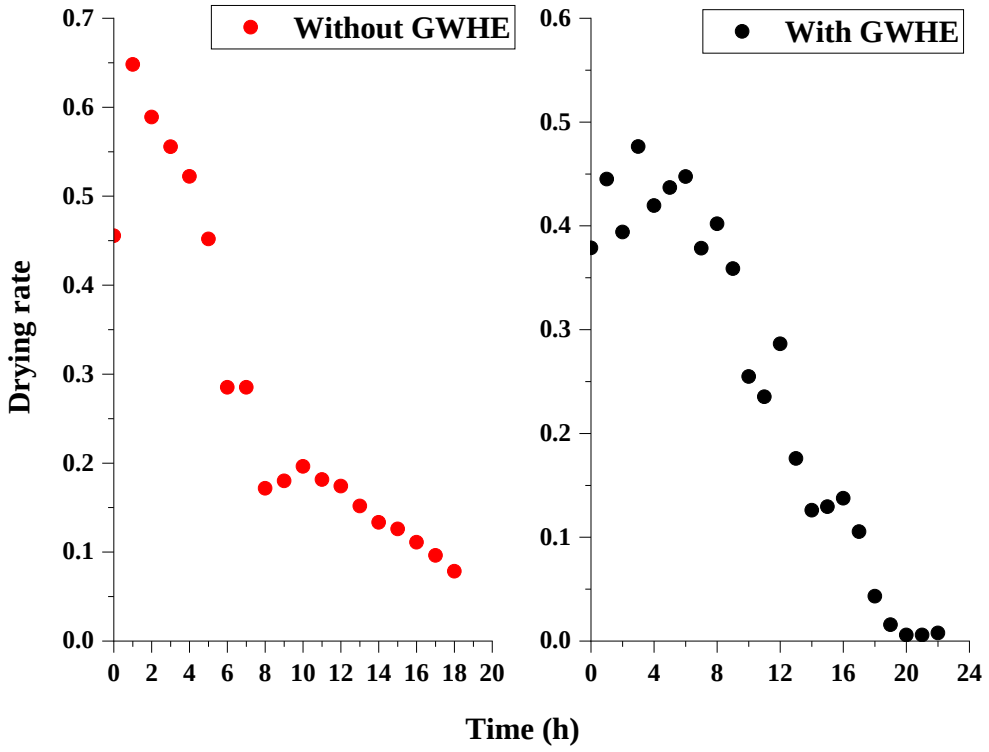

***Figure 3-7**: Drying rate Vs drying time*

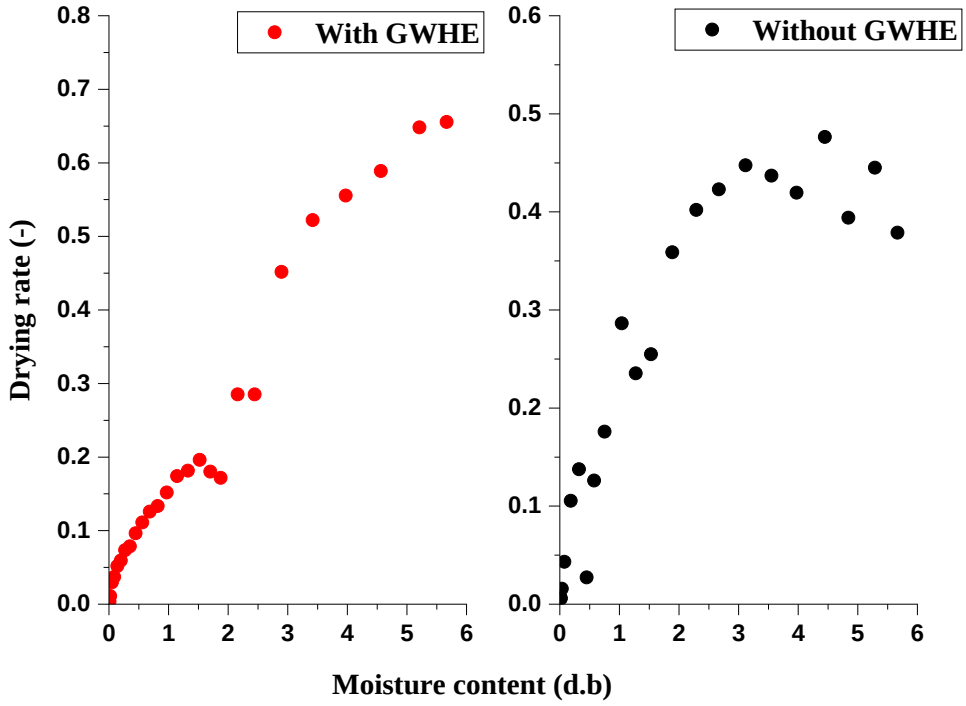

***Figure 3-8**: Drying rate Vs moisture content*

3.3.5 Determination of effective moisture diffusivity

A comparison of internal diffusion of tomato paste during solar drying with and without the usage of geothermal energy on the first day of the experiment was investigated. As described in Equations. (3.6) and (3.7), effective moisture diffusivity is determined by plotting empirical drying data in terms of ln (*MR*) against drying time. The natural logarithm of moisture ratio values "ln (*MR*)" are plotted against drying time "(t)" for different drying processes on the first day of the experiments. The linearity of the relationship between ln (*MR*) and drying time (t) with R^2 and slopes values are also illustrated in Figure (3.9). The value of R^2 is higher for drying processes inside a solar dryer with GWHE as compared to without GWHE. The instant moisture diffusivities between two points were also determined with an average value.

The effective moisture diffusivities were calculated by neglecting the air-surface interaction. The average values of effective moisture diffusivities were found to be 8.05×10^{-10} and 5.39×10^{-10} for samples dried with and without GWHE, respectively. The instant D_{eff} was found lower than the ones calculated with the slopes method which is a similar remark given by Badaoui et al., (2019). An increase in the effective moisture diffusivity was observed in solar drying with GWHE compared to the other process. D_{eff} increased from 1.202×10^{-9} m^2 s^{-1} to 1.617×10^{-9} m^2 s^{-1} due to increasing of drying air temperature over-drying process when using the geothermal energy as a supplementary thermal energy source. The values of D_{eff} validated with

the results obtained by Karathanos et al., (1990) and Sharma and Prasad (2004) for food. Indeed, the D_{eff} of food products varied between 10^{-12} and 10^{-8} ($m^2\ s^{-1}$), (Benhamou et al., 2008).

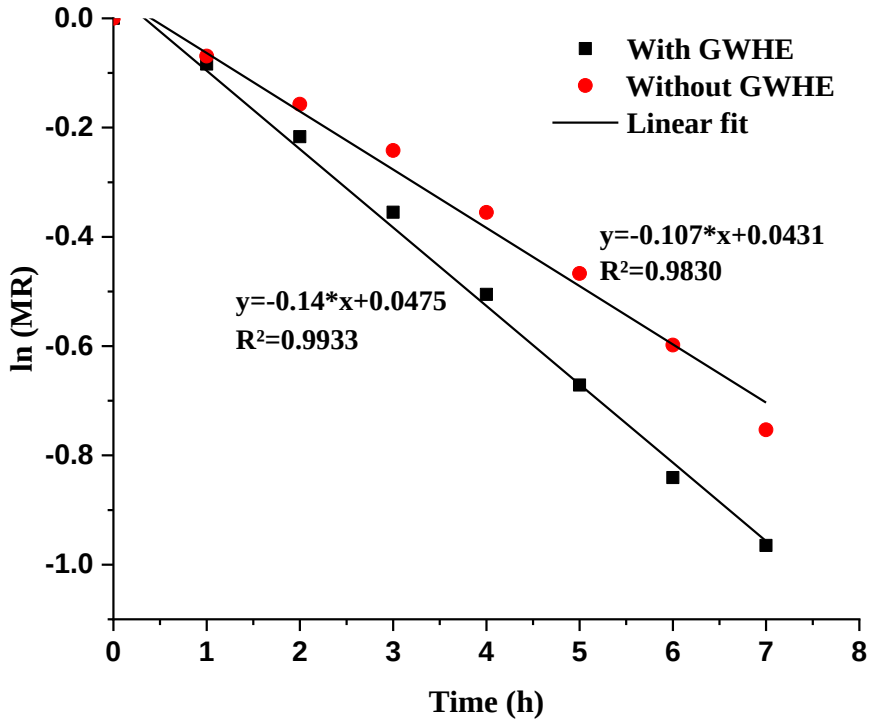

Figure 3-9 *ln (MR) versus drying time for the first day with and without GWHE*

3.3.6 Economic analysis

The techno-economic analysis of the developed system was done through the three methods namely: (i) annualized cost, (ii) life cycle, and (iii) payback time. The inflation rate and interest rate had taken as 8% and 3%, respectively. It should be noted that the electrical energy is used to operate the pump only since the water is hot at 67 °C come from the ground, and its value is calculated as 2634.66 DZD. The cost with economic parameters of both hybrid and basic dryers is given in Table (3- 2), where 1 USD equivalent to 128.41 DZD in 2020.

Table 3-2 *Cost and economic parameters of hybrid solar and basic solar dryers*

Parameter	*Solar dryer with GWHE*	*Solar dryer without GWHE*	*Unit*
Assumed dryer life	15	15	Year
Construction cost of the solar dryer	60000	45000	DZD
Cost of fresh tomato	20	20	DZD/kg
Electricity consumption cost	2634.66	0	DZD/kWh
Price of dried tomato paste	200	200	DZD

3.3.6.1 Annualized cost

The cost of maintaining the systems every year has been estimated to be 2% of the (C_{acc}). The salvage value has been considered to be 10% of the annual cost. The annual cost was estimated to be 9758.8 and 7977.7 DZD for a solar dryer with and without GWHE, respectively. Since the experiments were conducted at southern Algeria with abundant solar radiation round the year and geothermal energy, therefore the number of drying days were considered to be 365 days.

3.3.6.2 Life cycle savings

The daily saving is calculated as 82.3 and 18.7 DZD/day for a solar dryer with and without GWHE, respectively. The amount of cumulative present worth of yearly savings (P_{ws}) for drying tomato paste were 305922.4 and 69445.18 DZD, therefore incensement of 9758.81 DZD will save 305922.4 and 69445.18 DZD during the life span of hybrid and basic dryers respectively. The results of the economic analysis are summarized in Table (3-3).

Table 3-3 *Annual economic analysis during the life of the solar dryers with and without GWHE for drying of tomato paste*

Mode	*Solar drying with GWHE*				*Solar drying Without GWHE*			
year (j)	B_j	F_{pwf}	P_{was}	P_{ws}	*Bj*	F_{pwf}	P_{was}	P_{ws}
1	30059.37	0.925926	27832.75	9398.405	6823.55	0.925926	6318.1	27832.75
2	30961.15	0.857339	26544.2	54376.95	7028.26	0.857339	6025.6	12343.71
3	31889.99	0.793832	25315.3	79692.25	7239.1	0.793832	5746.63	18090.35
4	32846.69	0.73503	24143.29	103835.5	7456.28	0.73503	5480.59	23570.94
5	33832.09	0.680583	23025.55	126861.1	7679.97	0.680583	5226.86	28797.79
6	34847.05	0.63017	21959.55	148820.6	7910.37	0.63017	4984.87	33782.67
7	35892.46	0.58349	20942.91	169763.5	8147.681	0.58349	4754.094	38536.76
8	36969.23	0.540269	19973.33	189736.9	8392.111	0.540269	4533.997	43070.76
9	38078.31	0.500249	19048.64	208785.5	8643.875	0.500249	4324.089	47394.85
10	39220.66	0.463193	18166.75	226952.3	8903.191	0.463193	4123.9	51518.75
11	40397.28	0.428883	17325.7	244278	9170.287	0.428883	3932.979	55451.73
12	41609.2	0.397114	16523.59	260801.6	9445.395	0.397114	3750.896	59202.62
13	42857.47	0.367698	15758.6	276560.2	9728.757	0.367698	3577.244	62779.87
14	44143.2	0.340461	15029.04	291589.2	10020.62	0.340461	3411.631	66191.5
15	45467.5	0.315242	14333.25	305922.4	**10321.24**	0.315242	3253.685	69445.18

3.3.6.3 Payback period

The payback period (*N*) for tomato paste drying has been estimated to be 2.21 years (equal to 807 days). Similarly, for the basic dryer (*N*) is 8.44 years (equal to 3081 days). It is noticed that *N* of the hybrid dryer for a dryer life of 15 years is acceptable as compared with the basic dryer. Therefore, it's recommended to use the hybrid solar dryer with GWHE.

3.3.6.4 Net present worth (NPV)

The *NPV* is the amount between the present worth of savings and the cost of investment. It is observed that the *NPV* is found to be 64945.2 and 299922.5 DZD for basic and hybrid dryers, respectively, with an increase of 462%. Hence, the hybrid dryer with a life cycle of 15 years is recommended.

3.3.6.5 Benefit-cost ratio (BCR)

The benefit-cost ratios are calculated using Equation (3.25). The (*BCR*) are found to be 15.43 and 50.98 for a direct solar dryer with and without GWHE, respectively.

3.4 Conclusion

An experimental investigation and economic analysis of tomato paste drying inside a direct solar dryer with and without GWHE were done. The drying time and various economic parameters of the tomato paste thin layer were investigated. The finding is concluded as:

- The highest and lowest drying temperature was observed at 53.4 °C and 35.75 °C for a solar dryer with GWHE, while for the basic dryer were 41.95 °C and 17.76 °C, respectively.
- solar dryer integrated with GWHE ensures a salient difference between drying temperature and ambient temperature after sunset and at night reached 30.8 °C.
- The hybrid solar dryer provided with GWHE took 22 consecutive hours (day + night), while, the basic dryer without GWHE took 18 hours (day) through three days to reach desired moisture content 0.08 (d.b). Long time exposure means possibilities of deterioration.
- The hybrid dryer increases the effective moisture diffusivity from 1.202×10^{-9} to 1.617×10^{-9} m^2 s^{-1}.
- The cumulative present worth value (P_{ws}) of yearly savings for tomato paste drying was found to be 305922.4 and 69445.18 DZD for basic and hybrid dryer respectively.
- The payback period of the hybrid dryer with 2.21 years (807 days) is recommended for the drying of tomato paste.

- The net present values were 64945.2 and 299922.5 DZD, whereas, the benefit-cost ratio was 15.43 and 50.98 for basic and hybrid dryer respectively.
- Lower shrinkage of the final produce for drying with GWHE than the solar drying without GWHE. This result can be explained by the time that tomato paste was exposed to the solar radiation, while it was one and three days for drying with and without GWHE, respectively.

In conclusion, the hybrid system with GWHE ensures the drying operation after sunset, during nighttime, cloudy days, and reduced drying time. Otherwise, the economic analysis of both systems encourages investment with the hybrid dryer.

4 Modeling and Development of Characteristic Curve for Tomato Paste Drying

4.1 Introduction

Today, in light of increasing demand for agricultural products outside their harvest seasons, on one hand, and to preserve the state's financial resources by reducing the import bill, on the other hand, the Algerian government is working hard to remedy this deficiency through urgent solutions at the level of large farms and small farmers. In order to avoid the loss of their crops by drying means, Algerian farmers can make use and profit of the abundance of solar energy and geothermal energy as renewable sources, especially in the Algerian Sahara regions where high solar radiation and important geothermal water resources are available (Sandali et al., 2019).

Tomatoes with their versatile food ingredient and variable derived products, such as sauces, soups, ketchup, salsa, and juice, is considered as an important source of health-promoting nutraceuticals and micronutrients (Lu et al., 2020; Porretta, 2019). nonetheless, due to its fragility and the lack of conservation means and factories, tons of harvested tomatoes are thrown away every year in Algeria, namely in the southern hot climate regions. Therefore, there is an absolute necessity to preserve tomatoes by using drying techniques and hence extending their shelf life , improving their appearance, and enhancing their nutritional attributes, texture, and taste (Salehi et al., 2019).

From designing aspects viewpoint, several drying systems, destined to different crops and based on solar energy, have been developed as alternatives to the traditional crops drying under the open sun, especially in locations with abundant radiations (ELkhadraoui et al., 2015). As illustrative examples we can cite: (Adelaja and Ojolo, 2010; Amer et al., 2018; Arun et al., 2019; Baniasadi et al., 2017; Bhardwaj et al., 2019; Keawsuntia, 2014; Lakshmi et al., 2019; Mehran et al., 2019; Mewa et al., 2019; Sallam et al., 2015; Ssemwanga et al., 2020; Tagnamas et al., 2020; Zhong et al., 2012).

In the available literature, numerous studies have been developed dealing with the solar drying of tomatoes, to obtain different output products (Badaoui et al., 2019; Djebli et al., 2019; Dorouzi et al., 2018; Manaa et al., 2013; Milczarek et al., 2017; Nabnean et al., 2016; Prakash and Kumar, 2014; Ringeisen et al., 2014), covering a set of tomato products such as : dehydrated tomato concentrate; concentrated tomato products, either in puree or paste; pizza sauce, from peels and seeds; tomato powder, peeled tomato, whole or diced, etc.). Nevertheless, there is a lack of research on the drying process of tomato paste. In fact, the need for research investigation on tomato paste is well justified by the fact that several derived products are simultaneously obtained. Indeed, besides the easily reconstituted dried tomato paste, there is the tomato juice demanded on

the organic product market; thus, the rejects of skin and seeds constitute a good source of the antioxidant's product.

The present chapter aims to investigate the efficiency of free solar energy and geothermal water, on several solar drying methods of tomato paste. So this study will offer a more effective drying method to prevent the postharvest losses of tomatoes, in paste form, that is used as a biological product namely intended for children and elderly. For the aforementioned goals, improved direct solar drying of tomato paste using four drying techniques was conducted: (i) basic direct solar drying, (ii) direct solar drying provided with geothermal heat exchanger, (iii) direct solar drying with accelerated air drying using two electric DC fans generated by a P-V module, and (iv) combined direct solar drying between ventilated and heat exchanger mode. Drying kinetics and drying characteristic curves of tomato paste have been investigated. In order to make it possible to extrapolate the problem from laboratory scale to industrial application, this paper is also aimed to propose a mathematical comportment model to well describe the solar drying behavior of tomato paste.

4.2 Materials and methods

4.2.1 Experimental procedure

Ten (10) kilograms of tomato were bought from a central market of Ouargla city, in the northern of Algerian Sahara. Before drying experiments, tomatoes were properly washed then cut into halves and quarters, before being ground in a kitchen blender. Then, they were separated in a whole series of sieves with different sizes to remove the skin and the seeds from the paste. Finally, the mixture was drained in a tissue bag to obtain 1 kilogram of tomato paste, and 4 liters of tomato juice.

Solar drying of tomato paste with an initial moisture content of 5.8 (d.b) was carried out using a laboratory-scale direct solar dryer previously tested and developed at LENERZA laboratory (Ouargla University) by Mennouche et al., (2014). The drying procedure was conducted with four methods: (i) Basic Solar-drying mode, which is the basic solar dryer without any supplementary sources of energy (SDM), (ii) Solar/Geothermal Drying using a serpentine heat exchanger operated with geothermal water (SGD), (iii) Electric fan, Convective Ventilated Solar Drying (CVD), and (iv) solar dryer combined with both heat exchanger and ventilated mode (VHD). The drying experiments occurred in July using similar direct solar dryers. As a sample, Figure (4.1) presents the schematic of the solar dryer for VHD drying. The dryer consists mainly of a drying chamber (1 m × 0.7 m), a direct sun collector, and a chimney (1 m × 0.1 m) to accelerate the exhaust air. Two similar fans with a total power of 12 W were used to accelerate the dry air

entering the chamber. A P-V module of 150 W is used to feed these fans. The drying equipment is connected by an acquisition table that allows measuring the climate conditions such as sunshine and air temperature as well as drying temperatures and relative humidity of the drying chamber.

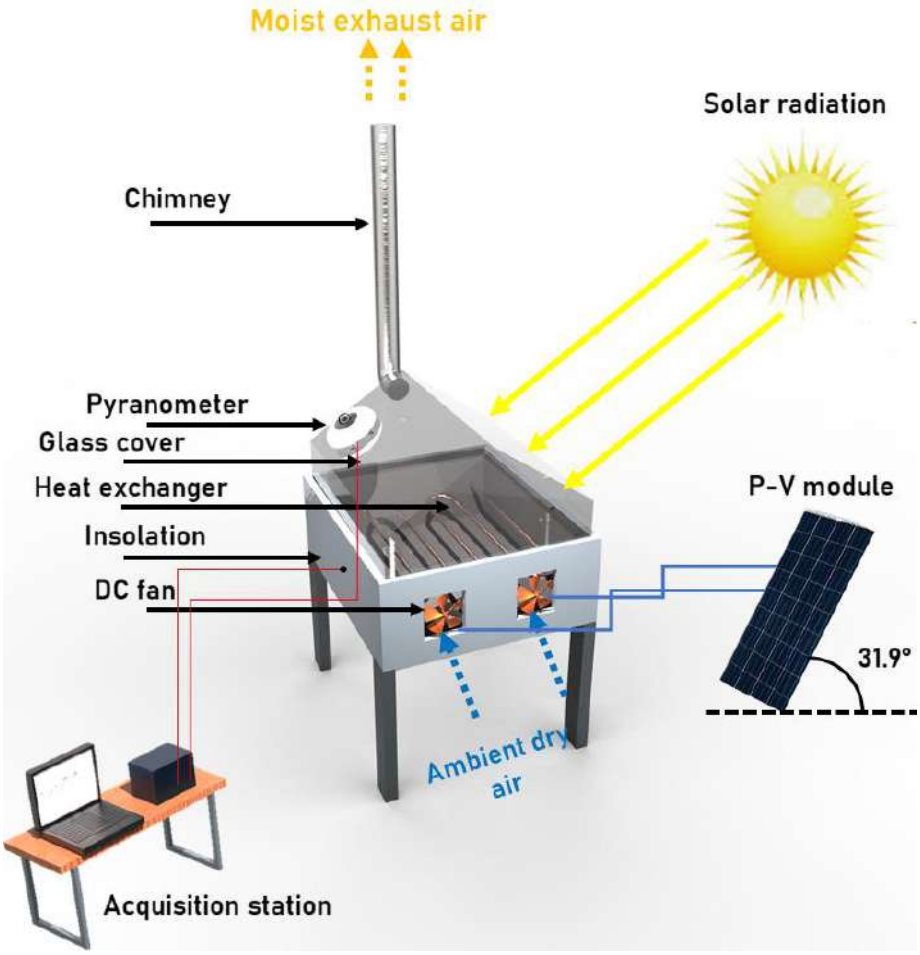

***Figure 4-1**: Schematic of the solar dryer for VHD drying*

The moisture content of tomato paste was reduced from 5.8 (g water/kg dry matter) to the desired level ≤ 0.1(g water/kg dry matter) using different solar drying data M_t, *MR*, and *DR* of tomato paste at any time.

Moisture content (M_t) on a dry basis can be defined by Equation (4.1), (El-Sebaii and Shalaby, 2013):

$$M_t = \frac{m_t - m_d}{m_d} \qquad \text{(Eq.4.1)}$$

Moisture content ratio (*MR*) can be calculated using Equation (4.2):

$$MR = \frac{M_t - M_e}{M_0 - M_e} \qquad \text{(Eq. 4.2)}$$

However, *MR* has been simplified to M_t/M_0 by assuming that M_e is very small compared to M_t and M_0.

Finally, the drying rate (*DR*) in (kg water/kg dry matter. h) can be defined by Equation (Eq. 4.3), (Doymaz, 2006):

$$DR = \frac{M_{t+\Delta t} - M_t}{\Delta t} \qquad \text{(Eq. 4.3)}$$

4.2.2 Characteristic drying curve

The Characteristic Drying Curve *CDC* defines the effect of various drying techniques as reported by Van Meel (1958). Such a *CDC* allowed determining the drying model of tomato paste. The curve established as the moisture ratio (*MR*) versus drying time to secondly be expressed as *f* = f(*MR*) (Borah et al., 2015):

$$f = \frac{(-dM/dt)_t}{(-dM/dt)_0} \qquad \text{(Eq. 4.4)}$$

4.2.3 Mathematical modeling

The drying curves expressed as natural logarithmic against drying time were fitted to eight mathematical models. The conventional modeling aims to predict the drying behavior of tomato paste solar drying using different modes. Origin software is used to fit the mathematical models in Table (4-1) with the experimental drying curve of moisture ratio.

***Table 4-1**: The eight mathematical models fitted to the drying curves*

Model name	*Equation*	*Reference*
Lewis	$MR = exp(-kt)$	(Bruce, 1985)
Page	$MR = exp(-kt^n)$	(PAGE, 1949)
Two-term	$MR = aexp(-kt) + bexp(-k_1 t)$	(Henderson, 1974)
Wangh and Singh	$MR = 1 + at + bt^2$	(Wang and Singh, 1978)
Diffusion approximation	$MR = aexp(-kt) + (1-a)exp(-kbt)$	(Kassem, 1998)
Henderson and Pabis	$MR = aexp(-kt)$	(Pabis, 1961)
Prakash and Kumar	$MR = at^3 + bt^2 + ct + d$	(Prakash and Kumar, 2014)
Proposed model	$MR = a\exp(-t/\alpha)^{\beta} + c$	Current paper

According to Midilli and Kucuk (2003), the main criterion for the selection of the best drying equation is the correlation coefficient (r), the lowest Root Mean Square ($RMSE$), and the lowest reduced chis-square (x^2). These parameters are defined as following, (Yaldiz et al., 2001):

$$r = \frac{\sum_{i=1}^{n}(MR_i - MR_{pre,i}).\sum_{i=1}^{n}(MR_i - MR_{\exp,i})}{\sqrt{\left[\sum_{i=1}^{n}(MR_i - MR_{pre,i})^2\right].\left[\sum_{i=1}^{n}(MR_i - MR_{\exp,i})^2\right]}} \quad \text{(Eq. 4.5)}$$

$$RMSE = \left[\frac{\sum_{i=1}^{n}(MR_{pre,i} - MR_{\exp,i})}{N}\right] \quad \text{(Eq. 4.6)}$$

$$x^2 = \frac{\sum_{i=1}^{N}(MR_{\exp,i} - MR_{pre,i})^2}{N - P} \quad \text{(Eq. 4.7)}$$

4.2.4 *Effective moisture diffusivity*

The diffusion coefficient (D_{eff}) is the most important criterion in the drying of fruits and vegetables and other materials for modelling the drying process. It characterizes a function of moisture content with respect to drying temperature in food (Oztop and Akpinar, 2008). D_{eff} of tomato paste was calculated by using the simplified Fick's second diffusion law as defined below:

$$\frac{\partial MR}{\partial t} = \nabla\left[D_{eff}\nabla\left(\frac{M_t - M_e}{M_0 - M_e}\right)\right] = D_{eff}\nabla^2\left(\frac{M_t - M_e}{M_0 - M_e}\right) \quad \text{(Eq. 4.8)}$$

Fick's second law can be used to solve Equation (4.8), assuming humidity transport by diffusion. The constant diffusivity, temperature, minimal shrinkage, and geometry without limits slab as proposed by Crank (1979) were used:

$$MR = \frac{8}{\pi^2}\sum_{n=1}^{\infty}\frac{1}{(2n+1)^2}\exp\left(-(2n+1)^2\pi^2\frac{D_{eff}.t}{4L^2}\right) \quad \text{(Eq. 4.9)}$$

For a sufficiently long drying time, Equation (4.9) becomes:

$$MR = \frac{8}{\pi^2}\exp\left(\pi^2\frac{D_{eff}.t}{4L^2}\right) \quad \text{(Eq. 4.10)}$$

The effective diffusivity can be calculated using the slope k of the straight-line of plotted experimental data of $ln\ (MR)$ against drying time (s):

$$D_{eff} = -\frac{4L^2}{\pi^2}k \qquad \text{(Eq. 4.11)}$$

4.3 Results and discussion

4.3.1 Drying kinetics

The moisture content and drying rate of tomato paste dried using four solar drying techniques is shown in Figures (4.2-3). The tomato paste with an initial moisture content of 5.8 (g water/kg dry matter) was dried to 0.08 (g water/kg dry matter). Under solar dryer conditions, the final moisture content reflects moisture balance between the sample and drying air where the product temperature reached the drying air temperature, beyond that no change in the weight of the sample might have occurred. Basic Solar-drying mode (SDM) took 10 h to reach the desired moisture content. Whereas, Solar/Geothermal Drying using a heat exchanger operated with geothermal water (SGD), ConvectionVentilated solar Drying mode (CVD), and the combined mode (VHD) took 9, 8, and 4.5 h, respectively. The results revealed a significant effect of combined mode between the heat exchanger and ventilated mode on drying time with a reduction of 120%, 100%, and 77% compared (SDM), to (SGD) and (CVD), respectively. This rise in drying time may be attributed to the increase of average drying temperatures and decrease of daytime average relative humidity of (VHD) as this state raises the vapor pressure as well as the evaporation rate of warm air (ELkhadraoui et al., 2015; Seerangurayar et al., 2019). Quite the reverse, the convection process reduces the external resistance and accelerates the removal of water by drying air.

In terms of drying rate, the Basic Solar-drying mode of tomato paste (SDM) was the least effective. It was intensified when coupled with geothermal drying (SGD), and even more so with convection/ventilation solar drying (CVD). The best yield was achieved by combining the solar drying with ventilation and heat exchanger drying (VHD). Similar results were obtained by Ali et al., (2016); Koukouch et al., (2017) and Shen et al., (2014). It should be noted that the influence of convection-ventilated solar drying (CVD) has less effect than SGD and VHD techniques resulting in a better heat input to air drying. The decrease in the drying rate with the reduced moisture content of the tomato paste can be due to the decreased presence of moisture in its free form as the product moisture interactions increase (Shivhare et al., 2004). This observation is in agreement with those of Mewa et al., (2019) for solar drying of beef.

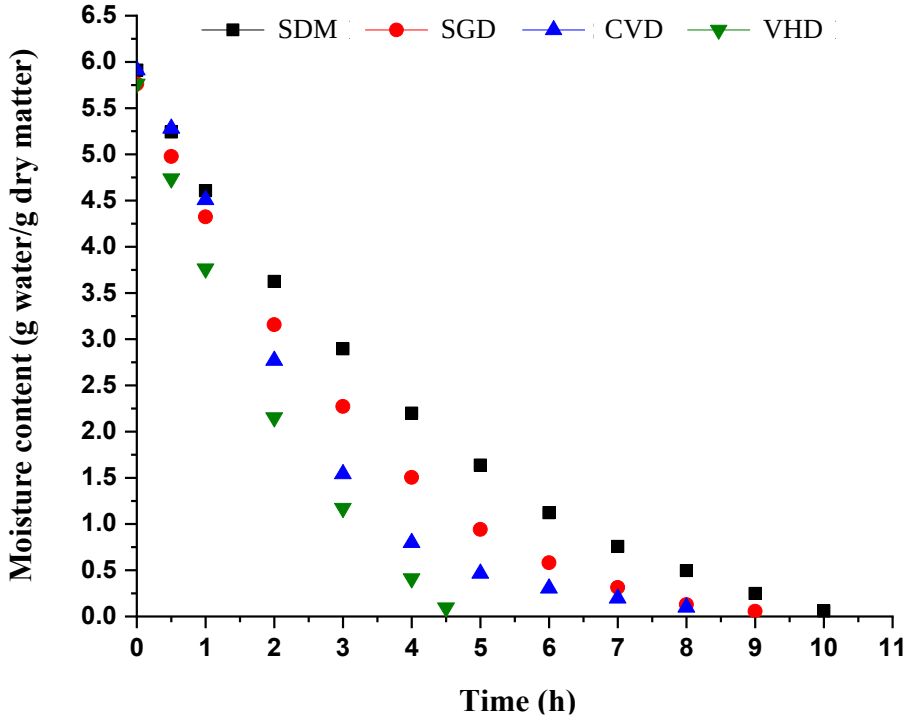

***Figure 4-2**: Evolution of moisture content drying time depending on drying techniques: basic solar drying (SDM), Solar-Geothermal Drying (SGD), Convection/Ventilated solar Drying (CVD), and Ventilation and Heat exchanger solar Drying (VHD)*

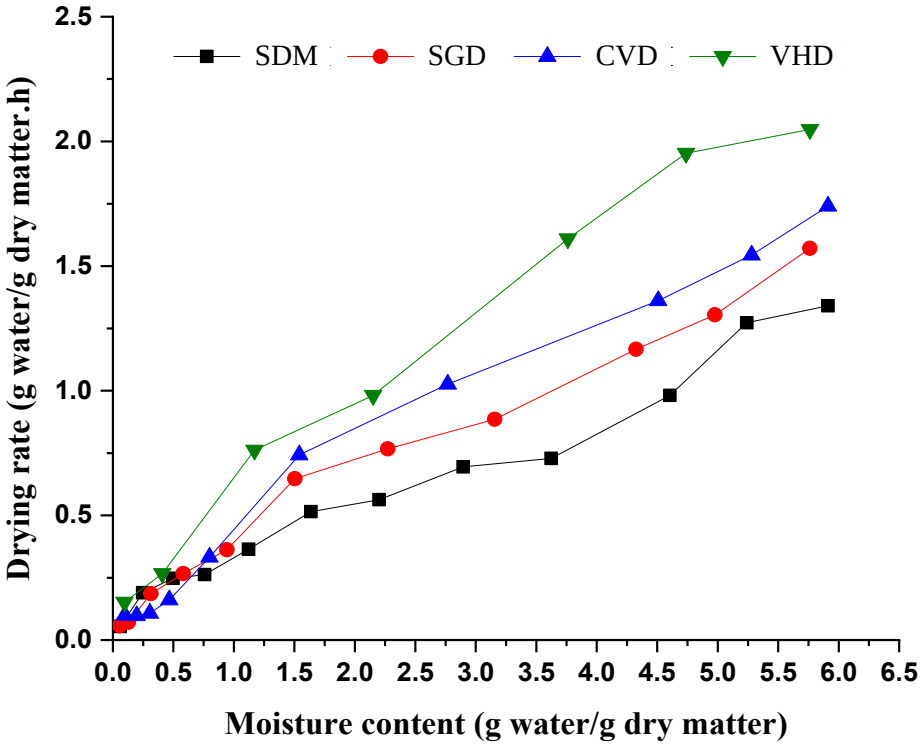

***Figure 4-3**: Variation of drying rate over moisture content depending of drying techniques: basic solar drying (SDM), Solar-Geothermal Drying (SGD), Convection/Ventilated solar Drying (CVD), and Ventilation and Heat exchanger solar Drying (VHD)*

4.3.2 Characteristic drying curve

Characteristic drying curve (*CDC*) of tomato paste presented in Figure (4.4) illustrates the experimental results. It is based on normalizing the kinetics of drying into a dimensionless drying rate based on experiments. The approach used was to produce a statistical association between typical kinetics of tomato paste in the form of a polynomial equation of the third-degree *MR* by non-linear optimization of Levenberg-Marquard using the Curve Expert 1.4 program (Huang et al., 2016).

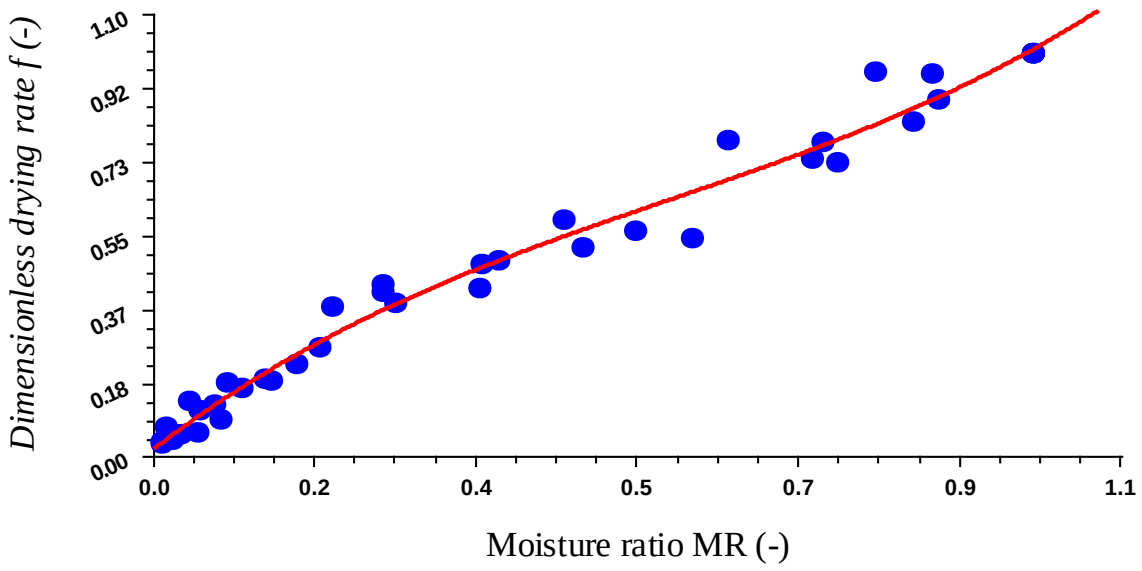

***Figure 4-4**: Characteristic drying curve of tomato paste*

The fitting of experimental data of *CDC* of tomato paste allowed defining the dimensionless drying rate equation (*f*): $f = 0.002 + 1.674MR - 1.592MR^2 + 0.908MR^3$

The best fit was obtained by the lowest standard error value (*RMSE*= 0.04643) and the highest correlation coefficient (r = 0.99128).

The *CDC* is characterized by its specific and simple use. It takes into consideration the combined impacts of the aerothermal conditions of the drying air (drying temperature, drying air velocity, relative humidity..etc.) and the drying behavior of the product through the drying process (Ali et al., 2016; Ferreira et al., 2014).

4.3.3 Mathematical modeling

To express the drying kinetics behavior of tomato paste, eight mathematical models based on the Levenberg-Marquard algorithm with Origin 8.5 software were used to fit the experimental curve. The statistical constants of these models with different drying techniques are given and summarized in Table (4-2). The obtained average statistical results for fitted experimental points

by the eight mathematical models are shown in Table (4-3). The tested mathematical models showed a high correlation coefficient values "*r*" ranged from 0.9864 and 0.9996. Nevertheless, the proposed model showed the highest average value of *r* (0.9996), the lowest values of x^2 (0.00009) and *RMSE* (0.0091). Consequently, among the tested models, the proposed one was the best one that accurately described the drying behavior of tomato paste using different drying techniques. The fitting of experimental data of various techniques of solar drying to the proposed mathematical model is presented in Figure (4.5).

***Table 4-2**:Constants of mathematical models*

Model name	*Constant*	*SDM*	*SGD*	*CVD*	*VHD*
Lewis	*k*	0.26667	0.33768	0.41376	0.51849
Page	*k*	0.21475	0.27036	0.28952	0.42244
	n	1.14767	1.17941	1.37094	1.27568
Two-term	*a*	0.51134	0.51544	0.51825	0.52137
	k_0	0.27312	0.34867	0.44334	0.54236
	b	0.51134	0.51544	0.55109	0.52138
	k_1	0.27312	0.34867	0.44347	0.54232
Wang and Singh	*a*	-0.19695	-0.24478	-0.30104	-0.37835
	b	0.01003	0.01526	0.02278	0.03601
Diffusion of Approximation	*a*	1	1	1	1
	k	0.26667	0.33768	0.41375	0.51845
	b	1	1	1	1
Henderson and Pabis	*a*	1.02273	1.03099	1.06935	1.04276
	k	0.27314	0.34876	0.44342	0.54236
Prakash and Kumar	*a*	-0.00054	-0.00074	-0.00138	-0.00292
	b	0.0172	0.02441	0.04012	0.05528
	c	-0.21656	-0.26935	-0.35894	-0.40883
	d	0.9909	0.99658	1.03924	1.00546
Proposed model	*a*	1.14354	1.1086	0.99922	1.27631
	α	21.34356	1.96316	0.27588	0.77727
	β	4.25747	0.54208	1.336	0.25885
	c	-0.14853	-0.10011	0.00088	-0.26849

***Table 4-3**: Average values of criteria for the used mathematical models*

Model	*r*	*RMSE*	x^2
Lewis	0.9864	0.04243	0.00189
Page	0.9975	0.01867	0.00037
Two-term	0.9893	0.04799	0.00247
Wang and Singh	0.9967	0.02058	0.00044
Diffusion of Approximation	0.9864	0.04892	0.00255
Henderson and Pabis	0.9906	0.03694	0.00142
Prakash and Kumar	0.9987	0.01327	0.00029
Proposed model	0.9996	0.0091	0.00009

Figure (4.6) shows the perfect alignment between the experimental and predicted values of *MR* resulted from the proposed model with $r = 0.9998$ and $RMSE = 0.00703$ using Curve Expert 1.4 software.

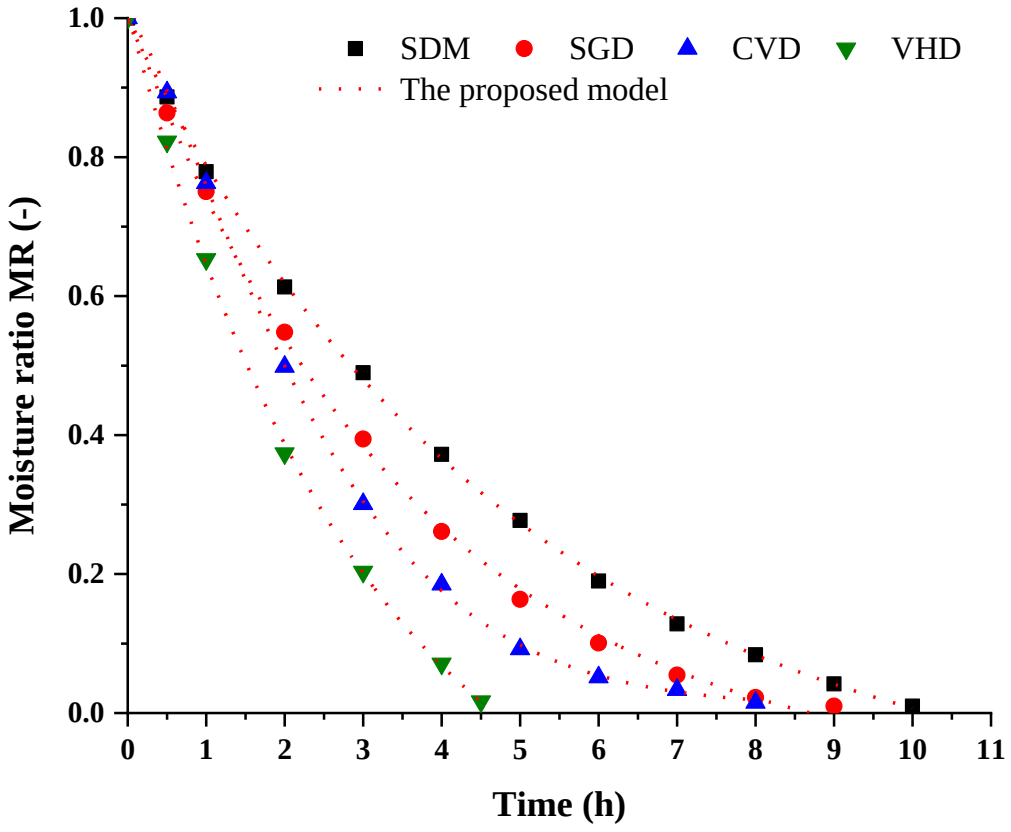

***Figure 4-5**: Experimental moisture ratio (MR) Vs drying time fitted with the new proposed model*

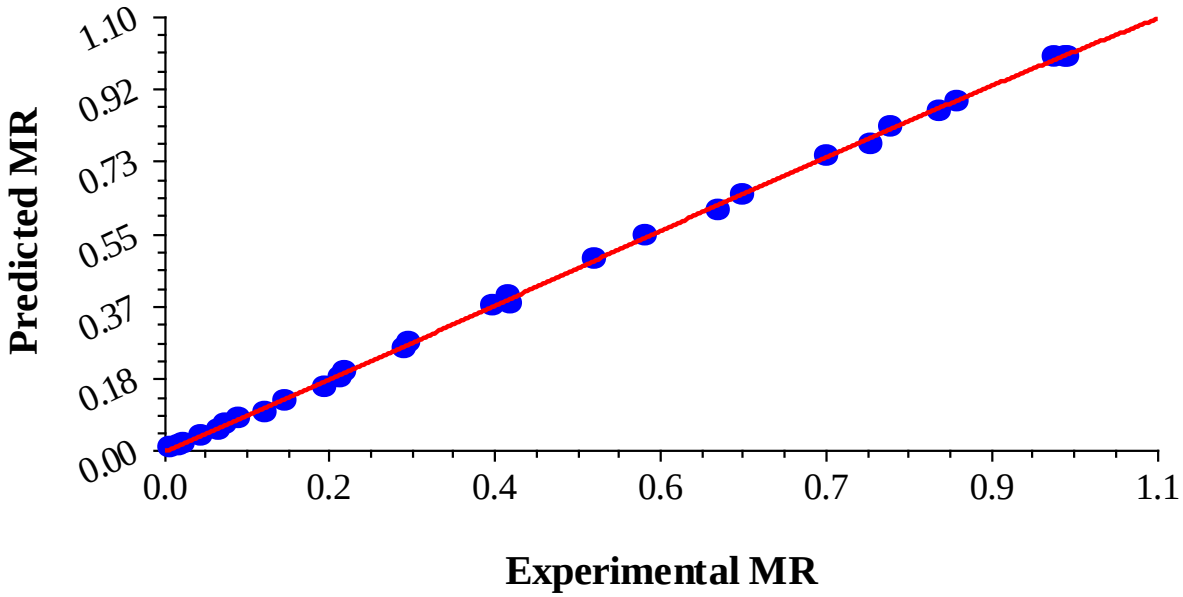

***Figure 4-6**: The predicted moisture ratio by the proposed mathematical model Vs experimental moisture ratio (MR)*

4.3.4 Determination of effective moisture diffusivity

Figure (4.7) illustrates the natural logarithmic ln (*MR*) values against drying time of tomato paste at different drying techniques. The figure showed that plots of natural logarithmic versus time deviated slightly from the linearity for all drying experiments.

According to Celma et al., (2009), the deviation of the plotted drying curve from linearity denotes that effective moisture diffusivity is correlated with the moisture content of the product at any time. Thus, drawing ln (*MR*) against drying time using a non-linear polynomial regression of the third degree was carried out with a good fitting of the experimental points, Equation (4.12):

$$\ln(MR) = A_0 + A_1 t + A_2 t^2 + A_3 t^3 \qquad (4.12)$$

Also; Figure (4.7) presents the effective moisture diffusivity values for different drying techniques. The obtained results showed a significant increase of D_{eff} from 1.1×10^{-9} to 2.298×10^{-9} $m^2\ s^{-1}$for (SDM), (SGD), (CVD), and (VHD), respectively. Drying tomato paste using (VHD) leads to the highest moisture diffusivity, so, an increase of heating energy and accelerating air drying would increase the activity of water molecules and reduce the surface air interaction between the air drying and tomato paste surface. A similar result was obtained by Xiao et al., (2010). The resulted D_{eff} was in the range of recent studies varied between 10^{-8} and 10^{-12} $m^2\ s^{-1}$ for dried agro-products (Zogzas et al., 1996).

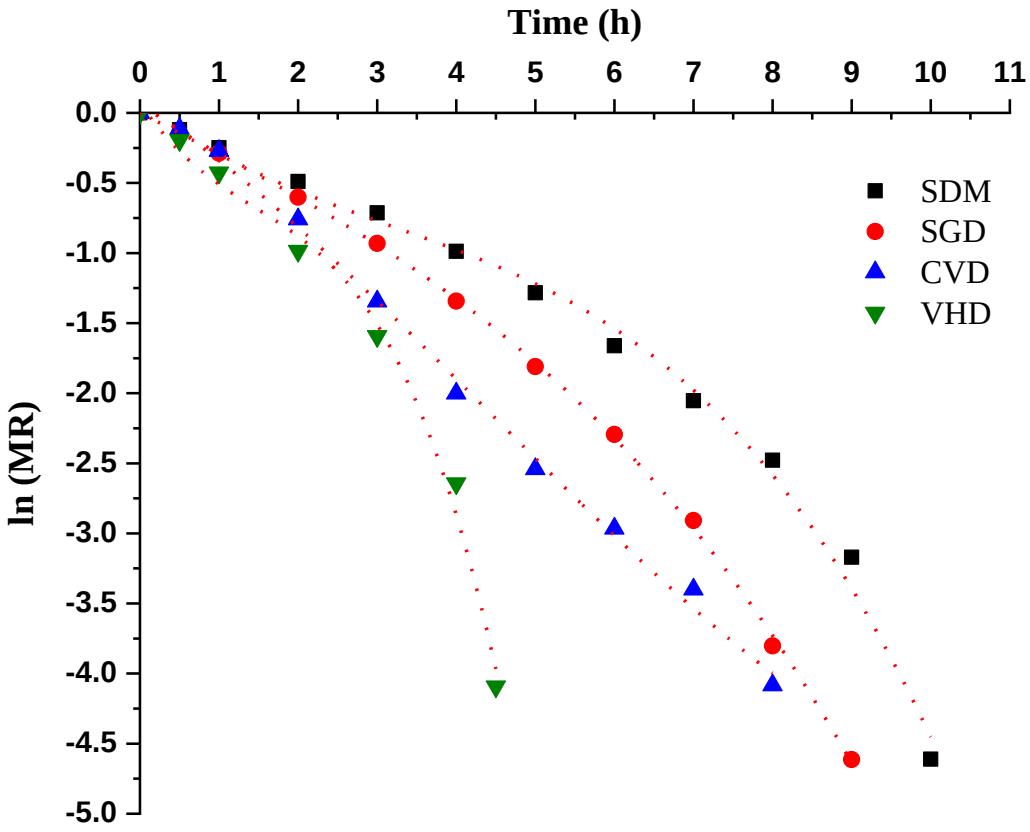

***Figure 4-7**: Effects of drying techniques on the effective diffusion coefficient of tomato paste*

The coefficients (A_0, A_1, $A2$, and A_3) of equation 12, the diffusion coefficient (D_{eff}), and the resultant of correlation coefficient (r) for different drying technics are given in Table (4-4).

***Table 4-4**: Equation's coefficients, effective moisture diffusivity, and correlation coefficient (r) for different drying techniques*

Drying technique	A_0	A_1	A_2	A_3	$D_{eff}\times 10^{-9}$ ($m^2\ s^{-1}$)	r
SDM	0.0691	-0.4211	0.0685	-0.0072	1.1	0.9942
SGD	0.0031	-0.2975	0.0036	-0.0031	1.374	0.9995
CVD	0.0654	-0.3621	-0.0463	0.0035	1.469	0.9971
VHD	0.0732	-0.8447	0.3406	-0.0783	2.298	0.9924

4.4 Conclusion

Solar drying of tomato paste was conducted using four drying techniques: (i) basic direct solar drying, (ii) direct solar drying assisted with heat exchanger, (iii) direct solar drying with ventilated mode, and (iv) direct solar drying with combined mode. The drying characteristic curve and drying kinetics of tomato paste were experimentally investigated. The obtained results of this chapter can be summarized as follow:

- Solar drying with combined mode decreased the drying time by 120% compared to the basic solar drying mode.
- The highest value of drying rate was observed for the solar drying with combined mode.
- The best fit for the characteristic drying curve was obtained by the evaluation of two criteria, the standard error value *RMSE* = 0.04643 and the correlation coefficient value *r* = 0.99128.
- Among eight mathematical models, the proposed mathematical model followed by Prakash and Kumar's model was selected as the most appropriate model describing the behavior of tomato paste and well predicting the changes in moisture content during the drying process with the highest average value of *r* = 0.9996, the lowest values of x^2 = 0.00009 and *RMSE* = 0.0091 using the four drying methods.
- The proposed model was found the be the most suitable to describe the drying behavior under the used drying techniques with r = 0.9998 and RMSE = 0.00703.
- The highest effective moisture diffusivity was recorded for the combined mode. D_{eff} ranged from 1.1×10^{-9} and 2.298×10^{-9} $m^2\ s^{-1}$.
- Improved solar drying in northern Algerian Sahara is recommended for reducing harvested losses of tomato and other seasonal crops.

5 Combined Solar Drying/Swell Drying of Tomato Paste

5.1 Introduction

Today, large quantities of tomatoes are produced in Algeria. According to (FAO, 2014), Algeria produced 1,065,609 tons per year with a world rank of 18 and a world share of 0.6%. Due to their fragility and the distances between the production and consumption zones, tons of harvested tomatoes are thrown away every year in Algeria, namely in southern hot climate regions. Therefore, there are considerable needs for preservation and processing techniques to extend the shelf life of tomatoes, improve their appearance, enhance nutritional attributes, texture, and taste (Salehi et al., 2019).

Tomatoes with their versatile food ingredient and derived products from them can be an important source of health-promoting nutraceuticals and micronutrients (Porretta, 2019).

For several years, researchers have been conducting research aimed at using solar and sun drying in different cases of fruit and vegetables. They usually defined and investigated the impact of several solar drying technics on drying kinetics. Normally, such experimental studies on several fruit and vegetables observed that the drying kinetics was only the falling-rate period, such as wood Khouya and Draoui (2009); grape Masmoudi et al., (2008); tomato Boughali et al., (2009); sugar beetroot VACCAREZZA et al., (1974); avocado ALZAMORA & CHIRIFE (1980); fish Bellagha et al., (2002); leaves Mohamed et al., (2005); grains and oilseeds Brooker et al., (1992); apple Doymaz (2009) and Kaya et al., (2007); chilli Gupta et al., (2002).

Moreover, in the available literature, numerous studies have been conducted on the solar drying of tomatoes (Badaoui et al., 2019; Djebli et al., 2019; Dorouzi et al., 2018; Manaa et al., 2013; Milczarek et al., 2017; Nabnean et al., 2016; Prakash and Kumar, 2014; Ringeisen et al., 2014) to obtain different output products. Nevertheless, there is a lack of research on the drying process of such kind of product. Furthermore, the need for research investigation on tomato paste manufacturing remains well justified by the fact that several derived products can be simultaneously obtained. So, besides the easily reconstituted dried tomato paste, there is the tomato juice demanded on the organic product market; thus, the rejects of skin and seeds can also constitute a good source of the antioxidant's product.

This situation urges us to study the whole dehydration including both mechanical dewatering and a new drying method for mainly increasing the operational performance through the internal water diffusion to reduce the processing time (less energy consumption) as well as improving the visual quality and preventing the throwing of surplus tomatoes. The first step of simple dewatering was followed by a drying step using two types of energy (solar energy, geothermal energy). Before reaching the final step of drying, we inserted a texturing by Instant

Controlled Pressure-Drop (DIC). In this chapter, the impact of DIC texturing was more particularly studied as well as the final solar drying.

5.2 Materials and methods

5.2.1 Raw material and sample processing way

Fresh local tomatoes (L. esculentum) were bought at a local market in Ouargla, southern of Algeria. The tomatoes were selected one by one using visual criteria such as color, size, absence of physical damage, and uniform ripeness. Tomatoes were properly washed under running water to remove the skin and then cut into halves or quarters. They were then crushed in a kitchen blender and separated in a series of sieves of different sizes to remove a part of its internal water and seeds from the flesh. Finally, the paste was partially removed from the freest part of its water by draining (dewatering) through a cotton cloth bag. A quantity of partially dewatered tomato paste was obtained, separated from another amount of tomato water. This tomato paste was enclosed in plastic bags and stored at 4°C.

5.2.2 Solar drying

5.2.2.1 Assessment of solar intensity

Experiments on continuous solar drying of tomato paste were carried out with a direct solar dryer using a Geothermal Water Heat Exchanger (GWHE). The continuity of the drying process was thus ensured during the night. The system presented in Figure (5.1) was built at the Laboratory for the Development of New and Renewable Energy in Arid and Saharan Zones, LENERZA, Faculty of Mathematics and Material Sciences, University of Kasdi Merbah Ouargla, Ouargla 30000, Algeria. The GWHE solar dryer was switched on even in the presence of sunlight, after sunset, and during the night. Geothermal water with a temperature of about 67 °C was pumped into the heat exchanger using an electric pump. The dryer was insulated with 2 cm thick polystyrene to reduce heat loss outside during the hours out of the sun, from 4:30 p.m. onwards and throughout the night. The experiment was stopped when the dried samples reached the desired moisture level. The dryer consists mainly of a drying chamber inclined at an angle of 31.9° (latitude of the city of Ouargla) with a base painted black to improve absorption of sunlight and connected to a cylindrical galvanized chimney to evacuate the humid air. The lower sides of the drying chamber are made of galvanized sheets insulated with polystyrene. The ambient air entering the drying chamber is heated when it comes into contact with the GWHE and the absorber. The hot air passes through the product, transports the moisture on its surface, and is exhausted to the outside through the chimney. The geometrical dimensions of the solar dryer are shown in Table (5-1).

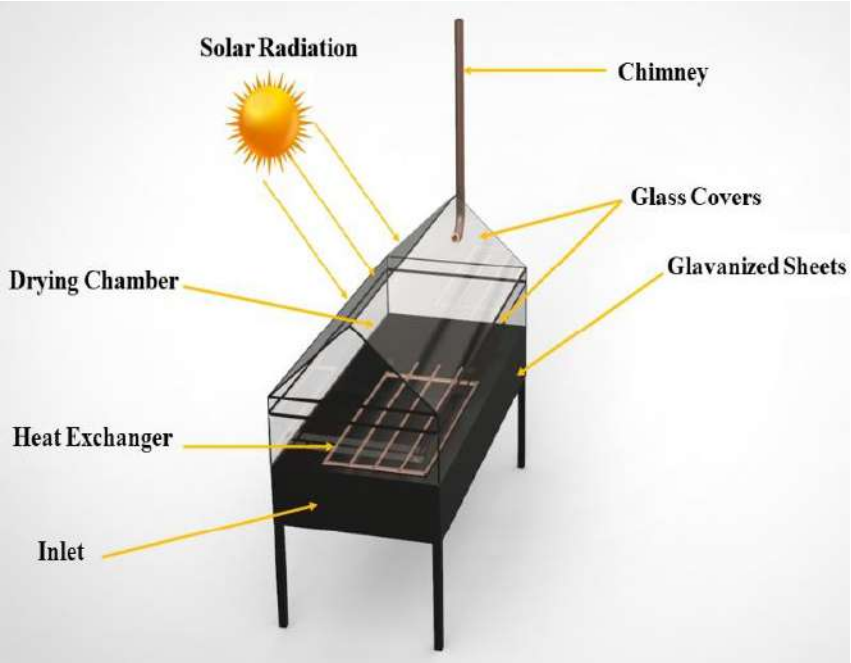

***Figure 5-1**: Schematic diagram of the used solar dryer*

***Table 5-1**: Dimensions of the dryer components*

Signification	*Values (m)*
Length of drying chamber	1.0
Width of drying chamber	0.8
Galvanized metal sheets insulated thickness	0.05
Glass covers thickness	0.004
Absorber thickness	0.02
Air inlet	0.015
Chimney diameter	0.1
Chimney length	1.0

5.2.2.2 Assessment of mass and water content evolutions versus time

Calibrated k-type sensors were used to record all temperatures every 15 min using a data acquisition system (NIcDAQ -9174). The display of the measurement results was provided by the "LabVIEW NXG" software. The solar radiation was recorded by a Solar Mac pyranometer in a range of 0 to 1000 W/m². The mass of the tomato paste was measured every 60 min using an electronic scale with a capacity of 10 kg with an accuracy of 0.01 kg.

The initial moisture content expressed in g H_2O/g dry basis (d.b) was measured by a moisture analyzer (IR 35, accuracy ± 0.001). A thin layer of tomato paste, 3 g thick, was placed

inside the temperature-controlled (105 °C) analyzer. The analyzer stops automatically when the weight of the tomato paste sample becomes stable.

The initial moisture content of the tomato paste samples was found to be 6.5 g H_2O/g dry basis (d.b). Otherwise, the initial moisture content of the fresh tomato was measured as a 7.4 g H_2O/g dry basis (d.b). Moisture content and relative moisture content (M_t and MR) were calculated using the following mathematical relationships:

$$M_t = \frac{m_t - m_d}{m_d} \quad \text{(Eq. 5.1)}$$

$$MR = \frac{M_t - M_e}{M_0 - M_e} \quad \text{(Eq. 5.2)}$$

However, MR was simplified to $M_t/M_0$by assuming that M_e is very small compared to M_t and M_0

5.2.3 Phenomenological modeling of drying kinetics

To assess whether the drying kinetics allow efficient moisture diffusivities and activation energy, phenomenological modeling must be investigated. The drying operations occur through three different stages:

(1) A surface interaction between the airflow and the exchange surface. This should be a short-time step of heat transfer by convection, solicitation, and evaporation of water present at the surface, and transport of vapor from the surface towards the surrounding environment.
(2) Stage of the diffusion of water from the matrix volume towards the exchange surface to be evaporated and transported through the airflow mass convection. This is mainly the main drying stage.
(3) The paradoxical stage of internal evaporating of water within the pores and the transfer of the vapor from the product core to its exchange surface. This famous paradoxical stage is a temperature depending process. The temperature and vapour pressure gradients are driven from the product surface to the core. Drying is then achieved by a gradual low water activity operation. Generally, no shrinkage is associated with this stage (Nguyen et al., 2016).

Only the second stage data of the drying can be used to calculate the diffusivity of water within the matrix. However, only once the airflow velocity value is higher than the critical airflow velocity (CAV) that this stage of the drying process is a diffusion-controlled process. Indeed, the higher the airflow velocity, the lower the external mass transfer resistance. Therefore, the negligible external resistance (NER) allows to identify the effective diffusivity of water within the

product from the experimental drying results. Moreover, the determination of diffusivity can't be carried out without having proved that the external transfer resistance is weaker than the internal diffusion resistance (Nguyen et al., 2016). To use drying data to determine the effective diffusivity, one has to first prove that the operation is independent of airflow velocity. Indeed, the drying becomes an internal diffusion-controlled process when increasing velocity cannot accelerate the drying process (Mounir et al., 2012). Then, it is worth noting that:

- When the airflow velocity is shorter than CAV, the drying kinetics doesn't permit the diffusion to be accessed because drying is "controlled" by the external change;
- When the airflow velocity is greater than CAV, the drying kinetics are "controlled" by the internal diffusion. Then, it is possible to calculate the effective water diffusivity from the drying kinetics.

CAV depends on the effective diffusivity, sample frame and size, and airflow humidity. In our experiment, airflow velocity is superior to 3 m s^{-1}, which allows us to reduce the external transfer stage.

5.2.4 Effective water diffusivity D_{eff}

The second Fick's law was used to calculate the effective water diffusivity by taking into a count the relationship with the reduced water content MR as a dependent variable. The reduced water content MR must be estimated differently than the conventional method (Queiroz et al., 2004). *MR* should be related to a time t_1 where one can assume that there is the second diffusion stage with negligible first stage contribution. Fick's second law solution was identified by seeing an infinite slab. We also assumed that:

(1) Isotropic drying system and uniform initial water content, temperature, and structure,

(2) no shrinkage accompanied of the product during drying process.

This gives the diffusion coefficient expressed as:

$$MR_{t_1} = \frac{W - W_\infty}{W_\infty - W_\infty} = \frac{8}{\pi^2}\sum_{i=1}^{\infty}\frac{1}{(2n+1)^2} exp\left(-(2n+1)^2\pi^2 D_{eff}\frac{t-t_1}{4L^2}\right) \quad \text{(Eq. 5.3)}$$

Where: D_{eff} = effective water diffusion (m^2 s^{-1}), L = half-thickness of the slab (m) and n = 1, 2, 3... the number of terms taken into consideration. For long drying times (MR < 0.6), (n) can be simplified to its first term. Thus, taking the natural logarithm on both sides, one may obtain the following relationship:

$$ln(MR_{t_1}) = ln\left(\frac{8}{\pi^2}\right) - \frac{\pi^2 D_{eff}}{4L^2}(t - t_1) \quad \text{(Eq. 5.4)}$$

The diffusion coefficient was determined by plotting the experimental data (for $t>t_1$) in terms of $ln(MR_{t_1})$ as a linear function of the drying time. The plot of this function gives a straight line with a slope equal to *k*:

$$k = -\frac{\pi^2 D_{eff}}{4L^2} \text{ or } \qquad D_{eff} = -\frac{4L^2}{\pi^2}k \quad \text{(Eq. 5.5)}$$

5.2.5 *Starting accessibility δWs*

The diffusion model of water content dry basis W=f(t) statistically is normally obtained from the data of $t > t_1$ experimental trials. This model can be extrapolated and the value of water content W_0 computed at $t = 0$ usually has a distinct value of the real initial water content W_i**.** The difference δW_s between these two values is the Starting Accessibility δW_s normally expressed as kg H_2O/kg db, (Queiroz et al., 2004)**:**

$$\delta W_s = W_i - W_0 \quad \text{(Eq. 5.6)}$$

The starting accessibility δW_srepresents the water quickly removed from the surface independently from the diffusion process. It's described to show the specific effect of the surface-hot air interaction. Generally, it ought to be positive $\delta W_s > 0$.

5.2.6 *Activation energy*

The activation energy in a drying process, E_a, is the minimum quantity of energy that must be overcome to make this process realizable. The E_a value is closely related to D_{eff}. The origin of the self-diffusion is the thermal agitation. The diffusion is thermally activated, and the diffusion coefficient is traditionally calculated by using the Arrhenius law (Madamba et al., 1996):

$$D_{eff} = D_0 exp\left(-\frac{E_A}{R_g T_p}\right) \quad \text{(Eq. 5.7)}$$

Where D_0 is the pre-exponential factor of Arrhenius equation ($m^2\ s^{-1}$), E_A is the activation energy (kJ mol^{-1}), R_g= the perfect gas constant (8.314 J $mol^{-1}\ K^{-1}$), and T_p (K) is the product temperature. T_p, which must be different from the drying air, is normally called wet-bulb temperature or better, evaporating-system temperature. The higher the evaporating rate, the higher the difference between airflow temperature and product temperature.

From Equation (5.7), a plot of ln (D_{eff}) vs $\frac{1}{T_p}$ gives a straight line whose slope is $\left(-\frac{E_A}{R_g}\right)$ which allows obtaining the activation energy.

5.2.7 Description and principle of DIC

5.2.7.1 DIC equipment

The DIC equipment has three parts as described by Allaf and Vidal (1988) in Figure (5.2):

- A treatment vessel in which the products are processed at high temperature/high-pressure of dry saturated steam (usually up to 1 MPa).
- A vacuum system consisting of a large vacuum tank (120 times the volume of the treatment chamber) and a vacuum pump to achieve and keep constant a vacuum of 5 ± 0.1 kPa in all our experiments, just before the pressure drops.
- A pneumatic valve of a large diameter (more than 200 mm) provides the connection/separation between the vacuum tank and the treatment chamber. It can be opened in time < 0.1 s, which ensures the 'instant' fall of the reactor pressure.

5.2.7.2 DIC treatment

Normally, DIC treatment included two main steps of 1/ high-temperature/high-pressure and 2/ Instant releasing toward a vacuum Such pressure-drop infers a partial auto-vaporization of water, as well as texturing and instant cooling of the samples.

A DIC cycle is also divided into four steps determined in Figure (5.3):

(1) An initial vacuum of 5 kPa as absolute pressure,

(2) Injection of dry saturated steam to maintain for the cycle thermal treatment time t of 5 to 55 s an absolute pressure P between 0.1 and 0.5 MPa. During this step, the product is exposed to a temperature T between 100 and 160 °C. The initial vacuum step is to substantially improve the next exchange between steam and exchange surface. The use of saturated dry steam permitted heating by condensation, with a heating rate that is thousands of times higher than the conventional convection of overheated steam. During this high-pressure/high-temperature heating stage, the temperature and the water content of the product must remain essentially homogenized for a period of time

(3) Abrupt pressure-drop towards a vacuum with an absolute pressure of 5 kPa, and a pressure-drop rate $\Delta P/\Delta t > 0.5$ MPa s^{-1}. This abrupt pressure-drop towards the vacuum allows the product as an “over-heated material” to be submitted to instant auto-vaporization and cooling towards the equilibrium temperature (here, about 30°C for 4-5 kPa). It also results

in a controlled expansion of the solid material. When it is adequate, the glass transition temperature allows for preserving the expanded texture.

(4) Releasing to the atmospheric pressure.

Besides, it is worth mentioning that the treatment of DIC can be achieved by multi-cycles. The number of cycles is the number of different vacuum pressure drops and the operation time is measured for the total cycles (Allaf and Allaf, 2016).

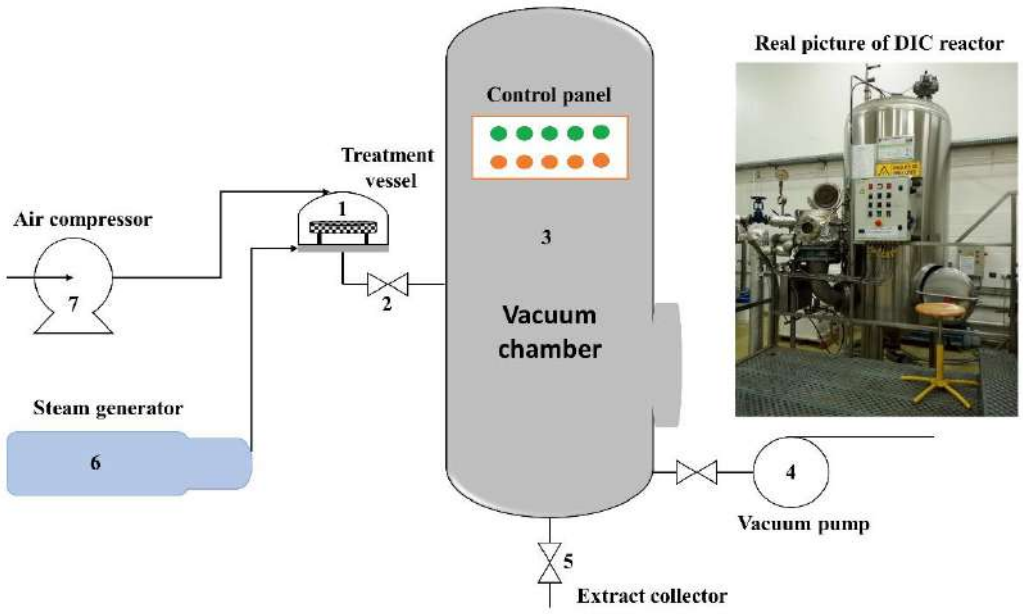

***Figure 5-2**: Schematic presentation of a typical DIC reactor: (1) treatment vessel, (2) controlled instant pressure drop valve, (3) vacuum tank with cooling jacket, (4) vacuum pump, (5) extract collection trap, (6) steam generator, and (7) air compressor*

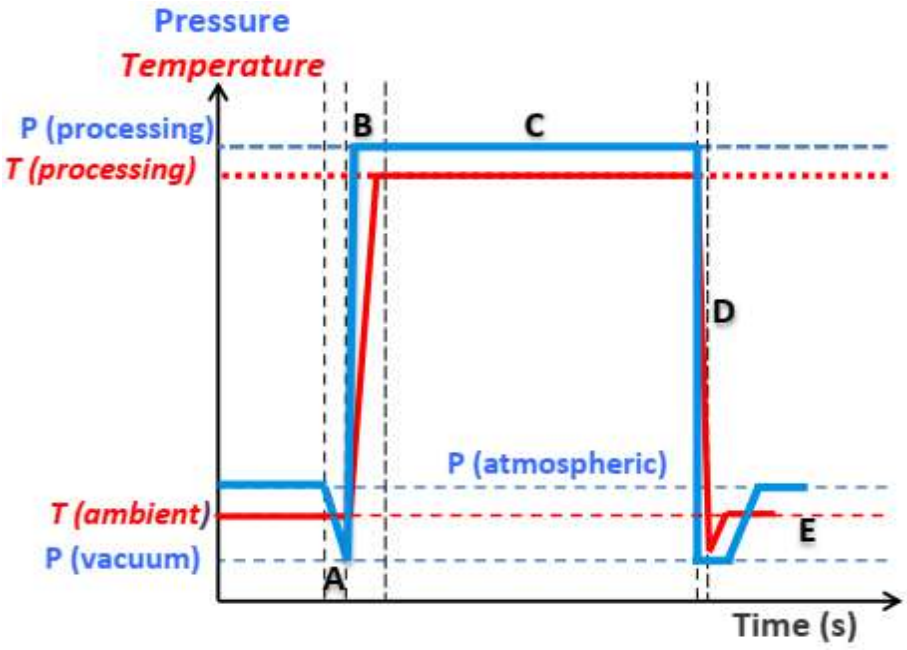

***Figure 5-3**: Evolution of the temperature and pressure during a DIC treatment*

5.2.8 Design of experiments "DoE" of DIC treatment

Design of Experiments (DoE) was used to empirically analyze the effect of instant controlled pressure drop, and optimize its operating parameters on textural, color, and effective diffusivity according to the preliminary trials. DoE was determined with two operating parameters; saturated steam pressure P and thermal holding time t, which respectively ranged from 0.1 to 0.5 MPa and from 10 to 50 s. The DoE we adopted was a 2-parameter, 5-level, and five triplicated-point of central composite rotatable design of experiments Table (5-2).

***Table 5-2**: DIC processing parameters and ranges of saturated steam pressure and thermal holding time*

The effects of these independent variables on responses as dependent variable parameters were evaluated through an RSM statistical treatment using (Statgraphics centurion XVIII, Stat Point Technologies, Inc., USA) Windows. Results were explained through Pareto charts, 3-D response surface, empirical mathematical model, and optimized conditions of instant controlled pressure drop. The Analysis of VAriance (ANOVA) is retained to select significant differences between independent operating variables.

5.2.9 Assessment of color parameters

Color measurements were performed by using a colorimeter (CR-400; Konica Minolta, Tokyo, Japan). Before measuring the color, a standard white ceramic plate was used to calibrate the colorimeter (L* = 96; a* = 0.13; b* = 1.63). L* denotes lightness (L* = 0 for black, L* = 100 for white), a* denotes intensity in red-green (a* > 0 for red, a* < 0 for green), b* denotes intensity in blue to yellow (b* > 0 for yellow, b* < 0 for blue). The average value of L*, a*, and b* were taken using five color measurements.

The brightness of the red color (*B*) was determined according to Toor et al., (2005) using Equation (5.8):

$$Brithnessofredcolor(B) = \frac{a^*}{b^*} \qquad \text{(Eq. 5.8)}$$

Chroma (*C**) is considered as a quantitative characteristic of colorfulness. Chroma (*C**) was calculated (Toor et al., 2005) using Equation (5.9).

$$C^* = \sqrt{a^{*2} + b^{*2}} \qquad \text{(Eq. 5.9)}$$

Overall color change (ΔE) indicates the magnitude of color difference between the two tomato paste samples. It was calculated according to Vega-Gálvez et al., (2012) as follows:

$$\Delta E = \sqrt{\Delta L^{*2} + \Delta a^{*2} + \Delta b^{*2}} \quad \text{(Eq. 5.10)}$$

5.3 Results and discussions

5.3.1 Preparation and draining

Forty (40) kg of tomatoes, similar in visual criteria and uniform maturation degree, were prepared at the laboratory. They were peeled and cut into halves or quarters. These tomato pieces were ground in a kitchen blender (8000 rpm for 30 s) and separated in a whole series of sieves with decreasing sizes to perfectly separate the skin and seeds from the paste. The amount of total wet skin and seeds was about 2.411±0.003 kg at 15.67±0.37 kg H_2O/kg db as water content.

Finally, the paste was drained in a tissue bag to obtain 14.61±0.02 kg of wet tomato paste at 5.82±0.37 kg H_2O/kg db as water content, 22.98 kg of tomato water whose °Brix was 5.3±1. Tomato paste was divided into parallelepiped plate samples of 5×5×0.5 cm^3.

***Table 5-3**: Balance of mechanical partial dewatering of tomato*

5.3.2 Solar and geothermal drying procedure of tomato paste

Samples of tomato pasta with an initial moisture content of 5.82 kg H_2O/kg db or 84.7 (% w.b) were first dried with a natural convection sun dryer as shown in Figure (5.2) at the Laboratory for the Development of New and Renewable Energies in Arid and Saharan Zones, LENREZA, University of Kasdi Merbah Ouargla (Algeria). An additional source of thermal renewable energy was provided by a counter-current heat exchanger of geothermal water at initially 67±2 °C. It ensured continuity in the drying process between sunrise and night in the same dryer, with an airflow of 1 m s^{-1}. The drying operation for the tomato samples took 15 hours to reach the desired moisture level of approximately 0.6 ±0.02 kg H_2O/kg db and 22 hours to reach the desired moisture level for the finished product (<0.1±0.02 kg H_2O/kg db).

For the main part of tomato paste samples, the continuous solar/geothermal drying was performed to obtain the moisture level of 0.6 ±0.02 kg H_2O/kg db, which was adequate for DIC texturing. This final drying stage was conducted under the operative parameters of input airflow temperature *DT* (°C) and relative humidity HR_{in} (%), and drying rate Q_{in} (kg s^{-1}), and solar radiation *I* (W m^{-2}) as determined and presented in Table (5-4) below:

***Table 5-4**: Operative parameters of pre-solar drying of tomato paste*

5.3.3 DIC treatment

DIC texturing differently pre-dried tomato paste were organized by a central two-parameter, five-level experimental design. However, preliminary trials with an initial moisture

content between 5.82 and 0.2 kg H_2O/kg db defined the most adequate moisture content value for DIC as 0.62 kg H_2O/kg db. Then, the other treatment parameters were the absolute pressure of the dry saturated steam between 0.1 and 0.5 MPa, i.e., a temperature between 100 and 152 °C, and treatment time between 10 and 50 sec. The thermo-mechanical DIC treatment is based on an abrupt pressure-drop rate of $\left(\frac{\Delta P}{\Delta t} > 0.5\ MPa\right)$towards a vacuum of absolute pressure of 5 kPa (Allaf and Allaf, 2016; Louati et al., 2019). Various physical, structural, color, and functional characteristics were used to identify the effects of the DIC conditions.

5.3.4 Hot air-drying operation

Hot air drying HAD was achieved on the tomato paste samples without (raw materials RM) and after DIC treatment. Drying airflow temperature of HAD studied at 39, 50, and 70 °C ± 1 °C with an airflow velocity higher than 3.5 m s^{-1}. Drying kinetics was studied for the range from 0.62 to 0.1 kg H_2O/kg db.

5.3.5 Drying procedure and DIC treatment

A combination between solar drying and Instant Controlled Pressure Drop treatment, "DIC" Détente Instantanée Contrôlée in French or texturing stage followed by hot air drying (HAD) at different operative parameters was conducted and presented in Figure (5.4) below:

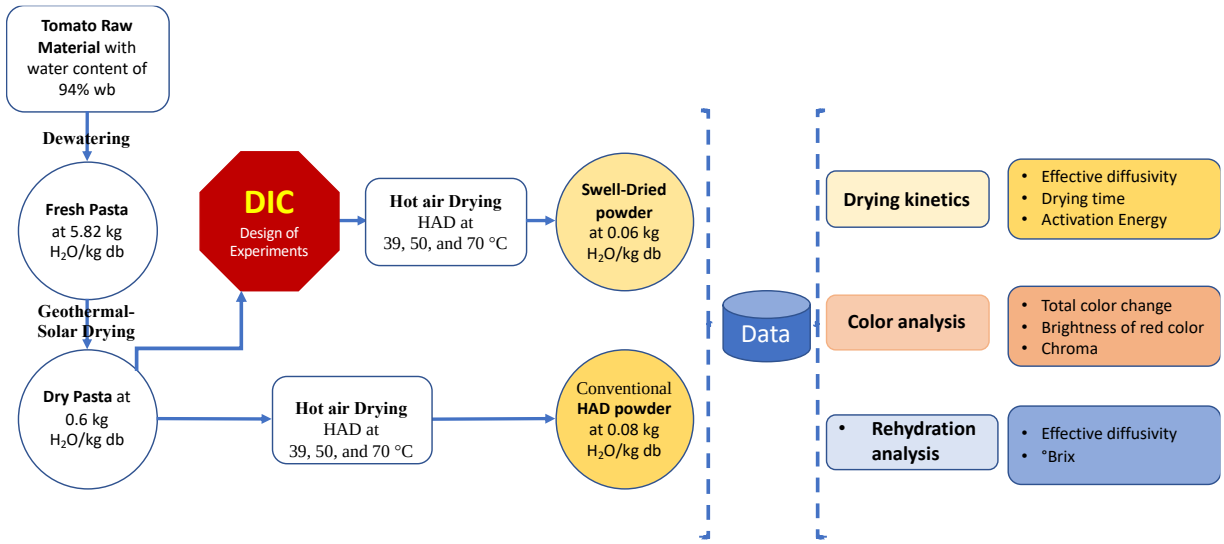

***Figure 5-4**: Dewatering and Drying procedures*

5.3.6 Drying time

Drying characteristic curves for DIC-treated and untreated tomatoes paste at different temperatures (39, 50, and 70 °C) are represented in Figure (5.5). It is clear that the DIC texturing stage has a significant influence on drying time. DIC treatment significantly reduces the drying time. A similar result was observed by Albitar et al., (2011) and Mounir et al., (2012). The drying

time of all DIC texturing stage was shorter than the controlThe obtained result is considered a crucial factor to determine the better drying process for many agricultural products in terms of reducing drying time.

***Figure 5-5**: Moisture content versus drying time*

***Figure 5-6**: Effect of DIC on drying time*

5.3.7 Determination of effective moisture diffusivity

As described in Equations (5.6-7), effective diffusivities (D_{eff}) are usually calculated by drawing experimental drying results in terms of ln (*MR*) Vs drying time; Figure (5.7).

***Figure 5-7**: ln (MR) versus time*

In one hand, the increase of drying temperature increases the effective moisture diffusivity from 1.41×10^{-9} to 3.67×10^{-9} $m^2\ s^{-1}$ for DIC treatment and from 2.95×10^{-10} to $1.43\times10^{-9} m^2\ s^{-1}$ for controlled samples. On the other hand, the texturing stage with DIC treatment improved systematically the effective diffusivity. DIC-texturing stage caused expanding the structure of tomato paste, as well as improve the effective water diffusivity. As an example, DIC texturing allowed effective diffusivity to be approximately 5 times greater than the controlled sample for T= 39°C. According to these results, on one hand, as expected D_{eff} is greater at higher drying air temperatures. Similar results were obtained by Mazzoleni et al., (2005). On the other hand, DIC treatment increases the D_{eff} of various agricultural products (Téllez-Pérez et al., 2019).

5.3.8 Activation energy

Activation energy is obtained by plotting ln (D_{eff}) against the reversed absolute temperature and calculation of the line slope, (Figure 9). Using Arhenius Equation and plotting ln (D_{eff}) against $1/T_p$, the experimental activation energy was calculated; Figure (5.8). The activation energy and D_0 at all tested temperatures are presented in Table (5-5). The activation energy, under different experimental conditions, was found to be 25.69 and 41.87 kJ mol-1 for DIC and controlled samples, respectively.

***Figure 5-8**: Ln D_{eff} versus 1/T (K^{-1})*

***Table 5-5**: Activation energy and effective diffusivity coefficient of tomato paste*

5.3.9 Visual quality

In the food industry, color is regarded to be the first creterion judged by the customers as the key product acceptance and costomers's demand.

Figure (5.9) displays the final dried product of tomato paste with SD + DIC + HAD (Solar Drying+DIC+Hot Air Drying); RM+SD+HAD (Raw Material+Solar Drying +Hot Air Drying), and tomato paste dried completely with solar drying (SD). It is worth noting that DIC texturing stage improve the final color of tomato paste compared with other drying methods (eg: for drying temperature of about 40 °C we noticed a considerable improvement in visual color and shrinkage for samples treated by DIC texturing stage compared with other processes). Also, no high correlation between drying temperature and final color or shrinkage for samples with DIC texturing stage of (P=0.3 MPa and t =30 s) was observed.

***Figure 5-9**: Visual quality of dried tomato paste with various drying methods*

5.3.10 Statistical study of the design of experiments DoE

Fourteen trials were carried out; 13 DIC textured samples and one triplicated raw-material RM (see Table 3). The dry basis water content just after the DIC treatment was $W_0 = 0.21 \pm 0.03$ gH_2O/g db (dry matter) and the final moisture content after 60 °C with 3 m s^{-1} hot air drying was $W = 0.12 \pm 0.01$ g H_2O/g db.

The impact of DIC treatment on drying kinetics was observed through three criterions: 1/ required drying time to reach the desired moisture level, from the initial moisture content, 2/ the internal effective water diffusivity, 3/ The quantified color characteristics such as intensity in red-green color, the brightness, the chroma, and the total color change. D_{eff} was determined from the slope "*k*" by drawing experimental drying results in terms of ln (*MR*) Vs drying time, considering the short time of surface air interaction at the initial time (t = 0) because of the high value of air-drying velocity superior to 5 m s^{-1}. Three samples of raw material were dried completely using HAD without DIC texturing stage. Table (5-6) also shows the middle values of drying time and D_{eff} for RM.

***Table 5-6**: Values of the process performance parameters through the drying kinetic parameters such as the drying time and the effective diffusivity, the color change such as intensity in red-green, brightness, chroma, and total color change*

5.3.10.1 Effective moisture diffusivity

Assuming that the transfer of the liquid occurs from the product core to its exchange surface, so, the drying process is completely diffusional. Figure (5.10) illustrates the impact of DIC operating parameters on effective moisture diffusivity for tomato paste samples. The obtained results showed that the higher the absolute saturated steam pressure and the thermal holding time (0.5 MPa, 30 s) correlated with the higher the effective moisture diffusivity. Statistical analysis allowed identifying the prediction models for the effective moisture diffusivity. At T= 60 °C the regression model was found with R^2= 87.19 %:

$$D_{eff} = 3.445\,10^{-9} - 1.6795\,10^{-8}P + 0.00726\,10^{-9}t + 2.5867\,10^{-8}P^2 + 1.9503\,10^{-10}Pt - 0.0008\,10^{-9}t^2$$

5.3.10.2 Determination of color parameters (a, a*/b*, C* and ΔE)*

The obtained results showed that the higher the absolute saturated steam pressure and the thermal holding time (P =0.5 MPa and t =30 s) was recorded for the higher the a^* (40.08). Statistical analysis allowed identifying the prediction models for the red color.

$$a^* = 29.917 + 2.2696P + 0.232t + 52.551P^2 - 0.8612Pt + 5.0299\ 10^{-4}t^2$$

Brightness of red color (B= a^*/b^*) of tomato paste varied between 0.68 and 0.82 for DIC texturing of (P =0.3 MPa and t =30 s) and (P =0.1 MPa and t =30 s), respectively. We observed that steam pressure plays a vital role in increasing B, decrease of "P" increases systematically B with the low effect of holding time "t". The mathematical model presents the evolution of B versus p and t is determined as follow:

$$B = 0.9497 - 0.4593P - 0.0035t + 0.2055P^2 + 0.0019Pt + 1.2669\ 10^{-5}t^2$$

Chroma (C^*) may be used to evaluate the level of color in dried food products, the grater the Chroma value, the greater the color intensity of samples viewed by customers. The obtained results show that the color intensity of tomato paste varied after DIC texturing with a variation of operative parameters. The value of C^* ranged between 51.73 and 69.04, and the maximum value was recorded for DIC texturing of (P =0.5 MPa and t = 30 s). Pareto chart in Figure (5.10) showed a significant positive effect of steam pressure "P" in an increase of C^* with a low negative effect of holding time "t". The mathematical model obtained for the evolution of "C^*" is presented below:

$$C^* = 41.9781 + 18.62P + 0.5191t + 84.3941P^2 - 1.4146Pt + 2.973910^{-4}t^2$$

A high positive relationship was noticed between the total color change and absolute steam pressure with the negative effect of holding time. The highest total color change was recorded (43.08) for (P =0.5 MPa and t =30 s) with a high correlation of a^*. The mathematical model describes the variation of total color change with the operative parameters "p" and "t" is presented below:

$$\Delta E = 23.1791 - 9.6913P + 0.4145t + 114.905P^2 - 1.2582Pt + 1.472810^{-3}t^2$$

With regard to the effect of operative parameters of DIC texturing (P, t) on D_{eff} and color quantification of tomato paste, the saturated steam pressure was found to have a significant effect on total color change, color quality, and diffusion stage with varied effects of holding time value. Hence, the central point (P =0.3 MPa and t =30 s) is taken as the suitable operative parameters for DIC texturing stage to study the drying kinetics of pre-solar dried tomato paste under (T= 39, 50, and 70 °C).

***Figure 5-10**: Impact of DIC parameters; pressure (MPa) and time (s) on the effective moisture diffusivity; red color a*; the ratio a*/b*; the Chroma C*, and the total color change ΔE: a) Pareto chart; b) Response surface*

5.3.11 Energy balance and industrial application

The study of the industrialization of the combined processes of mechanical dewatering by draining, drying by solar energy possibly joined with heat exchange with geothermal water, DIC texturing, and finally, airflow drying is mainly motivated by the energy balance in comparison with the conventional system of drying by hot air convection. The industrial partner has set a target of producing 1 ton per day of tomato powder at 0.04 kg H_2O/kg db. The mechanical dewatering can be assumed as resulting in negligible energy consumption while drying should require about 1 kWh/kg of removed vapor.

The total quantity of fresh tomatoes needed for such a daily production is estimated to be 20 tons. The tomato water resulting from the mechanical draining dewatering is about 11 tons. The Ultra High-Temperature UHT process of debacterization requires about:

4.2 (kJ kg^{-1} K^{-1}) ×100 K×11000 kg=1300 kWh

The amount of solar and geothermal energy required to dry the tomato paste from 5.82 to 0.6 kg H_2O/kg db implies the use of 5220 kWh of energy. The energy consumed by the DIC

processing of this quantity of 1.6 tons of wet tomato paste is estimated at 420 kWh. Finally, the drying of this paste from 0.6 to 0.05 kg H_2O/kg db requires a quantity of 600 kWh of heat energy.

The total energy thus implied for the production of 1 ton of tomato powder is 7600 kWh against 19000 kWh for conventional drying. It is worth noticing that the tomato water also has a clear commercial value.

5.4 Conclusion

The dewatering by draining of tomato mixture allowed removing/separating tomato water from tomato paste whose water content was about 5.82 kg H_2O/kg db (dry basis). Solar drying possibly coupled with high-temperature geothermal water was used to reduce the water content of this tomato paste to reach about 0.6 ±0.02 kg H_2O/kg db, with good preservation of the visual quality. This level of water content investigating the instant controlled pressure drop DIC texturing. The DIC texturing stage was applied on various samples, and its impacts were identified and optimized for absolute steam pressure and thermal holding time of p=0.3 MPa and t=30 s, respectively. Hot air drying (HAD) was carried out at airflow temperature of 39, 50 and 70 °C (±1 °C), velocity superior to 3 m s^{-1} to reach the desired final moisture content < 0.1 (d.b). Finally, Effective moisture diffusivities and activation energy were determined. Drying kinetics were calculated by using a model that considers the starting accessibility, the internal diffusion model with Fick's law, and the paradoxical stage. The DIC process improves the drying kinetics; this behavior could be related to the increase of water activity "a_w". Although, activation energy is reduced when rapidly increasing of a_w, because of the new expanded structure obtained by the high-porosity DIC textured paste. A comparison of visual quality revealed a high correlation between DIC texturing stage and visual quality improvement, with a low effect of drying temperature. As a conclusion, compared with the conventional drying methods (Hot-air drying HAD or solar drying SD), this new dehydration operation coupling the various processes of draining dewatering, solar/geothermal drying, DIC texturing / Swell-drying stage had a significant effect on improving the drying kinetics, greatly reducing the energy consumption, and increasing the visual quality.

6 Exergy and Energy Analysis of Hybrid Solar Electric Drying of Garlic

6.1 Introduction

Garlic (Allium sativum L., Alliaceae) has been playing one of the most important dietary and medicinal roles in human beings for centuries (Bozin et al., 2008). Fresh garlic yields the sulfur-containing compounds allicin, ajoene, diallyl polysulfides, vinyldithiins, and S-allylcysteine; as well as enzymes, saponins, flavonoids, and Maillard reaction products, which are not sulfur-containing compounds ("https://en.wikipedia.org/wiki/Garlic," 2021). It has been yielded since ancient times, used as a powder and flavors, and has been used in many cultures due to its benefits in curative and preventive medicine. Due to a lack of transference, conversion, and storage, 30% of the world garlic production is thrown away every year (Younis et al., 2018).

In many regions in the world, where garlic is cultivated, the drying process is the most commonly used to preserve the surplus. Nowadays, open sun drying of crops takes a lot of time and harms the environment by smells (Ali et al., 2016). Therefore, several scientific works provide an innovative drying process, with significant efficacy.

Various researches using hybrid solar drying systems have been carried out for drying of ago-products. In Algeria, many researches using experimental investigations and mathematical modelling studies have been carried out to improve the solar drying of various agro-products such as tomato Djebli et al., (2019); Manaa et al., (2013) and Mennouche et al., (2018), potatoes Chouicha et al., (2013), dates Boubekri et al., (2009) and Mennouche et al., (2017), pumpkin slice Benseddik et al., (2018), henna leaves Bennaceur et al., (2015), camel meat Chaouch et al., (2018). However, with the increase of garlic produce in Algeria, there is a real research gap in the treatment of garlic by solar drying means. According to the Algerian Ministry of Agriculture ("www.radioalgerie.dz/news/ar/article/20190521/170361.html," 2019.), in 2019, Algeria has achieved a large excess in garlic production reached 8 thousand tons with a total area planted of 11700 hectares. The price of one kilogram reached 0.078 USD in the harvest season and most of the producers then suffered from large losses of surplus production which were eventually burned. On the other hand, it reached 15.5 USD in the rest of the seasons due to the lack of an effective way of preservation. As a result, the present study was conducted, using a hybrid solar-electric dryer (HSED). The HSED operated with three drying temperatures; 50, 60, and 70 °C under natural convection (NC) and air velocity of 4.1 and 6.9 m s^{-1}. Therefore, the primary objectives of the presented chapter are:

(i) Mathematical modelling and characteristic drying curve of dried garlic.

(ii) Environmental analysis and energy payback time of the HSED.

(iii) Exergy analysis of the drying chamber, waste exergy ratio, sustainability exergy index, and improvement potential as well as the environmental impact factor was determined.

6.2 Methods and materials

6.2.1 Determination of moistures and drying rate

Twenty kilograms of fresh garlic cloves were dried in these experiments. The cloves of 1.5 cm thickness were selected out one by one using a visual criterion such as height, lack of physical injury, and uniform ripening degree. The garlic cloves were unpeeled and sliced into half of 0.75 cm thickness garlic cloves.

The initial moisture content of garlic cloves was measured by using the oven technique at 105 °C for 24 h. Average moisture content was found to be 2.35 (d.b) or 70 % (w.b). The moisture content at any time (M), moisture ratio (MR), and drying rate (DR) values were determined using Equations (6.1-3) as follows:

$$M_t = \frac{m_t - m_d}{m_d} \quad \text{(Eq. 6.1)}$$

$$MR = \frac{M_t - M_e}{M_0 - M_e} \quad \text{(Eq. 6.2)}$$

$$DR = \frac{M_{t+\Delta t} - M_t}{\Delta t} \quad \text{(Eq. 6.3)}$$

6.2.2 Solar dryer description

The present dryer consists mainly of (i) a drying chamber (1 m^3) and a solar collector (2 m^2) containing an absorbent plate and directly attached to the drying chamber without any air conduct being used; (ii) an electric fan of 10 cm diameter, used to accelerate the drying air; and (iii) an electric resistance used as an auxiliary heating system placed inside the drying chamber (2kW: accuracy ± 2%). The collector is fixed and tilted at 30° to the south-facing horizontal. A schematic of the used dryer is shown in Figure (6.1).

The HSED operates as follows: The inlet air to the solar collector is heated by the absorbent plate and greenhouse effect due to the exposure of solar intensity on the glass cover. The heated air arrives at the inlet of the dryer chamber with variable temperature. Inside the chamber, the air can be heated by an auxiliary heating system to meet and control the desired drying temperature. The drying air is then extracted by the exhaust fan. The rotating velocity of the electric fan could be controlled, by adjusting the electric power delivered.

Previous work was performed to estimate and model the temperature field and drying airflow profile inside the chamber, shows that the temperature variation does not exceed 1.4 °C in both natural and forced convection (Zoukit et al., 2019).

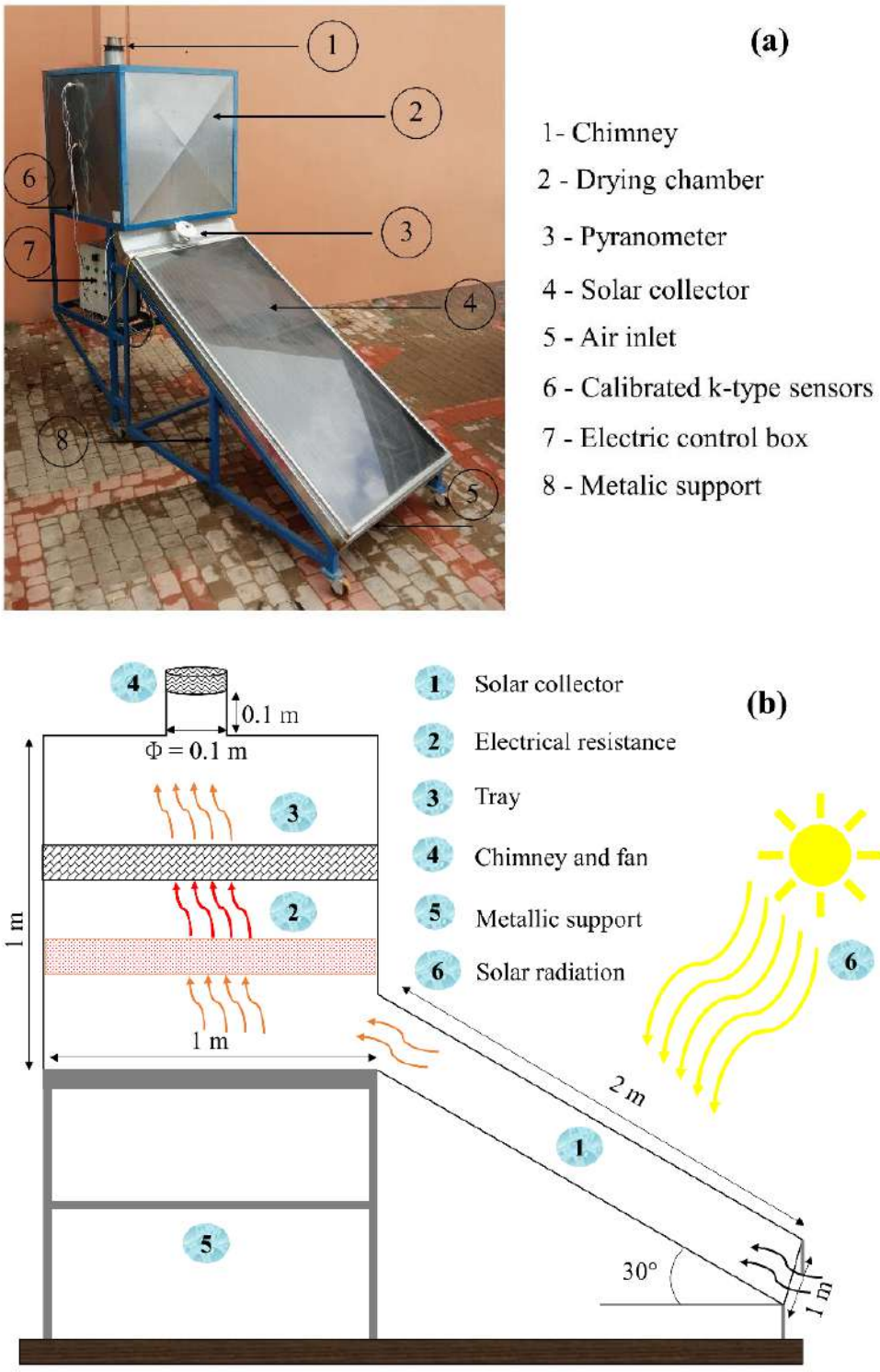

***Figure 6-1**: a: Picture of the HSED, b: Schematic of the HSED*

As shown in Table (6-1), nine experiments of hybrid solar-electric drying of garlic slice at drying temperatures of 50, 60, and 70°C were carried out with non-controlled natural ventilation and artificial ventilation at 4.1 and 6.9 m s^{-1}.

***Table 6-1**: Experimental conditions of the hybrid solar-electric drying of garlic cloves*

Run	*Relative humidity (%)*	*V (m s^{-1})*	*T (°C)*	*Drying time (h)*	*Drying time (min)*
1	23.26	---	50	20	1200
2	19.5	---	60	14	840
3	13.6	---	70	5	300
4	15.58	4.1	50	7	420
5	13.1	4.1	60	5	300
6	10.9	4.1	70	3	180
7	14.37	6.9	50	3.5	210
8	12.1	6.9	60	3	180
9	8.44	6.9	70	2.5	150

6.2.3 Determination of characteristics drying curve (CDC)

The characteristics drying curve (*CDC*) permits to determine the impact of drying temperature on garlic cloves drying kinetics, using Van Meel (1958) theory of the(*CDC*). This characteristic curve is obtained under constant drying temperature, drying air velocity, and relative humidity through a uniform drying rate curve. Firstly, the experimental moisture content values in dry basis were transformed to the moisture ratio (*MR*) expression and fit the curve to the drying time for the specified drying model. Secondly, this curve of moisture ratio (*MR*) can be used to extend the use of the data in the solar dryer with an additional heating and ventilation system. Finally, the *CDC* equation is defined by f = f(*MR*) and detailed in Equation (6.4), (Borah et al., 2015):

$$f = -\left(\frac{dM}{dt}\right)_t / -\left(\frac{dM}{dt}\right)_0 \qquad \text{(Eq. 6.4)}$$

For suitable constant experimental parameters as temperature, drying air velocity, humidity, and size of the garlic cloves, the characteristic drying curve has to verify the properties mentioned below (Koukouch et al., 2015).

$$f = 0 \quad for\ MR = 0 \qquad \text{(Eq. 6.5)}$$

$$0 \leq f \leq 1 \quad for \quad 0 \leq MR \leq 1 \qquad \text{(Eq. 6.6)}$$

6.2.4 *Fitting of the solar drying curves*

The experimental outputs were fitted to nine empirical and semi-empirical models to predict the variation in the moisture content of garlic cloves during hybrid solar-electric drying. Among the tested models, the most appropriate one was selected according to the statistical parameters given in Equations (6.7-9). Origin software is used for the regression analyses. The obtained drying curves of experimental *MR* were fitted with nine models are given in Table (6-2).

***Table 6-2**: Moisture ratio equations applied to the experimental drying curves*

Model name	*Model*	*Reference*
Lewis	$MR = exp(-kt)$	(Bruce, 1985)
Page	$MR = exp(-kt^n)$	(PAGE, 1949)
Logarithmic	$MR = a\,exp(-kt) + c$	(Toğrul and Pehlivan, 2002)
Two-term	$MR = a\,exp(-kt) + b\,exp(-k_1 t)$	(Henderson, 1974)
Wangh and Singh	$MR = 1 + at + bt^2$	(Wang and Singh, 1978)
Verma et al.	$MR = aexp(-kt) + (1-a)exp(-gt)$	(Verma et al., 1985)
Diffusion of approximation	$MR = aexp(-kt) + (1-a)exp(-kbt)$	(Kassem, 1998)
Midili and Kucuk	$MR = aexp(-kt^n) + bt$	(Midilli et al., 2002)
Henderson and Pabis	$MR = a\,exp(-kt)$	(Pabis, 1961)

Based on Akpinar and Bicer (2008) hypothesis, the highest correlation coefficient (r), the lowest mean bias error (*MBE*), and the lowest reduced chi-square (χ^2) can be selected for the most appropriate drying model. These statistical parameters are given as follows:

$$r = \frac{\sum_{i=1}^{n}(MR_i - MR_{pre,i}) \cdot \sum_{i=1}^{n}(MR_i - MR_{\exp,i})}{\sqrt{\left[\sum_{i=1}^{n}(MR_i - MR_{pre,i})^2\right] \cdot \left[\sum_{i=1}^{n}(MR_i - MR_{\exp,i})^2\right]}} \quad \text{(Eq. 6.7)}$$

$$MBE = \left[\frac{\sum_{i=1}^{n}(MR_{pre,i} - MR_{\exp,i})}{N}\right] \quad \text{(Eq. 6.8)}$$

$$\chi^2 = \frac{\sum_{i=1}^{N}(MR_{exp,i} - MR_{pre,i})^2}{N - P} \quad \text{(Eq. 6.9)}$$

6.2.5 *Determination of effective moisture diffusivity*

The effective moisture diffusivity is defined by the term (D_{eff}) in ($m^2\ s^{-1}$) and used to describe all means of transporting water inside a sample. It's the main physical property in the

drying of food and other materials allow to model the moisture movement from the core to the surface. It characterizes a function of drying temperature and moisture content evolution in material (Oztop and Akpinar, 2008). Commonly, the effective moisture diffusivity was calculated by using the second simplified Fick's law as given in Equation (6.10):

$$\frac{\partial MR}{\partial t} = \nabla\left[D_{eff} \nabla\left(\frac{M_t - M_e}{M_0 - M_e} \right) \right] = D_{eff} \nabla^2 \left(\frac{M_t - M_e}{M_0 - M_e} \right) \quad \text{(Eq. 6.10)}$$

Based on Crank (Crank, 1979) correlation, solving Fick's second law by assuming:

1. The drying process is totally diffusional;
2. The diffusion coefficient and product temperature are constants;
3. Neglected shrinkage during the drying process;
4. Infinite slab geometry.

$$MR = \frac{8}{\pi^2} \sum_{n=1}^{\infty} \frac{1}{(2n+1)^2} \exp\left(-(2n+1)^2 \pi^2 \frac{D_{eff}.t}{4L^2} \right) \quad \text{(Eq. 6.11)}$$

For a considerably longer drying time, all terms of the above series are marginal relative to the first term. Thus, Equation (Eq. 6.12) becomes:

$$MR = \frac{8}{\pi^2} \exp\left(-\pi^2 \frac{D_{eff}.t}{4L^2} \right) \quad \text{(Eq. 6.12)}$$

Effective moisture diffusivity was determined by plotting experimental drying results for ln (*MR*) vs drying time(s). After the slope of the straight line is determined, D_{eff} has been calculated using Equation (6.13):

$$Slope = -\frac{\pi^2 D_{eff}.t}{4L^2} \quad \text{(Eq. 6.13)}$$

6.2.6 Determination of activation energy

The activation energy (E_a) in (kJ mol^{-1}) is the relative ease with which water molecules override an energy obstacle as it is transported through the pores of the product. The reliance between the diffusion process and absolute temperature can be defined by an Arrhenius type equation as follows:

$$D_{eff} = D_0 \exp\left(-\frac{E_a}{RT_{abs}} \right) \quad \text{(Eq. 6.14)}$$

The activation energy values can be calculated as follow:

In the first step, by entering the natural logarithm on both sides, Equation (6.14) becomes:

$$\ln(D_{eff}) = \ln(D_0) - \frac{E_a}{R}\frac{1}{T_{abs}} \quad \text{(Eq. 6.15)}$$

In the second step, E_a is calculated by plotting the natural logarithmic of effective moisture diffusivity $\ln(D_{eff})$ against the reciprocal of the absolute temperature $(1/T_{abs})$. Finally, the slopes $(-E_a / R)$ for each temperature determine the numerical values of activation energy.

6.2.7 Energy analysis

Energy analysis in industrial systems plays a vital role in global and national companies. It is extremely important for solar thermal systems such as solar dryers, to save energy, reduce the cost price, reduce the energy payback time, and mitigate the carbon credit. In the present work, energy analysis is studied for drying temperatures ranged between 50 and 70°C, with non-controlled artificial ventilation (passive mode) and drying air velocity of 4.1 and 6.9 m s^{-1} (active mode).

6.2.7.1 Embodied Energy (E_m)

The embodied energy (E_m) in (kWh) is the required energy to produce any body, thing, or service. The embodied energy is considered a crucial criterion for measuring the intensity of carbon dioxide that causes global warming due to the large consumption of energy.

Table (6-3) presents the conventional values of the embodied energy coefficient with the total energy for the used materials in the manufacture of the active HSED. The total embodied energy of the hybrid solar dryer under passive mode is estimated to be 917.66 (kWh).

***Table 6-3**: Embodied energy and embodied energy coefficient for active HSED construction*

Material	*Quantity (kg)*	*E_m*	*Total (kWh)*	*Reference*
Aluminium	7.84	55.28	433.3952	(Baird et al., 1997)
Glass cover	10.12	7.28	73.6736	(Baird et al., 1997)
Steel sheet	11.34	8.89	100.8126	(Baird et al., 1997)
Iron	7.3	25	182.5	(Baird et al., 1997)
Plastic	0.1	19.44	1.944	(Baird et al., 1997)
Coper	3	19.61	58.83	(Baird et al., 1997)
Paint	1.35	25.11	33.8985	(Baird et al., 1997)
Fittings (nuts, bolts, screw and rivets)	1	8.89	8.89	(Baird et al., 1997)
Glass fiber insulation (glass-wood)	6.35	4.044	25.6794	(Baird et al., 1997)
Total (kWh)			**919.6233**	

6.2.7.2 Energy payback time (EPBT)

The required time in years to pay back the embodied energy of any system is called energy payback time (*EPBT*). It's defined by the next equation (Vijayan et al., 2020):

$$\text{Energy payback time (EPBT)} = \frac{\text{Embodied Energy}}{\text{Annual Energy Output}} \qquad \text{(Eq. 6.16)}$$

6.2.7.3 CO_2 emission of the dryer

The average CO_2 emission is equivalent to approximately 0.98 kg CO_2 / kWh for coal-generated electricity case. Equation (6.17) determines the annual carbon dioxide emissions (Chauhan et al., 2018).

$$CO_2 \text{ emissions per year} = \frac{\text{Embodied energy} \times 0.98}{\text{Lifetime}} \qquad \text{(Eq. 6.17)}$$

According to the designer, lifetime is approximately 13 years.

6.2.7.4 Carbon dioxide mitigation

Carbon dioxide (CO_2) mitigation in kilowatt-hour is the main criterion used for determining climate change.

A carbon credit is described as "a crucial element of national and international emissions trading strategies that have been introduced to reduce global warming." Carbon credit trade can be purchased on the foreign market or as a company at the market valuation.

The daily efficiency (η_d) can be defined as:

$$\eta_d = \frac{\text{Daily output energy}}{\text{Daily input energy}} = \frac{M\,\lambda}{I_m(t)A_c}10^2 \qquad \text{(Eq. 6.18)}$$

Where:

M is the evaporated moisture in (kg), λ presents the latent heat of evaporation in (J/kg) and taken 2. 26 $\times 10^6$J/kg; I_m is the average solar radiation falling on the hybrid dryer; A_c is the collector area. In the current study, I_m and A_c are taken 500 W/m^2 and 2 m^2, respectively.

$$\text{The daily thermal output of the dryer (kWh)} = \frac{\text{Evaporated moisture (kg)} \times \text{ latent heat of evaporation (J/kg)}}{3.6\ 10^6} \qquad \text{(Eq. 6.19)}$$

$$\text{The annual thermal output energy of the dryer } (E_{\text{aout}}) = \text{Daily thermal output energy of dryer} \times N_d \qquad \text{(Eq. 6.20)}$$

The drying system allows evaporating a total of 8.8 kg/day of moisture. The annual thermal output of the dryer is the result of the daily thermal output of the dryer and the number of total assumed sunshine days in a year (N_d) i.e. 305 days.

$$\text{Daily input energy (kWh)} = \mathrm{I}_m(t) \times N_h \times A_c \times 10^{-3} \quad \text{(Eq. 6.21)}$$

Where, N_h presents the sunshine hours per day, which is taken as 7 h.

If the losses caused by distribution and transmission effect L_{td} are considered as 45% and domestic losses L_{a} are taken as 10%. Therefore, the amount of CO_2 mitigation of the system (X) would be:

$$X = \frac{1}{1 - L_a}\frac{1}{1 - L_{\mathrm{td}}}\ 0.98 \approx 2\ \mathrm{kg} \quad \text{(Eq. 6.22)}$$

$$\mathrm{CO_2}\ \text{mitigation in the lifetime of the dryer} = E_m\ X \quad \text{(Eq. 6.23)}$$

$$\text{The net mitigation of } \mathrm{CO_2} \text{ over lifetime(kg)} = \text{Total } \mathrm{CO_2} \text{ mitigation - Total } \mathrm{CO_2} \text{ emission} = [E_{\mathrm{aout}}.n.X - E_m] \quad \text{(Eq. 6.24)}$$

Where n is the lifespan of the HSED, which is considered 25 years.

6.2.7.5 Carbon credit earned of the dryer

Generally, the mitigation of 1 ton of emission is comparable to one carbon credit. Carbon credit earned value can be defined as following, (Tiwari and Tiwari, 2016):

$$\text{Earned carbon credit} = \text{Net mitigation of } \mathrm{CO_2} \text{ in lifespan (tonnes)} \times D \quad \text{(Eq. 6.25)}$$

Where D is the cost of carbon credit, which varies from USD5 to USD20/ton of CO_2 mitigation, and since USD1 is equal to almost 129 DZD (Algerian Dinar) or 10 MAD (Moroccan Dirham).

6.2.8 Exergy analysis

The basic procedure for exergy analysis of the drying chamber in (kJ s^{-1}) unit is to determine the exergy values at the steady-state regime and the reason for the exergy variation for the process. The general equation representing the total exergy of a system can be expressed as follow:

$$Ex_{tot} = Ex_{ph} + Ex_c + Ex_k + Ex_p \quad \text{(Eq. 6.26)}$$

Where Ex_{tot} is the total exergy of the drying system, Ex_{ph}, Ex_c, Ex_k, and Ex_p are the physical exergy, the chemical exergy, the kinetic exergy, and the potential energy, respectively.

Or, by expanding the terms:

$$Ex_{tot} = (U - U_0) + p_0(V - V_0) - T_0(S - S_0) + \frac{1}{2}mv^2 + mgz + (Ex_R + Ex_N) \quad \text{(Eq. 6.27)}$$

Where the "0" subscript denotes the thermodynamic environment conditions, and Ex_R and Ex_N are respectively the reactive and the non-reactive exergy.

Some assumptions must be made to obtain the total exergy equation as follows:

(i) Steady flow and constant pressure i.e., (V=V_0);
(ii) Negligible kinetic energies of the system and environment i.e., Ex_k=0;
(iii) Negligible gravitational effects i.e., Ex_p= 0;
(iv) Absence of chemical reactions i.e., Ex_c= 0.

According to the above assumptions the total exergy is consists of physical exergy due to deviation in temperature alone as pressure deviation is neglected. Therefore, the total exergy expression can be deduced as shown as follow (Benhamza et al., 2021):

$$Ex_{tot} = E_{ph} = \Delta U_0 - T_0\Delta S_0 = \dot{m}C_p(T - T_0) - T\dot{m}C_p \times \ln\left(\frac{T}{T_0}\right) \quad \text{(Eq. 6.28)}$$

For a unit mass, the flow rate of drying air is:

$$Ex = c_p\left[(T - T_0) - T_0 \times \ln\left(\frac{T}{T_0}\right)\right] \quad \text{(Eq. 6.29)}$$

The equations of exergy inflow and outflow for the drying chamber are as below:

$$Ex_i = \dot{m}C_p\left[(T_i - T_0) - T_0 \ln\frac{T_i}{T_0}\right] \quad \text{(Eq. 6.30)}$$

$$Ex_o = \dot{m}C_p\left[(T_o - T_0) - T_0 \ln\frac{T_o}{T_0}\right] \quad \text{(Eq. 6.31)}$$

Hence, the exergy loss is determined by:

$$Ex_l = Ex_i - Ex_o \quad \text{(Eq. 6.32)}$$

And the exergy efficiency η is given by:

$$\eta = 1 - \frac{Ex_l}{Ex_i} \quad \text{(Eq. 6.33)}$$

6.2.8.1 Exergy-based sustainability indexes

Since drying operations encompass developing and convicting heat transfer, its environmental impact is considered for sustainable development.

$$W = \frac{E\,x_l}{E\,x_i} \quad \text{(Eq. 6.34)}$$

$$S_i = \frac{1}{1-\eta} \quad \text{(Eq. 6.35)}$$

$$I_p = (1-\eta)Ex_l \quad \text{(Eq. 6.36)}$$

Where I_p is the Improvement potential, W is the Waste exergy ratio, and S_i is the Sustainability index.

6.2.8.2 Environmental impact factor

The environmental impact factor (E_{IF}) can be deduced by the flowing formula:

$$E_{IF} = W\frac{1}{\eta} \quad \text{(Eq. 6.37)}$$

6.3 Results and discussion

6.3.1 Drying time and drying phases

The evolution of moisture content at different experimental conditions against drying time is presented in Figure (6.2). It was observed a high decrease in drying time with controlled temperature without ventilation (In natural convection (NC)), and low influence for high velocity of 4.1 and 6.9 m s^{-1} at similar drying temperature, so, drying temperature played a vital role in the decrease of drying time by increasing the mass transfer from the core to the garlic surface. The values of drying time at different experimental conditions are presented above in Table (6.1).

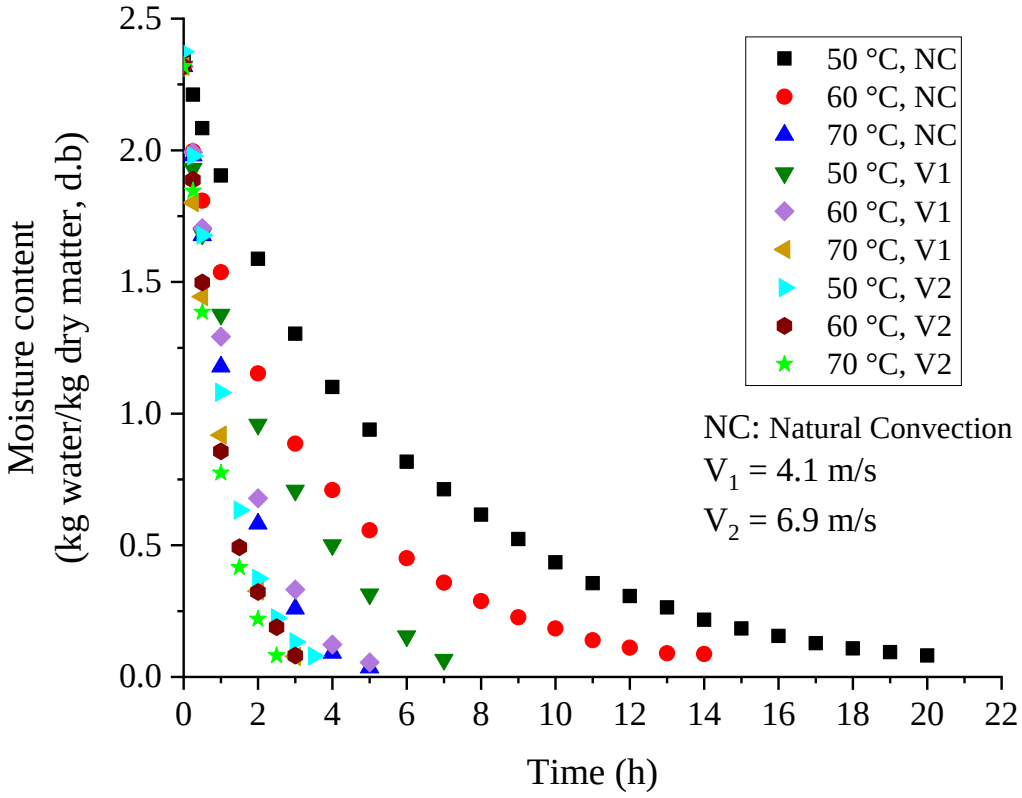

***Figure 6-2**: Influence of experimental conditions on the drying time*

Otherwise; Figure (6.3) displays the effect of drying air velocity on the drying process. It is observed for T = 50 and 60 °C without ventilation, the presence of phase I and phase II, and only phase II for T = 70 °C. The increase of drying air velocity revealed the absence of phase I, and the drying process was conducted in phase II for the used drying temperatures. The increase of drying air velocity leads to limit the surface-air interaction and allows the supply energy to warm the garlic cloves and evaporate the water vapor, so the process is totally controlled by the internal diffusion.

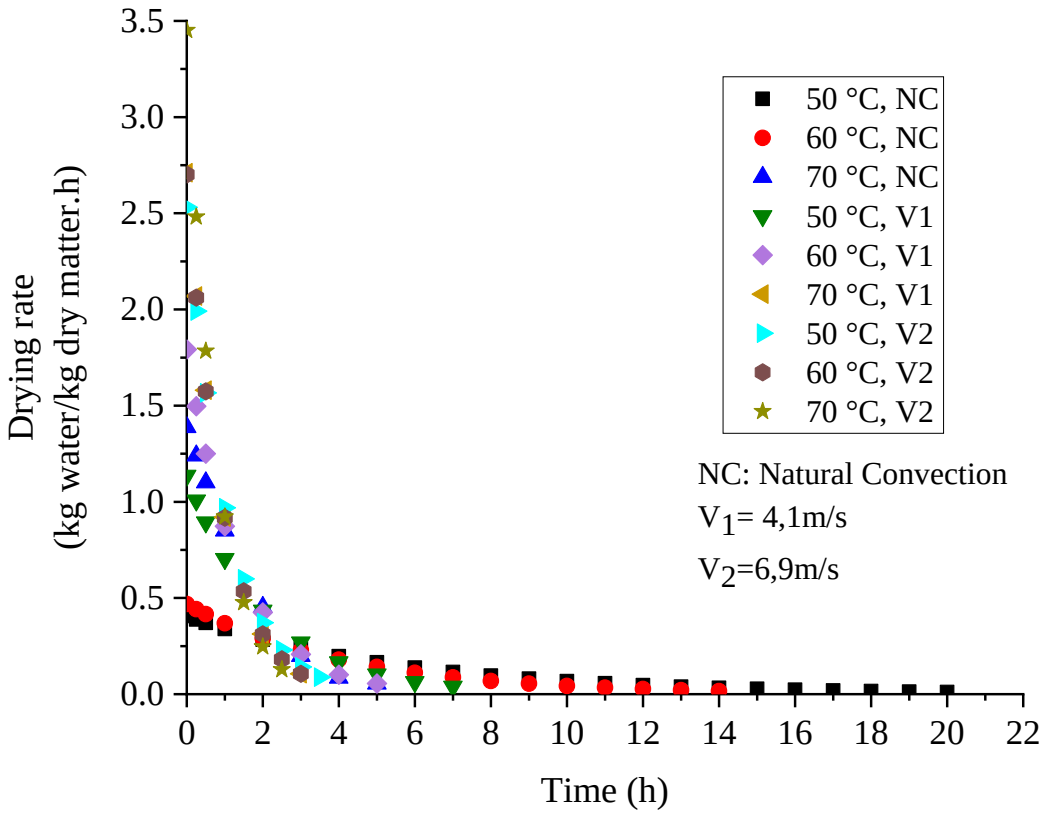

***Figure 6-3**: Drying rate (DR) against drying time for the experimental conditions*

6.3.2 Influence of experimental conditions on drying rate

Figure (6.4) illustrates the influence of drying air temperature and drying air velocity on drying kinetics of garlic for three drying temperatures (50, 60, and 70 °C) in cases of non-ventilated process and ventilated process with two different air-drying velocities. We can notice that, for the same drying air velocity, the increase in drying temperature increases systematically the drying rate. Thus, as expected, the drying kinetics of garlic cloves are affected by the drying temperature. This result is in line with previous work established in similar configurations for the drying of agro-products (Koukouch et al., 2017). Otherwise, the obtained results revealed a low impact of drying air velocity at high temperatures to 70°C, and it becomes more significant at the lowest temperatures of 50 and 60 °C. The same trend has been postulated by Mghazli et al., (2017).

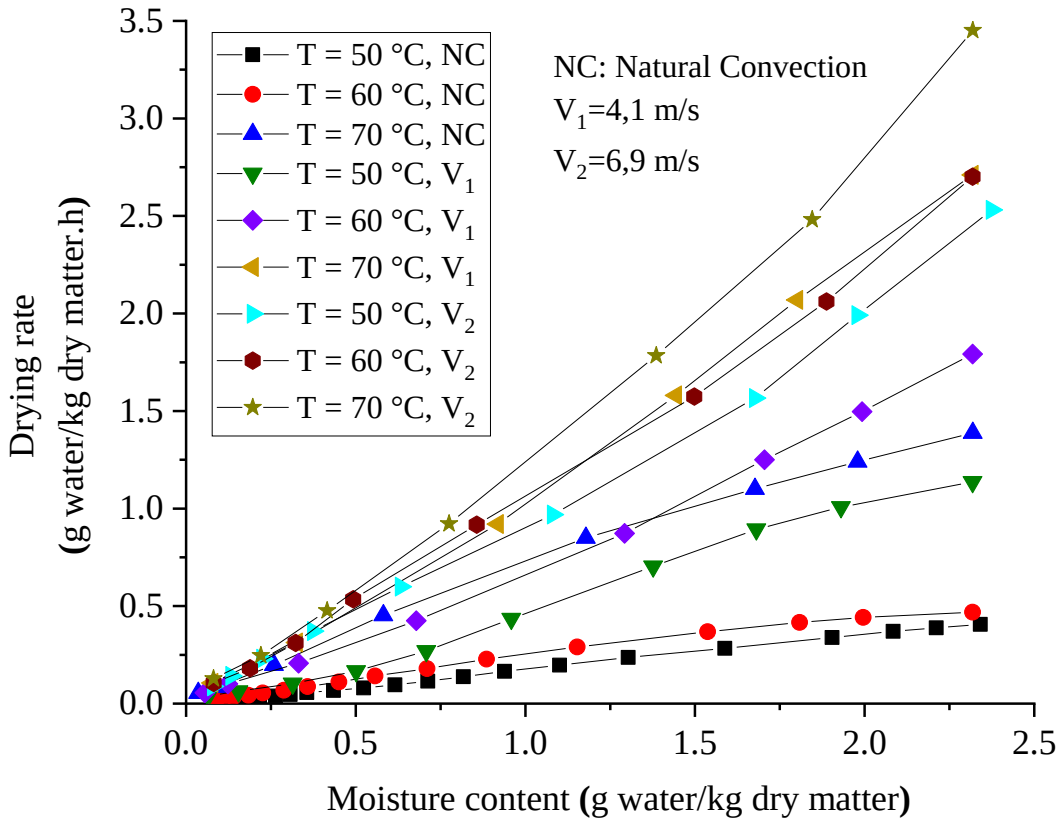

***Figure 6-4**: Impact of experimental drying conditions on the drying rate of garlic cloves*

6.3.3 Determination of characteristic drying curve CDC

Figure (6.5) shows the plot of the *CDC*; it consists of summarizing the results obtained based on the performed experiments by normalizing the drying kinetics of garlic cloves in a theoretical experiment-based model. The approved method was to create a reliance between the drying kinetics of garlic cloves in the form of a third-order polynomial of moisture ratio *MR* equation employing nonlinear optimization Levenberg-Marquard (Huang et al., 2016).

The dimensionless drying rate (*f*) can be defined by fitting the experimental data of garlic characteristic drying curves as bellow:

$$f = 0.752MR + 0.249MR^2 + 0.002MR^3 \qquad \text{(Eq. 6.37)}$$

Two criteria were considered to assess the best fit (mean bias error, *MBE* = 0.01135, and the correlation coefficient, *r* = 0.99936)

The benefit of this characteristic curve is its individuality and ease of use. It considers the combined impacts of the aerothermal factors of the drying air and the garlic behavior through the drying process.

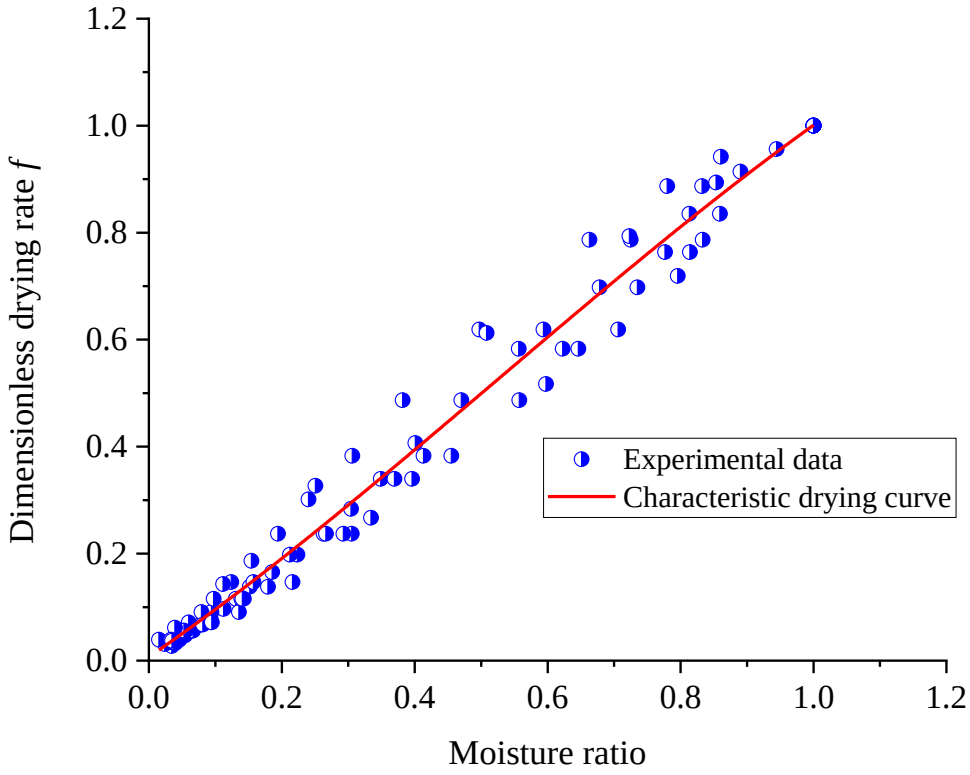

***Figure 6-5**: Characteristic drying curve of garlic cloves*

6.3.4 Modeling of the drying curves

The experimental curves were adjusted by nine mathematical models to provide an appropriate description of the drying kinetics. The adjustment was fulfilled by using the nonlinear optimization method based on the Levenberg-Marquard algorithm. The statistical parameters in each case were calculated and summarized in Table (6-4).

The results of the statistical average calculations of the parameters have been collated in Table (6.5). Although the correlation coefficient "*r*" remains high for the nine empirical models (0.9783 and 0.9992), it seems that Midilli-Kucuk model displayed the highest average value of (r = 0.9992), the lowest values of (χ^2 = 0.00016) and (MBE = 0.0018). This model was spotted to describe the drying behavior of garlic in the temperature range [50°C-70°C].

To highlight the temperature effect on the Midilli-Kucuk model coefficients, the a, k, n, and b expressions are written in the function of the drying temperature between 50 and 70 °C as follow:

$$a = 0.9572 + 0.0008T + 0.000007T^2$$
$$k = 1.3767 - 0.0382T + 0.0005T^2$$
$$n = -1.3624 + 0.0603T - 0.0004T^2$$
$$b = -0.1794 + 0.0062T - 0.00046T^2$$

Figures (6.6-7) show a good enough alignment of experimental values of moisture ratios and the calculated values delivered by Midilli-Kucuk's model.

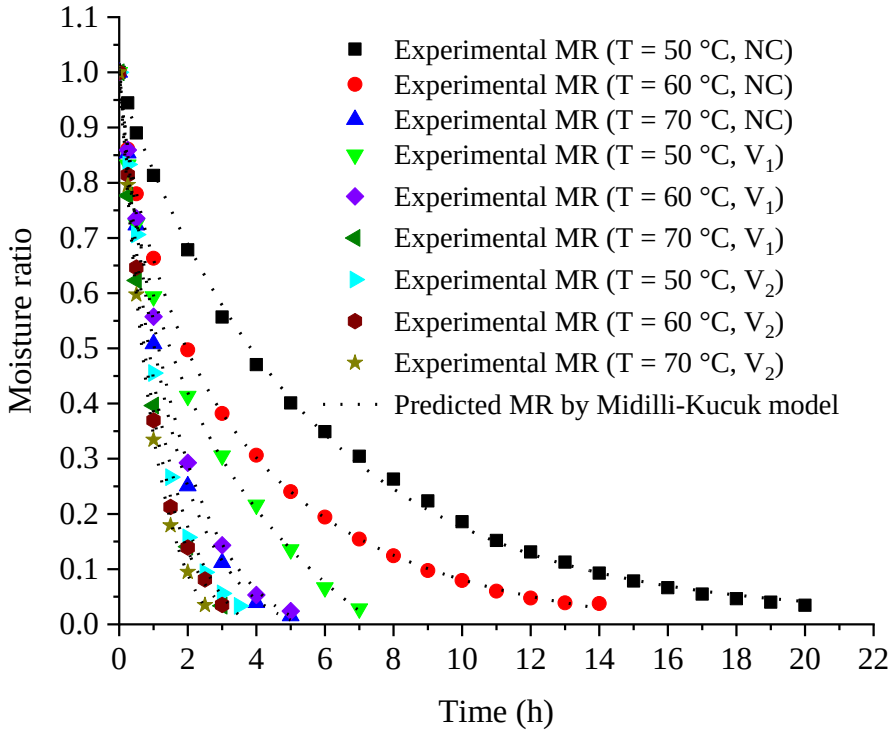

***Figure 6-6**: Experimental moisture ratio versus drying time fitted with Midilli-Kucuk model*

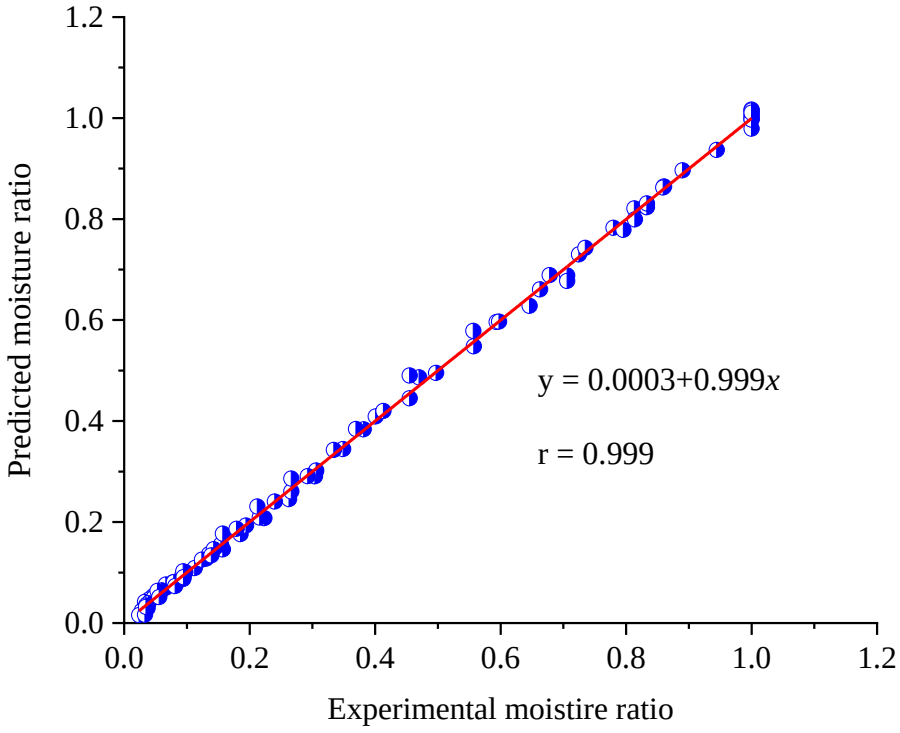

***Figure 6-7**: Predicted values of moisture ratio by Midilli-Kucuk's model versus experimental values (MR)*

***Table 6-4**: The average statistical parameters of fitted mathematical models*

Models	*Cst*	*50°C*	*60°C*	*70°C*	*50°C, V_1*	*60°C, V_1*	*70°C, V_1*	*50°C, V_2*	*60°C, V_2*	*70°C, V_2*
Lewis	*k*	0.176	0.303	0.693	0.444	0.625	0.9625	0.845	0.972	1.096
Page	*k*	0.207	0.410	0.676	0.520	0.607	0.9635	0.809	0.963	1.101
	n	0.915	0.781	1.070	0.828	1.061	1.0192	1.163	1.102	1.123
Logarithmic	*a*	0.964	0.900	1.037	0.938	1.045	1.0288	1.076	1.045	1.072
	k	0.178	0.319	0.649	0.414	0.562	0.8837	0.757	0.923	0.975
	c	0.014	0.041	-0.032	0.004	-0.047	-0.036	-0.05	-0.030	-0.061
Two-term	*a*	0.097	0.214	0.506	0.130	0.504	0.4997	0.514	0.510	0.511
	k_0	0.895	1.846	0.706	5.210	0.632	0.9618	0.873	0.997	1.124
	b	0.901	0.78	0.506	0.870	0.504	0.4997	0.514	0.510	0.511
	k_1	0.159	0.232	0.706	0.373	0.632	0.9617	0.873	0.997	1.124
Wang and Singh	*a*	-0.124	-0.194	-0.492	-0.321	-0.459	-0.736	-0.63	-0.733	-0.832
	b	0.004	0.009	0.060	0.027	0.053	0.1402	0.103	0.141	0.182
Verma *et al.*	*a*	0.901	0.216	-6.147	0.870	-0.559	10.324	-8.78	-10.94	-7.573
	k	0.159	1.948	0.459	0.373	0.307	0.9616	1.42	0.649	0.645
	k_0	0.906	0.232	0.485	5.194	0.484	0.9615	1.34	0.671	0.686
Diffusion of Approximation	*a*	1	1	9.751	1	1	1	1	1	1
	k	0.176	0.303	0.693	0.444	0.625	0.9625	0.845	0.972	1.096
	b	1	1	1	1	1	1	1	1	1
Midilli-Kucuk	*a*	0.964	0.997	1.037	1.001	1.045	1.0287	1.076	1.045	1.072
	k	0.422	0.409	0.805	0.487	0.750	0.9400	0.870	0.961	0.987
	n	0.422	0.761	0.805	0.681	0.750	0.9400	0.870	0.961	0.987
	b	0.014	-0.001	-0.032	-0.019	-0.047	-0.036	-0.05	-0.030	-0.061
Henderson and Pabis	*a*	0.974	0.925	1.013	0.942	1.008	0.9994	1.029	1.021	1.022
	k	0.171	0.275	0.706	0.409	0.632	0.9617	0.873	0.997	1.124

***Table 6-5**: Average values of modeling parameters (R, MBE, and x^2)*

Models	*r*	*MBE*	χ^2
Lewis	0.9942	0.0238	0.00068
Page	0.9989	0.0109	0.00016
Logarithmic	0.9977	0.0159	0.00034
Two-term	0.9981	0.0193	0.00044
Wang and Singh	0.9783	0.0471	0.00274
Verma *et al.*	0.9991	0.0108	0.00015
Diffusion of approximation	0.9942	0.0274	0.00088
Midilli-Kucuk	0.9992	0.0018	0.00016
Henderson and Pabis	0.9964	0.0208	0.00048

6.3.5 Effective moisture diffusivity

Figure (6.8) presents the variation of ln (*MR*) versus time (t) in hours. A slight deviation of the logarithm from the linearity can be noticed for the experimental data delivered by the conducted drying tests. This deviation can be explained by multiple effects: e.g. non-uniformity of initial moisture content, a fluctuation in product temperature during experiments, a variation of the moisture diffusivity according to the moisture content, and the shrinkage effect of the product.

The deviation from the linearity of the experimental logarithmic drying curve means that D_{eff} is reliant on the moisture content (Celma et al., 2009). Thus, the plot of ln (*MR*) against drying time (t) was represented using nonlinear regression of a quadratic polynomial equation with a good fit of experimental results:

$$\ln(MR) = A_0 + A_1 t + A_2 t^2 \qquad \text{(Eq. 6.27)}$$

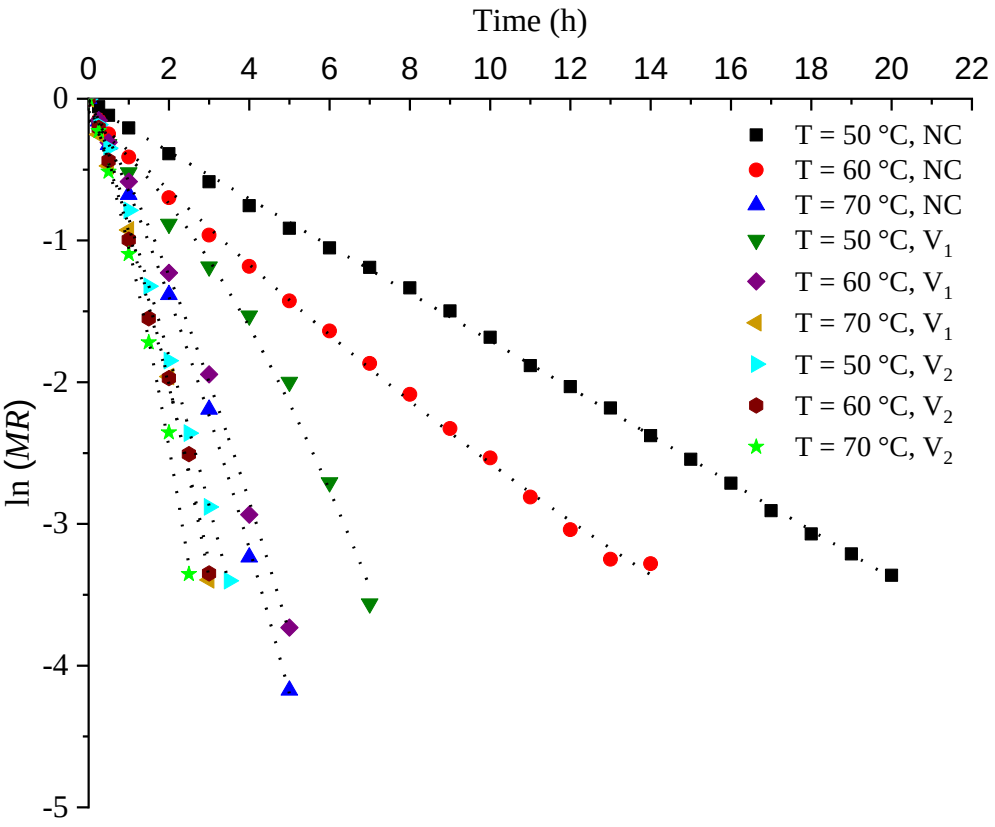

***Figure 6-8**: Influence of drying temperatures and air velocity on the diffusion coefficients of garlic cloves*

Where A_0, A_1, and A_2 are the regression coefficients of Equation (6.27) and the results of correlation coefficient (*r*) are given in Table (6-6).

***Table 6-6**: Regression coefficients and correlation coefficient of ln (MR) for all drying experiments*

Air velocity ($m\ s^{-1}$)	*Drying temperature (°C)*	A_0	A_1	A_2	*r*
NC	50	-0.04018	-0.16603	-0.00005	0.9994
	60	-0.09049	-0.2842	0.00362	0.9981
	70	-0.00683	-0.60062	-0.04751	0.9995
$V_1 = 4.1$	50	-0.15474	-0.22165	-0.03546	0.9913
	60	-0.01096	-0.52857	-0.04465	0.9989
	70	-0.04352	-0.73063	-0.1268	0.9992
$V_2 = 6.9$	50	0.04156	-0.84319	-0.04241	0.9992
	60	-0.00641	-0.85771	-0.07639	0.9964
	70	-0.01938	-0.84461	-0.18712	0.9981

The same figure displays the impact of drying temperature for each air velocity on the diffusion coefficient of garlic cloves. Plots were established between the ln (*MR*) against drying time. The diffusivity values are given in Table (6-7). It can be observed, as expected, that the increase in drying temperature necessarily leads to an increase in D_{eff} values. This phenomenon was observed and discussed by Guiné (2005). By considering the product with high porosity, the increase of drying temperature increases systematically the phenomena of mass transfer, consequently, the increase of effective moisture diffusivity: liquid movement to the surface due to capillary forces; diffusion of vapor due to gradients of partial vapor pressure; transport of liquid or vapor caused by increasing drying temperature. The values of D_{eff} obtained from recent studies range generally between 10^{-8} and $10^{-12} m^2\ s^{-1}$ for dried food products (Zogzas et al., 1996).

***Table 6-7**: Effective moisture diffusivity of hybrid solar-electric drying conditions*

Air Velocity ($m\ s^{-1}$)	*Drying temperature (°C)*	*Effective moisture diffusivity $\times 10^{-9} (m^2\ s^{-1})$*
NC	50	0.264
	60	0.374
	70	1.309
$V_1 = 4.1$	50	0.721
	60	1.174
	70	1.754
$V_2 = 6.9$	50	1.561
	60	1.710
	70	2.063

6.3.6 Activation energy

Activation energy (E_a) values were determined from the slope of Figure (6.9). E_a values for the nine experimental tests are given in Table (6-8) and ranged from 12.76 to 73.28 kJ mol^{-1}. We noticed that smaller activation energy values are remarked for greater effective moisture diffusivity values. This conclusion is similar to the one reported by Younis et al., (2018) concerning infra-red thin-layer drying of garlic cloves. Otherwise, In the current study, E_a values were found to be lower than those mentioned by Feng et al., (1999) for the drying of agro-products and ranged from 130 to 280 kJ mol^{-1}. As a conclusion, the value of E_a decreases due to the increase of internal diffusion.

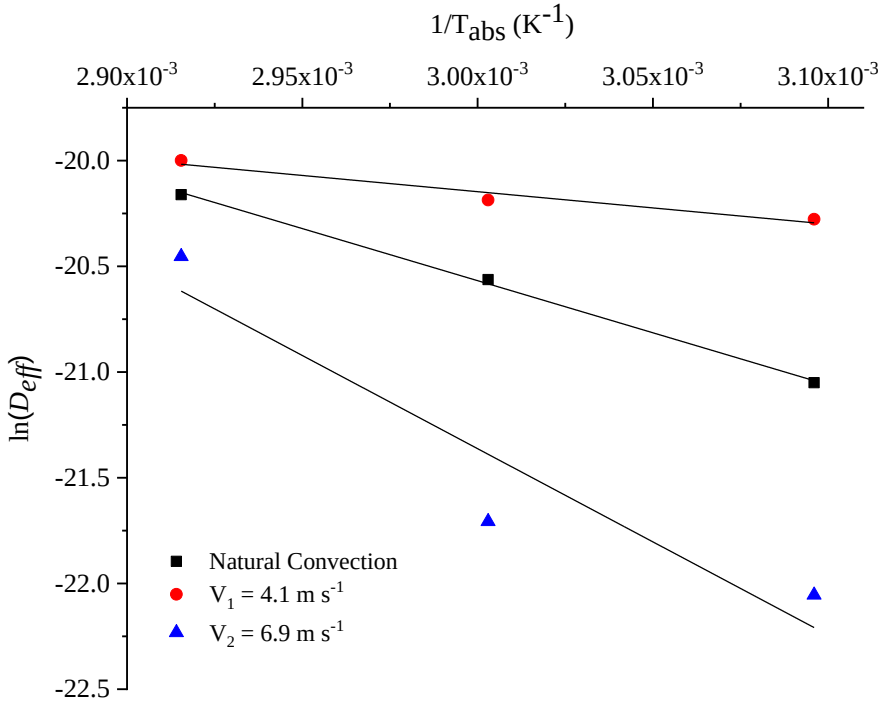

***Figure 6-9**: ln (D_{eff}) versus 1/T_{abs}*

***Table 6-8**: Activation energy values and pre-exponential factor at experimented conditions*

Air velocity (*m s^{-1}*)	*Drying temperature* (*°C*)	$D_0 \times 10^{-9}$ (*m² s^{-1}*)	E_a (*kJ mol^{-1}*)
NC	50	0.2715	73.28
	60	0.3841	
	70	1.3443	
4.1	50	0.7321	40.97
	60	1.1914	
	70	1.7794	
6.9	50	1.5693	12.76
	60	1.7183	
	70	2.0722	

6.3.7 Energy Analysis

The current dryer is made from various items and the total system mass is estimated to be 48.4kg. The mass ratios of the used items are presented in Figure (6.10). The steel sheet material comprises the main portion of 24% or 11.34 kg, next to the glass cover which takes 21% or 10.12 kg, and the residual amount of mass was divided for the other materials such as aluminium, iron, copper, etc. The percentage of embodied energy for each material used in the manufacture of the active solar-electric dryer is shown in Figure (6.11). The current dryer is with the total embodied energy of about 919.62 kWh. The aluminium metal with a share of 32 % consumes the highest percentage of the total embodied energy. Compared with aluminium, paint and iron come in the second rank with a contribution of 15 % for each material. Moreover, the embodied energy for glass fibre insulation is approximately 2% because it does not take a lot of energy to be manufactured.

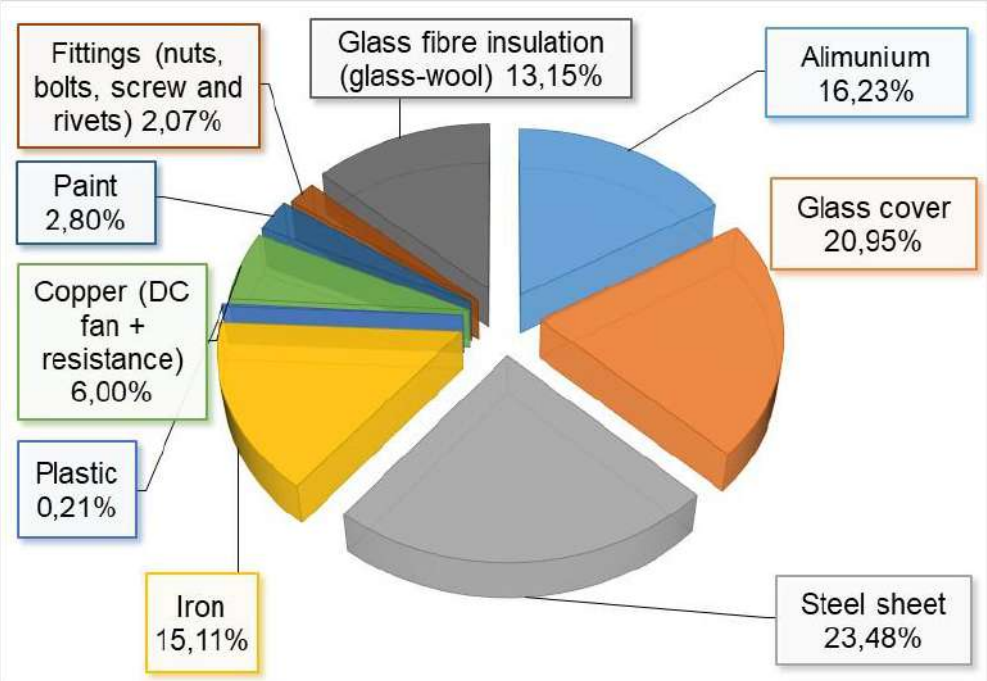

***Figure 6-10**: Break-up of the material masses used for the HSED operated under active mode*

The HSED operated under active mode at T = 70 °C and V_2 = 6.9 m s^{-1} allows to evaporate 6.75 kg of water in 2.5 h, and the dryer is available to run from 9 am to 5 pm, or 8 hours per day. However, this time of operation can differ based on the season. On an average for air drying velocity of 6.9 m s^{-1}, the evaporation capacity of the active solar-electric dryer is taken as 13 kg per day to dry the garlic twice per day. Otherwise, for the air-drying velocity of 4.1 m s^{-1}, the solar dryer evaporates the same moisture in 3, 5 and 7 h for T = 50, 60, and 70 °C, respectively. The

average evaporated moisture per day for the latter conditions is estimated to be 6.75 kg per day. The latent heat of moisture vaporization is taken as 2×106 J/kg. The energy payback time for the hybrid-solar electric dryer is found to be 0.62 and 0.32 years for both velocities are very low as compared to all solar dryers mentioned by (Prakash and Kumar, 2014; Vijayan et al., 2020). This EPBT is also much lower when compared to the lifetime of the designed solar dryer (13 years).

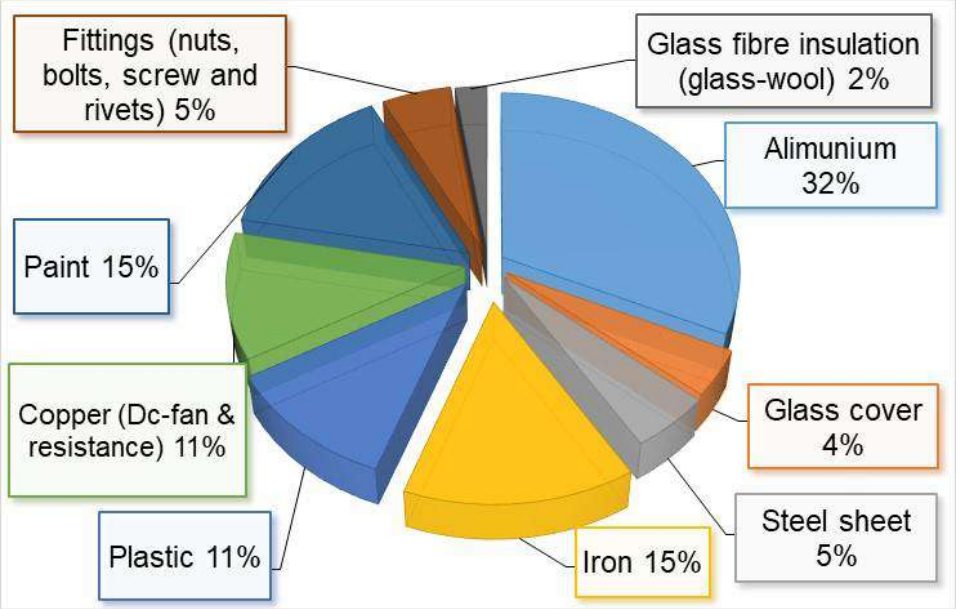

***Figure 6-11**: Embodied energy ratio of different materials used in the HSED operated under active mode*

The calculated net CO_2 mitigation of the active solar dryer for a life span of 25 years, hence the average earned carbon credit traded from 5 to 20 USD per tones of CO_2 mitigation is presented in Table (6-9).

***Table 6-9**: Environmental impact results of the comparison for garlic cloves drying (Assumed life span 25 years)*

Air velocity ($m\ s^{-1}$)	*Embodied energy (kWh)*	*EPBT (year)*	*CO_2 emission (kg/year)*	*Net CO_2 mitigation (tons)*	*Earned carbon credit (USD)*
4.1	919.62	0.62	1820	72	363.3-1453.4
6.9	919.62	0.32	1820	140	704-2816.2

*1 USD is equal to almost 129 DZD (Algerian Dinar) or 10 MAD (Moroccan Dirham) in 2020.

6.3.8 Exergy analysis

The total exergy of a drying system has always been dependent on the airflow stream and it can be suitable for the drying process with a steady-state (Hatami et al., 2020). However, the

evaporation of water that occurred during the drying process can't be considered as a steady stream, and the exergy definition of the dryer should be independent of the material amount of the product (Ndukwu et al., 2020). The exergy inflow, outflow, and loss through the drying chamber were calculated in the current study and presented in Table (6-10), considering the ambient temperature varied from 19 to 21 °C. The inflow exergy was ranged between 3.96 and 11.360 kJ s^{-1}. The outflow exergy was ranged between 0.593 and 10.226 kJ s^{-1}. The lowest loss through the drying chamber was recorded at 2.471 kJ s^{-1} for drying temperature of 70 °C under natural convection, while the highest value was recorded for drying temperature of 70 °C under air velocity of 6.9 m s^{-1}. Increasing both the drying temperature and the air velocity simultaneously, decrease the exergy loss and the system took the maximum inflow exergy to evaporate water from the product. Similar result was observed and investigated by Nwakuba et al. (2020) for drying of tomato slices under drying temperatures of 50, 60, and 70 °C with air velocities of 0.1, 1, and 1.5 m s^{-1} using HSED. The exergy efficiencies of the drying chamber under the experimented condition are shown in Table (6-11). The highest exergy efficiency of 89.86% was attained at 50 °C under natural convection mode. Whereas, the lowest value of exergy efficiency of 69.61% was obtained at 70 °C and 6.9 m s^{-1} air velocity. These values suggest that the exergy outflow is the main parameter for thermodynamic in efficiency, indicating that the exhaust air wasted a substantial quantity of heat exergy from the provided energy to the dryer. They are similar to the obtained result by Nwakuba et al. (2020) with exergy efficiency varied between 32.2 and 87.9 %.

***Table 6-10**: Exergy inflow, outflow, and losses at different temperatures and air velocities*

V (m s^{-1})	NC			4.1			6.9		
Ex (kJs^{-1})	Ex_i	Ex_o	Ex_l	Ex_i	Ex_o	Ex_l	Ex_i	Ex_o	Ex_l
T = 50 °C	3.502	3.147	0.355	3.784	3.323	0.547	4.083	3.517	0.566
T = 60 °C	5.408	4.622	0.786	5.086	4.32	0.765	5.408	4.24	1.167
T = 70 °C	7.483	6.015	1.467	7.483	5.609	1.874	8.266	5.889	2.376

***Table 6-11**: Exergy efficiencies of the drying system*

V (m s^{-1})	NC			4.1			6.9		
T (°C)	50	60	70	50	60	70	50	60	70
η (%)	89.86	85.46	80.38	84.90	82.01	74.95	82.74	78.41	69.61

Researcher Castro et al. (2018) indicated that as drying is in progress, the sustainability of exergy differs with temperature and velocity of air. In this research, the improvement potential, the ratio of waste energy, the sustainability index of exergy sustainability, and the environmental impact factor are all regarded and calculated. For a solar drying system, the environmental impact factor (E_{IF}) was defined as a function of waste exergy ratio and exergetic efficiency. The environmental impact factor is an important parameter that indicates whether the environment has

been damaged or not due to the waste energy output (Midilli and Kucuk, 2015). The E_{IF} values are shown in Table (6-12).

The variation of the waste exergy ratio, exergetic sustainability index, and the improvement potential factor with different drying conditions are given in Figures (6. 12-14), respectively. The waste exergy value varied from 10.1 to 30.3 %. The *W* values increased in line with the dying time or decreasing of drying temperature and air velocity. The decrease of exergy efficiency caused by the increase of exergy losses through the drying chamber led to an increase in the value of *W*. Similar result was obtained by Akpinar (2019). The value of exergetic sustainability index (S_i) changed from 9.86 and 3.29. The S_i has a negative correlation with both the drying temperature and air velocity and a positive correlation with the drying time. The I_p factor varied from 0.036 and 1.693 kW, it's increased with the increase of drying temperature and air velocity, as well as the decrease of drying time.

The environmental impact factor (E_{IF}) was calculated and deduced depending on the exergy efficiency of the drying chamber. The E_{IF} values varied from 11.28 to 40.35. As shown in Table (6-12), the E_{IF} increases with the decrease of exergy efficiency. The increased η resulted in reduced environmental damage to the solar drying system. A similar trend was found by (Midilli and Kucuk (2015).

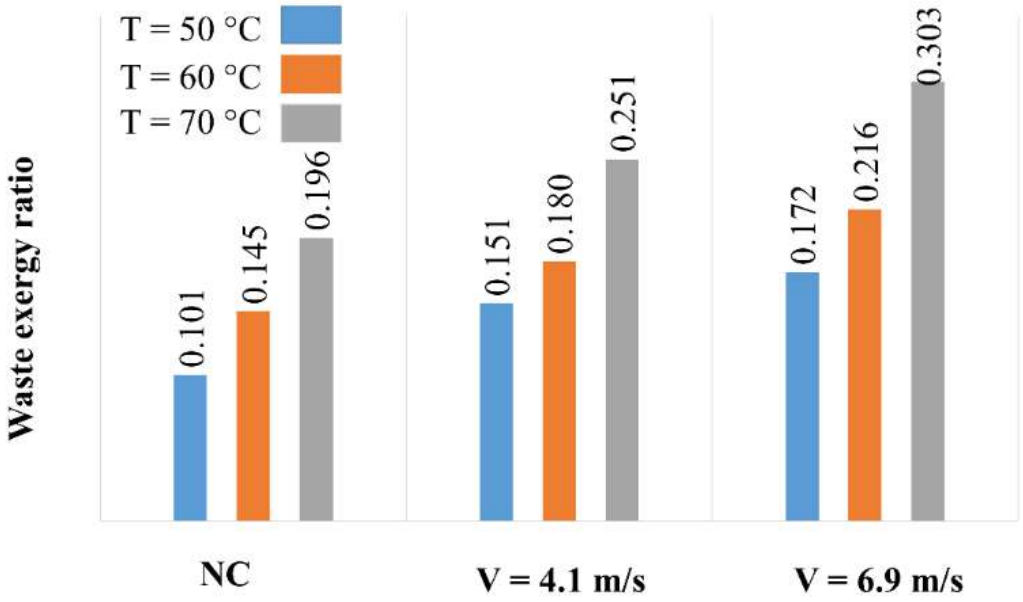

***Figure 6-12**: Waste exergy ratio of HSED*

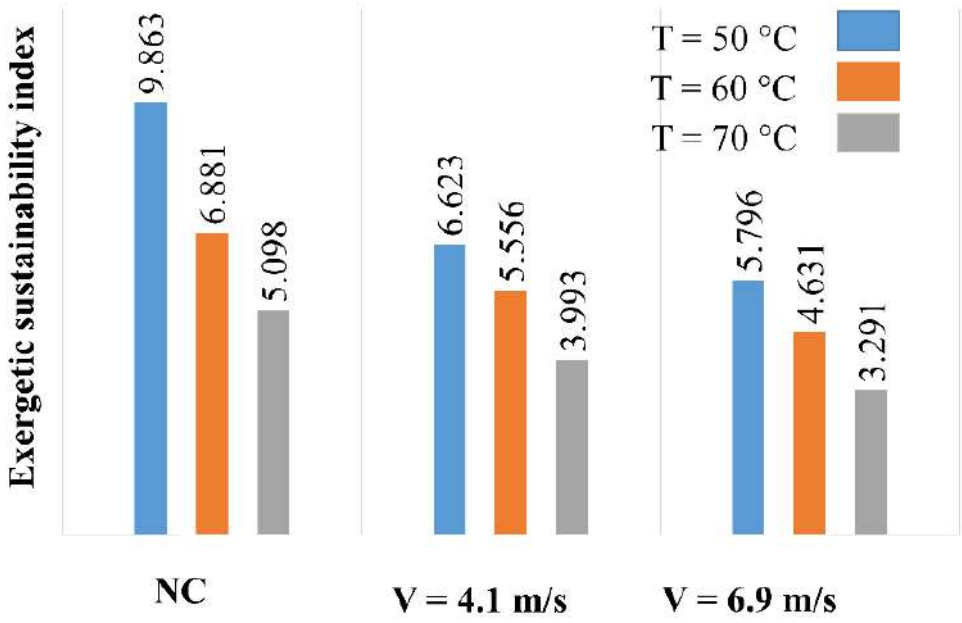

***Figure 6-13**: Exergetic sustainability index of drying unit*

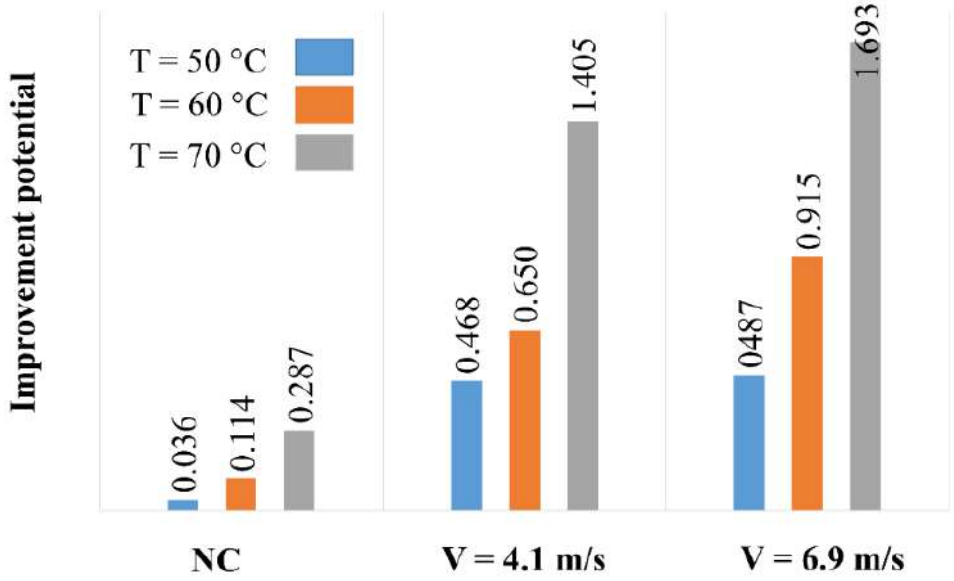

***Figure 6-14**: Variation of improvement potential*

***Table 6-12**: Environmental impact factor for different drying conditions*

V (m s^{-1})	NC			4.1			6.9		
T (°C)	50	60	70	50	60	70	50	60	70
W_{IF} (%)	11.28	17.01	24.40	16.90	17.71	33.41	16.08	27.54	40.35

6.4 Conclusion

In this chapter, mathematical modelling and characteristics drying curve of garlic cloves were performed using a HSED. Additionally, environmental and exergy analysis of the HSED were investigated. The main results are presented below:

- The drying temperature had the main effect on drying time. An increase in drying temperature decreases significantly the drying time. But the drying air velocity effect is limited and very low.
- The drying rate increased mainly when the moisture content increased, with a low effect of drying air velocity at a high temperature of 70°C.
- The fitting of the (*CDC*) experimental data of garlic cloves was expressed with the equation of the dimensionless drying rate of third nominal order with the standard error (*MBE* = 0.01135) and the correlation coefficient (r = 0.99936).
- Among nine mathematical models, Midilli-Kucuk model was selected as the most appropriate mathematical model predicting the change in the moisture of garlic cloves during the drying process with the highest average value of (r = 0.9992), the lowest values of (χ^2 = 0.00016) and (*MBE* = 0.0018).
- The effective moisture diffusivity increased with the increase of drying temperature and varied from 2.64 10^{-10} to 2.063 10^{-9} m^2 s^{-1}.
- Activation energy increased with the increase of drying temperature, (E_a) ranged from 12.76 to 73.28 kJ mol^{-1}, which expressed the effect of drying temperature on the diffusion coefficient.
- The energy payback time for the HSED varied between 0.32 and 0.62 years.
- For a life span of 25 years for the studied dryer, net CO_2 mitigation was found to be 72 and 140 tons, hence the average earned carbon credit varied between 363.3-1453.4 USD for 4.1 m s^{-1} and, between 704-2816.2 USD for 6.9 m s^{-1} drying air velocity, respectively.
- The exergy efficiency varied from 69.61% to 89.86%. The highest value was recorded for natural convection mode at 50 °C due to the lowest outflow exergy losses of 0.355 kJ s^{-1}. Sustainable exergy index and improvement potential were in the range of 3.29-9.86 and 0.036-1.693 kW, respectively. The highest environmental impact factor of 40.35% was achieved at the maximum exergy efficiency.

According to the results above, the HSED is highly recommended for the Algerian farmers for drying of garlic and other crops. It is much sustainable environmentally.

This chapter is valorised as a research paper entitled " 3E analysis and mathematical modelling of garlic drying process in a hybrid solar-electric dryer", (Hadibi et al., 2021).

General Conclusion

Preservation of tomato in paste form and garlic has been carried out by using solar drying assisted with other technics which are, geothermal energy, DIC technic, and hybrid electric-solar drying. These kinds of crop are widely cultivated in Algeria, with high losses due to the shortcoming of preservation and transport means. These products are dried with specific ways and materials appropriate with the availability of free energy and materials.

The current thesis is with six chapters, five of them are experimental investigation or mathematical modelling of the tomato paste and garlic. These chapters are presented with the main findings bellow:

1. Solar Drying Systems and Innovative Drying Process (Swell Drying)

A brief review on solar dryer's classification according to the mode of heat transfer on one hand, and a well description with some studies examples of innovative technic used for contributing in drying sector called "DIC" or instant controlled pressure drop, on the other hand.

2. Hot Air Convective Drying of Tomato Paste Under Near Solar Drying Operating Conditions

The drying of tomato paste was then established using an automated laboratory drying loop (LETTM, El-Manar University of Tunis).

- The effects of two drying parameters (air temperature, air velocity) on drying time and drying kinetics of dried tomato paste were investigated. They were conducted under air conditions as constant relative humidity of 16%, temperatures 45°C, 50°C, 60°C with airflow velocity of 1.5 and 2.5m s^{-1}. Obtained drying kinetics showed only falling periods and led to drying time ranged between 11.16 and 5.32 hours.
- Evaluation of the suitable mathematical models, describing thin-layer drying behavior of tomato paste with several drying conditions revealed that Demir et al. model was the best fitted among nine investigated models, followed by Midilli *et al*. model.
- The highest moisture diffusivities were 4.62449. 10^{-9} m^2 s^{-1} and 4.65409. 10^{-9} m^2 s^{-1} for the highest air-drying temperature 60°C, for both air velocities, respectively.
- Finally, the activation energies were found to be 44.836 and 38.159 kj/mol for air velocities 1.5 and 2.5 m s^{-1} respectively.

3. Kinetics and Economic Analysis of Hybrid Solar Drying of Tomato Paste

An experimental investigation and economic analysis of tomato paste drying inside a direct solar dryer with and without GWHE were done. The drying time and various economic parameters of the tomato paste thin layer were investigated. The finding is concluded as:

- The ambient temperature during daytime experimentation was varied between 18.08 and 23.05 °C.
- The highest and lowest drying temperature was observed at 53.4 °C and 35.75 °C for a solar dryer with GWHE, while for the basic dryer were 41.95 °C and 17.76 °C, respectively.
- solar dryer integrated with GWHE ensures a salient difference between drying temperature and ambient temperature after sunset and at night reached 30.8 °C.
- Hybrid solar drying took 22 h with the continuous drying process, whereas, the basic dryer took 18 h in three days for the desired final moisture content 0.08 (d.b). Long time exposure means possibilities of deterioration.
- The hybrid dryer increases the effective moisture diffusivity from 1.202×10^{-9} to 1.617×10^{-9} m^2 s^{-1}.
- The cumulative present worth value (P_{ws}) of yearly savings for tomato paste drying was found to be 305922.4and 69445.18 DA for basic and hybrid dryer respectively.
- The payback period of the hybrid dryer with 2.21 years (807 days) is recommended for the drying of tomato paste.
- The net present values were 64945.2 and 299922.5 DA, whereas, the benefit-cost ratio was 15.43 and 50.98 for basic and hybrid dryer respectively.

In conclusion, the hybrid system with GWHE ensures the drying operation after sunset, during nighttime, cloudy days, and reduced drying time. Otherwise, the economic analysis of both systems encourages investment with the hybrid dryer.

4. Modeling and Development of Characteristic Curve for Tomato Paste Drying

Tomato paste was dried using four drying techniques: (i) basic direct solar drying, (ii) direct solar drying assisted with heat exchanger, (iii) direct solar drying with ventilated mode, and (iv) direct solar drying with combined mode.

- Solar drying with combined mode decreased the drying time by 120% compared to the basic solar drying mode. The best fit for the characteristic drying curve was obtained by the evaluation of two criteria, the standard error value *RMSE* = 0.04643 and the correlation

coefficient value R^2= 0.99128. The highest effective moisture diffusivity was recorded for the combined mode. D_{eff} ranged from 1.1×10^{-9} and 2.298×10^{-9} m² s^{-1}.

5. Combined Solar Drying / Swell Drying of Tomato Paste

Combined solar drying with swell drying leads to the main folloing results:

- The DIC process improves the drying kinetics; this behavior could be related to the increase of water activity "a_w".
- A comparison of visual quality revealed a high correlation between DIC texturing stage and visual quality improvement, with a low effect of drying temperature.

As a conclusion, compared with the conventional drying methods (Hot-air drying HAD or solar drying SD), this new dehydration operation coupling the various processes of draining dewatering, solar/geothermal drying, DIC texturing / Swell-drying stage had a significant effect on improving the drying kinetics, greatly reducing the energy consumption, and increasing the visual quality.

6. Exergy and Energy Analysis of Hybrid Solar Electric Drying of Garlic

The characteristics drying curve of garlic cloves and energy analysis was performed by using a HSED.

- The fitting of the (*CDC*) experimental data of garlic cloves was expressed with the equation of the dimensionless drying rate of third nominal order with the standard error *MBE* = 0.01135 and the correlation coefficient *r* = 0.99936.
- Among nine mathematical models, Midilli-Kucuk model was selected as the most appropriate mathematical model predicting the change in the moisture of garlic cloves during the drying process with the highest average value of *r* = 0.9992, the lowest values of χ^2 = 0.00016 and *MBE* = 0.0018.
- The energy payback time for the HSED varied between 0.32 and 0.62 years.

For a life span of 25 years for the studied dryer, hence the average earned carbon credit varied between 363.3-1453.4 USD for 4.1 m s^{-1} and, between 704-2816.2 USD for 6.9 m s-^{1} drying air velocity, respectively.

- The highest value was recorded for natural convection mode at 50 °C due to the lowest outflow exergy losses of 0.355 kJ s^{-1}. Sustainable exergy index and improvement potential were in the range of 3.29-9.86 and 0.036-1.693 kW, respectively. The highest environmental impact factor of 40.35% was achieved at the maximum exergy efficiency.

From the above remarks, the hybridization of solar drying system shows a significant improvement on diffusional stage where the effective moisture diffusivity increased from 1.1×10^{-9} to 2.298×10^{-9} $m^2\ s^{-1}$ for ventilated geothermal assisted solar drying of tomato paste. The system can achieve a difference between drying/ambient temperature up to 33 °C for a cold night with 4 °C ambient temperature. Otherwise, the hybridization with geothermal is not much sustainable economically with a payback period at 2.21 years. This value can be reduced by increasing the dryer volume and adding another energy source such as thermal storage. The new drying process, mechanical dewatering followed by solar drying combined to DIC-swell drying was found to be much economically. DIC technique can save more energy consumption by reducing significantly the drying time and can improve the quality of final dried product. DIC-swell drying is highly recommended for the industrial in Algeria with abundant free solar and geothermal energy which can be used to achieve the desired moisture level of about 20% before treating by DIC. On the other hand, this new drying process improved the diffusional process compared to other drying techniques. The hybrid solar-electric drying of garlic revealed a significant effect of controlled drying temperature on stabilization of the product during drying. Low temperature up 60 °C was recommended. However, with 1,820 kg / year of CO_2 emissions, the system proved to be quite affected by relatively significant damage to the environment.

Perspective

The current thesis did not reach all the stated goals at the beginning. Because of the lack of means to do some complementary experiments or the time factor. The most important of these goals that we seek to achieve in the future are summarized in three points as follow:

- Quality analysis of tomato paste (Lycopene, Total Phenol Compound, Flavonoids…etc);
- Combined solar drying/swell drying of garlic;
- Solar drying system integrated with thermal storage medium for tomato paste and garlic drying.

Bibliography

Adelaja, A.O., Ojolo, S.J., 2010. Design, analysis and experimental evaluation of photovoltaic forced convection solar dryer for the tropics, in: International Journal of Engineering Research in Africa. Trans Tech Publ, pp. 49–61.

Agarwal, A., Sarviya, R.M., 2016. An experimental investigation of shell and tube latent heat storage for solar dryer using paraffin wax as heat storage material. Engineering Science and Technology, an International Journal 19, 619–631.

Akpinar, E.K., 2019. The effects of some exergetic indicators on the performance of thin layer drying process of long green pepper in a solar dryer. Heat and Mass Transfer 55, 299–308.

Akpinar, E.K., Bicer, Y., 2008. Mathematical modelling of thin layer drying process of long green pepper in solar dryer and under open sun. Energy Conversion and Management 49, 1367–1375.

Akpinar, E.K., Bicer, Y., Midilli, A., 2003. Modeling and experimental study on drying of apple slices in a convective cyclone dryer. Journal of Food Process Engineering 26, 515–541.

Al Haddad, M., Mounir, S., Sobolik, V., Allaf, K., 2008. Fruits & vegetables drying combining hot air, DIC technology and microwaves. International Journal of Food Engineering 4.

Albitar, N., Mounir, S., Besombes, C., Allaf, K., 2011. Improving the drying of onion using the instant controlled pressure drop technology. Drying Technology 29, 993–1001.

Ali, I., Abdelkader, L., El Houssayne, B., Mohamed, K., El Khadir, L., 2016. Solar convective drying in thin layers and modeling of municipal waste at three temperatures. Applied Thermal Engineering 108, 41–47.

Allaf, K., Vidal, P., 1988. Feasibility study of a new process of drying/swelling by instantaneous decompression toward vacuum of in pieces vegetables in view of a rapidfire-hydration. Gradient activity plotting university of technology of compiegne utc. In.

Allaf, T., Allaf, K., 2016. Instant controlled pressure drop (DIC) in food processing. Springer.

Allaf, T., Allaf, K., 2014. Instant controlled pressure drop DIC in food processing.

Allaf, T., Tomao, V., Ruiz, K., Chemat, F., 2013. Instant controlled pressure drop technology

and ultrasound assisted extraction for sequential extraction of essential oil and antioxidants. Ultrasonics Sonochemistry 20, 239–246.

Alonzo-Macías, M., Cardador-Martínez, A., Mounir, S., Montejano-Gaitán, G., Allaf, K., 2013. Comparative study of the effects of drying methods on antioxidant activity of dried strawberry (Fragaria Var. Camarosa). Journal of Food Research 2, 92–107.

ALZAMORA, S.M., CHIRIFE, J., 1980. Some factors controlling the kinetics of moisture movement during avocado dehydration. Journal of Food Science 45, 1649–1651.

Amer, B.M.A., Gottschalk, K., Hossain, M.A., 2018. Integrated hybrid solar drying system and its drying kinetics of chamomile. Renewable energy 121, 539–547.

Amer, B.M.A., Hossain, M.A., Gottschalk, K., 2010. Design and performance evaluation of a new hybrid solar dryer for banana. Energy conversion and management 51, 813–820.

Arun, K.R., Srinivas, M., Saleel, C.A., Jayaraj, S., 2019. Active drying of unripened bananas (Musa Nendra) in a multi-tray mixed-mode solar cabinet dryer with backup energy storage. Solar Energy 188, 1002–1012.

Asioli, D., Rocha, C., Wongprawmas, R., Popa, M., Gogus, F., Almli, V.L., 2019. Microwave-dried or air-dried? Consumers' stated preferences and attitudes for organic dried strawberries. A multi-country investigation in Europe. Food Research International 120, 763–775.

Azaizia, Z., Kooli, S., Hamdi, I., Elkhal, W., Guizani, A.A., 2020. Experimental study of a new mixed mode solar greenhouse drying system with and without thermal energy storage for pepper. Renewable Energy 145, 1972–1984.

Badaoui, O., Hanini, S., Djebli, A., Haddad, B., Benhamou, A., 2019. Experimental and modelling study of tomato pomace waste drying in a new solar greenhouse: Evaluation of new drying models. Renewable energy 133, 144–155.

Bagheri, H., Arabhosseini, A., Kianmehr, M.H., Chegini, G.R., 2013. Mathematical modeling of thin layer solar drying of tomato slices. Agricultural Engineering International: CIGR Journal 15, 146–153.

Baird, G., Alcorn, A., Haslam, P., 1997. The energy embodied in building materials-updated

New Zealand coefficients and their significance. Transactions of the Institution of Professional Engineers New Zealand: Civil Engineering Section 24, 46.

Bal, L.M., Satya, S., Naik, S.N., 2010. Solar dryer with thermal energy storage systems for drying agricultural food products: A review. Renewable and Sustainable Energy Reviews 14, 2298–2314.

Baniasadi, E., Ranjbar, S., Boostanipour, O., 2017. Experimental investigation of the performance of a mixed-mode solar dryer with thermal energy storage. Renewable Energy 112, 143–150.

Banout, J., 2017. Solar Drying Systems, in: Solar Drying Technology. Springer, pp. 39–67.

Belghith, A., Azzouz, S., ElCafsi, A., 2016. Desorption isotherms and mathematical modeling of thin layer drying kinetics of tomato. Heat and Mass Transfer 52, 407–419.

Bellagha, S., Amami, E., Farhat, A., Kechaou, N., 2002. Drying kinetics and characteristic drying curve of lightly salted sardine (Sardinella aurita). Drying Technology 20, 1527–1538.

Benhamou, A., Idlimam, A., Lamharrar, A., Benyoucef, B., Kouhila, M., 2008. Diffusivité hydrique et cinétique de séchage solaire en convection forcée des feuilles de marjolaine. Revue des Energies renouvelables 11, 75–85.

Benhamza, A., Boubekri, A., Atia, A., El Ferouali, H., Hadibi, T., Arıcı, M., Abdenouri, N., 2021. Multi-objective design optimization of solar air heater for food drying based on energy, exergy and improvement potential. Renewable Energy. https://doi.org/https://doi.org/10.1016/j.renene.2021.01.086

Bennaceur, S., Draoui, B., Touati, B., Benseddik, A., Saad, A., Bennamoun, L., 2015. Determination of the moisture-sorption isotherms and isosteric heat of henna leaves. Journal of Engineering Physics and Thermophysics 88, 52–62.

Benseddik, A., Azzi, A., Zidoune, M.N., Allaf, K., 2018. Mathematical empirical models of thin-layer airflow drying kinetics of pumpkin slice. Engineering in Agriculture, Environment and Food 11, 220–231.

Bhardwaj, A.K., Kumar, R., Chauhan, R., 2019. Experimental investigation of the performance

of a novel solar dryer for drying medicinal plants in Western Himalayan region. Solar Energy 177, 395–407.

Blanco-Cano, L., Soria-Verdugo, A., Miguel Garcia-Gutierrez, L., Ruiz-Rivas, U., 2016. Evaluation of the maximum evaporation rate in small-scale indirect solar dryers. Journal of Solar Energy Engineering 138.

Borah, A., Hazarika, K., Khayer, S.M., 2015. Drying kinetics of whole and sliced turmeric rhizomes (Curcuma longa L.) in a solar conduction dryer. Information Processing in Agriculture 2, 85–92.

Boubekri, A., Benmoussa, H., Mennouche, D., 2009. Solar drying kinetics of date palm fruits assuming a step-wise air temperature change. Journal of Engineering science and Technology 4, 292–304.

Boughali, S., Benmoussa, H., Bouchekima, B., Mennouche, D., Bouguettaia, H., Bechki, D., 2009. Crop drying by indirect active hybrid solar–Electrical dryer in the eastern Algerian Septentrional Sahara. Solar energy 83, 2223–2232.

Bozin, B., Mimica-Dukic, N., Samojlik, I., Goran, A., Igic, R., 2008. Phenolics as antioxidants in garlic (Allium sativum L., Alliaceae). Food chemistry 111, 925–929.

Brooker, D.B., Bakker-Arkema, F.W., Hall, C.W., 1992. Drying and storage of grains and oilseeds. Springer Science & Business Media.

Bruce, D.M., 1985. Exposed-layer barley drying: Three models fitted to new data up to 150°C. Journal of Agricultural Engineering Research 32, 337–348. https://doi.org/https://doi.org/10.1016/0021-8634(85)90098-8

Castro, M., Román, C., Echegaray, M., Mazza, G., Rodriguez, R., 2018. Exergy analyses of onion drying by convection: influence of dryer parameters on performance. Entropy 20, 310.

Celma, A.R., Cuadros, F., López-Rodríguez, F., 2009. Characterisation of industrial tomato by-products from infrared drying process. food and bioproducts processing 87, 282–291.

Chaouch, W.B., Khellaf, A., Mediani, A., Slimani, M.E.A., Loumani, A., Hamid, A., 2018. Experimental investigation of an active direct and indirect solar dryer with sensible heat

storage for camel meat drying in Saharan environment. Solar Energy 174, 328–341.

Chauhan, P.S., Kumar, A., Nuntadusit, C., 2018. Thermo-environomical and drying kinetics of bitter gourd flakes drying under north wall insulated greenhouse dryer. Solar Energy 162, 205–216.

Chouicha, S., Boubekri, A., Mennouche, D., Berrbeuh, M.H., 2013. Solar drying of sliced potatoes. An experimental investigation. Energy Procedia 36, 1276–1285.

Coşkun, S., Doymaz, I., Tunçkal, C., Erdoğan, S., 2017. Investigation of drying kinetics of tomato slices dried by using a closed loop heat pump dryer. Heat and Mass transfer 53, 1863–1871.

Crank, J., 1979. The mathematics of diffusion. Oxford university press.

da Silva, W.P., e Silva, C.M., Farias, V.S.O., Gomes, J.P., 2012. Diffusion models to describe the drying process of peeled bananas: optimization and simulation. Drying Technology 30, 164–174.

Demir, V., Gunhan, T., Yagcioglu, A.K., 2007. Mathematical modelling of convection drying of green table olives. Biosystems engineering 98, 47–53.

Diamante, L.M., Munro, P.A., 1991. Mathematical modelling of hot air drying of sweet potato slices. International journal of food science & technology 26, 99–109.

Djebli, A., Hanini, S., Badaoui, O., Boumahdi, M., 2019. A new approach to the thermodynamics study of drying tomatoes in mixed solar dryer. Solar Energy 193, 164–174.

Dorouzi, M., Mortezapour, H., Akhavan, H.-R., Moghaddam, A.G., 2018. Tomato slices drying in a liquid desiccant-assisted solar dryer coupled with a photovoltaic-thermal regeneration system. Solar Energy 162, 364–371.

Doymaz, I., 2009. An experimental study on drying of green apples. Drying technology 27, 478–485.

Doymaz, I., 2007. Air-drying characteristics of tomatoes. Journal of Food engineering 78, 1291–1297.

Doymaz, I., 2006. Thin-layer drying behaviour of mint leaves. Journal of Food Engineering 74, 370–375.

Duffie, J.A., Beckman, W.A., 1991. Solar engineering of thermal processes. Wiley New York.

Ekechukwu, O. V, 1999. Review of solar-energy drying systems I: an overview of drying principles and theory. Energy conversion and management 40, 593–613.

El-Sebaii, A.A., Shalaby, S.M., 2013. Experimental investigation of an indirect-mode forced convection solar dryer for drying thymus and mint. Energy Conversion and Management 74, 109–116.

El-Sebaii, A.A., Shalaby, S.M., 2012. Solar drying of agricultural products: A review. Renewable and Sustainable Energy Reviews 16, 37–43.

ELkhadraoui, A., Kooli, S., Hamdi, I., Farhat, A., 2015. Experimental investigation and economic evaluation of a new mixed-mode solar greenhouse dryer for drying of red pepper and grape. Renewable energy 77, 1–8.

FAO, 2014. Food and agricultural organization.

Feng, H., Tang, J., Cavalieri, R.P., 1999. Combined microwave and spouted bed drying of diced apples: effect of drying conditions on drying kinetics and product temperature. Drying technology 17, 1981–1998.

Ferreira, A.G., Gonçalves, L.M., Maia, C.B., 2014. Solar drying of a solid waste from steel wire industry. Applied thermal engineering 73, 104–110.

Fudholi, A., Sopian, K., Ruslan, M.H., Alghoul, M.A., Sulaiman, M.Y., 2010. Review of solar dryers for agricultural and marine products. Renewable and sustainable energy reviews 14, 1–30.

Ghasemkhani, H., Keyhani, A., Aghbashlo, M., Rafiee, S., Mujumdar, A.S., 2016. Improving exergetic performance parameters of a rotating-tray air dryer via a simple heat exchanger. Applied Thermal Engineering 94, 13–23.

Ghatrehsamani, S.H., Dadashzadeh, M., Zomorodian, A., 2012. Kinetics of apricot thin layer drying in a mixed and indirect mode solar dryer. International Journal of Agriculture

Sciences 4, 262.

Guiné, R.P.F., 2005. Drying kinetics of some varieties of pears produced in Portugal. Food and Bioproducts Processing 83, 273–276.

Gupta, P., Ahmed, J., Shivhare, U.S., Raghavan, G.S. V, 2002. Drying characteristics of red chilli. Drying technology 20, 1975–1987.

Haddad, J., Louka, N., Gadouleau, M., Juhel, F., Allaf, K., 2001. Application du nouveau procédé de séchage/texturation par Détente Instantanée Contrôlée DIC aux poissons: Impact sur les caractéristiques physico-chimiques du produit fini. Sciences des aliments 21, 481–498.

Hadibi, T., Boubekri, A., Mennouche, D., Benhamza, A., Abdenouri, N., 2021. 3E analysis and mathematical modelling of garlic drying process in a hybrid solar-electric dryer. Renewable Energy 170, 1052–1069. https://doi.org/https://doi.org/10.1016/j.renene.2021.02.029

Hatami, S., Payganeh, G., Mehrpanahi, A., 2020. Energy and exergy analysis of an indirect solar dryer based on a dynamic model. Journal of Cleaner Production 244, 118809.

Henderson, S.M., 1974. Progress in developing the thin layer drying equation. Transactions of the ASAE 17, 1167–1168.

Hernandez-Escobedo, Q., Rodríguez-García, E., Saldaña-Flores, R., Fernández-García, A., Manzano-Agugliaro, F., 2015. Solar energy resource assessment in Mexican states along the Gulf of Mexico. Renewable and Sustainable Energy Reviews 43, 216–238.

https://en.wikipedia.org/wiki/Garlic, 2021.

Huang, Y.W., Chen, M.Q., Jia, L., 2016. Assessment on thermal behavior of municipal sewage sludge thin-layer during hot air forced convective drying. Applied Thermal Engineering 96, 209–216.

Kamal, I.M., Sobolik, V., Kristiawan, M., Mounir, S.M., Allaf, K., 2008. Structure expansion of green coffee beans using instantaneous controlled pressure drop process. Innovative Food Science & Emerging Technologies 9, 534–541.

Karathanos, V.T., Villalobos, G., Saravacos, G.D., 1990. Comparison of two methods of

estimation of the effective moisture diffusivity from drying data. Journal of food science 55, 218–223.

Kassem, A.S., 1998. Comparative studies on thin layer drying models for wheat, in: 13th International Congress on Agricultural Engineering. pp. 2–6.

Kaviti, A.K., Deep, H., 2017. Thermal Energy Storage in Solar Dryer, in: Solar Drying Technology. Springer, pp. 603–617.

Kaya, A., Aydın, O., Demirtaş, C., 2007. Drying kinetics of red delicious apple. Biosystems Engineering 96, 517–524.

Keawsuntia, Y., 2014. Experimental investigation of active solar dryer for drying of chili, in: Advanced Materials Research. Trans Tech Publ, pp. 16–19.

Khouya, A., Draoui, A., 2009. Détermination des courbes caractéristiques de séchage de trois espèces de bois. Revue des énergies renouvelables 12, 87–98.

Kipcak, A.S., 2018. Effect of pre-treatment and air temperature on drying time of cherry tomato. Journal of Thermal Engineering 4, 1648–1655.

Kouchakzadeh, A., 2013. The effect of acoustic and solar energy on drying process of pistachios. Energy Conversion and Management 67, 351–356.

Koukouch, A., Idlimam, A., Asbik, M., Sarh, B., Izrar, B., Bah, A., Ansari, O., 2015. Thermophysical characterization and mathematical modeling of convective solar drying of raw olive pomace. Energy Conversion and Management 99, 221–230.

Koukouch, A., Idlimam, A., Asbik, M., Sarh, B., Izrar, B., Bostyn, S., Bah, A., Ansari, O., Zegaoui, O., Amine, A., 2017. Experimental determination of the effective moisture diffusivity and activation energy during convective solar drying of olive pomace waste. Renewable Energy 101, 565–574.

Krokida, M.K., Karathanos, V.T., Maroulis, Z.B., Marinos-Kouris, D., 2003. Drying kinetics of some vegetables. Journal of Food engineering 59, 391–403.

Lakshmi, D.V.N., Muthukumar, P., Layek, A., Nayak, P.K., 2019. Performance analyses of mixed mode forced convection solar dryer for drying of stevia leaves. Solar Energy 188,

507–518.

Lešková, E., Kubíková, J., Kováčiková, E., Košická, M., Porubská, J., Holčíková, K., 2006. Vitamin losses: Retention during heat treatment and continual changes expressed by mathematical models. Journal of Food Composition and analysis 19, 252–276.

Louati, I., Bahloul, N., Besombes, C., Allaf, K., Kechaou, N., 2019. Instant controlled pressure-drop as texturing pretreatment for intensifying both final drying stage and extraction of phenolic compounds to valorize orange industry by-products (Citrus sinensis L.). Food and bioproducts processing 114, 85–94.

Lu, Y., Mu, K., McClements, D.J., Liang, X., Liu, X., Liu, F., 2020. Fermentation of tomato juice improves in vitro bioaccessibility of lycopene. Journal of Functional Foods 71, 104020.

Madamba, P.S., Driscoll, R.H., Buckle, K.A., 1996. The thin-layer drying characteristics of garlic slices. Journal of food engineering 29, 75–97.

Manaa, S., Younsi, M., Moummi, N., 2013. Solar drying of tomato in the arid area of Touat (Adrar, Algeria). Energy Procedia 36, 511–514.

Masmoudi, G., Hermassi, I., Azzouz, S., Belghith, A., 2008. Caractérisation expérimentale du raisin sultanine: Cinétique de séchage et rhéologie. Revue des Energies Renouvelables SMSTS'08 193–202.

Mazzoleni, V., Dallagiovanna, L., Trevisan, M., Nicelli, M., 2005. Persistent organic pollutants in cork used for production of wine stoppers. Chemosphere 58, 1547–1552.

Mehran, S., Nikian, M., Ghazi, M., Zareiforoush, H., Bagheri, I., 2019. Experimental investigation and energy analysis of a solar-assisted fluidized-bed dryer including solar water heater and solar-powered infrared lamp for paddy grains drying. Solar Energy 190, 167–184.

Mennouche, D., Boubekri, A., Bouchekima, B., Boughali, S., Moumeni, R., Boutadjine, D., 2018. Valorization of the tomato to obtain a powder rich in antioxidant constituents, in: IDS 2018. 21st International Drying Symposium Proceedings. Editorial Universitat Politècnica de València, pp. 715–722.

Mennouche, D., Boubekri, A., Chouicha, S., Bouchekima, B., Bouguettaia, H., 2017. Solar drying process to obtain high standard “deglet-nour” date fruit. Journal of Food Process Engineering 40, e12546.

Mennouche, D., Bouchekima, B., Boubekri, A., Boughali, S., Bouguettaia, H., Bechki, D., 2014. Valorization of rehydrated Deglet-Nour dates by an experimental investigation of solar drying processing method. Energy conversion and management 84, 481–487.

Mewa, E.A., Okoth, M.W., Kunyanga, C.N., Rugiri, M.N., 2019. Experimental evaluation of beef drying kinetics in a solar tunnel dryer. Renewable energy 139, 235–241.

Mghazli, S., Ouhammou, M., Hidar, N., Lahnine, L., Idlimam, A., Mahrouz, M., 2017. Drying characteristics and kinetics solar drying of Moroccan rosemary leaves. Renewable Energy 108, 303–310.

Midilli, A., Kucuk, H., 2015. Assessment of exergetic sustainability indicators for a single layer solar drying system. International Journal of Exergy 16, 278–292.

Midilli, A., Kucuk, H., 2003. Mathematical modeling of thin layer drying of pistachio by using solar energy. Energy conversion and Management 44, 1111–1122.

Midilli, A., Kucuk, H., Yapar, Z., 2002. A new model for single-layer drying. Drying technology 20, 1503–1513.

Milczarek, R.R., Ferry, J.J., Alleyne, F.S., Olsen, C.W., Olson, D.A., Winston, R., 2017. Solar thermal drum drying performance of prune and tomato pomaces. Food and Bioproducts Processing 106, 53–64.

Misha, S., Mat, S., Ruslan, M.H., Salleh, E., Sopian, K., 2015. Performance of a solar assisted solid desiccant dryer for kenaf core fiber drying under low solar radiation. Solar Energy 112, 194–204.

Mohamed, L.A., Kouhila, M., Jamali, A., Lahsasni, S., Kechaou, N., Mahrouz, M., 2005. Single layer solar drying behaviour of Citrus aurantium leaves under forced convection. Energy Conversion and Management 46, 1473–1483.

Mounir, S., Allaf, K., 2008. Three-stage spray drying: new process involving instant controlled pressure drop. Drying technology 26, 452–463.

Mounir, S., Allaf, T., Mujumdar, A.S., Allaf, K., 2012. Swell drying: Coupling instant controlled pressure drop DIC to standard convection drying processes to intensify transfer phenomena and improve quality—An overview. Drying Technology 30, 1508–1531.

Mustayen, A., Mekhilef, S., Saidur, R., 2014. Performance study of different solar dryers: A review. Renewable and Sustainable Energy Reviews 34, 463–470.

Nabnean, S., Janjai, S., Thepa, S., Sudaprasert, K., Songprakorp, R., Bala, B.K., 2016. Experimental performance of a new design of solar dryer for drying osmotically dehydrated cherry tomatoes. Renewable energy 94, 147–156.

Nayak, S., Naaz, Z., Yadav, P., Chaudhary, R., 2012. Economic analysis of hybrid photovoltaic-thermal (PVT) integrated solar dryer. International journal of engineering inventions 1, 21–27.

Ndukwu, M.C., Simo-Tagne, M., Abam, F.I., Onwuka, O.S., Prince, S., Bennamoun, L., 2020. Exergetic sustainability and economic analysis of hybrid solar-biomass dryer integrated with copper tubing as heat exchanger. Heliyon 6, e03401.

Nguyen, T.H., Lanoisellé, J.-L., Allaf, T., Allaf, K., 2016. Experimental and fundamental critical analysis of diffusion model of airflow drying. Drying Technology 34, 1884–1899.

Nwakuba, N., Okafor, V.C., Okorafor, O.O., 2020. Techno-economic analysis of a hybrid solar-electric dryer. Energy Sources, Part A: Recovery, Utilization, and Environmental Effects 1–25.

O'callaghan, J.R., Menzies, D.J., Bailey, P.H., 1971. Digital simulation of agricultural drier performance. Journal of Agricultural Engineering Research 16, 223–244.

Okos, M.R., Narsimhan, G., Singh, R.K., Weitnauer, A.C., 1992. Food Dehydration Handbook of Food Engineering. Ch 1, 1–10.

Overhults, D.G., White, G.M., Hamilton, H.E., Ross, I.J., 1973. Drying soybeans with heated air. Transactions of the ASAE 16, 112.

Oztop, H.F., Akpinar, E.K., 2008. Numerical and experimental analysis of moisture transfer for convective drying of some products. International Communications in Heat and Mass Transfer 35, 169–177.

Pabis, S.M.H.S., 1961. Grain drying theory. II. Temperature effects on drying coefficients. Journal of Agricultural Engineering Research 6, 169–174.

PAGE, G.E., 1949. Factors influencing the maximum rates of air drying shelled corn in thin layer. Masters thesis Purdue University.

Pardhi, C.B., Bhagoria, J.L., 2013. Development and performance evaluation of mixed-mode solar dryer with forced convection. International journal of energy and environmental engineering 4, 23.

Perea-Moreno, A.-J., Juaidi, A., Manzano-Agugliaro, F., 2016. Solar greenhouse dryer system for wood chips improvement as biofuel. Journal of Cleaner Production 135, 1233–1241.

Porretta, S., 2019. Traditional Tomato Products and the Need for Innovation, in: Tomato Chemistry, Industrial Processing and Product Development. pp. 304–329.

Prakash, O., Kumar, A., 2014. Environomical analysis and mathematical modelling for tomato flakes drying in a modified greenhouse dryer under active mode. International journal of food engineering 10, 669–681.

Queiroz, R., Gabas, A.L., Telis, V.R.N., 2004. Drying kinetics of tomato by using electric resistance and heat pump dryers. Drying Technology 22, 1603–1620.

Rayaguru, K., Routray, W., 2012. Mathematical modeling of thin layer drying kinetics of stone apple slices. International Food Research Journal 19.

Ringeisen, B., Barrett, D.M., Stroeve, P., 2014. Concentrated solar drying of tomatoes. Energy for sustainable development 19, 47–55.

Sacilik, K., Keskin, R., Elicin, A.K., 2006. Mathematical modelling of solar tunnel drying of thin layer organic tomato. Journal of food Engineering 73, 231–238.

Sahin, F.H., Aktas, T., Orak, H., Ulger, P., Sahin, H., Aktas, T., Ulger, P., 2011. Influence of pretreatments and different drying methods on color parameters and lycopene content of dried tomato. Bulgarian Journal of Agricultural Science 17, 867–881.

Salehi, B., Sharifi-Rad, R., Sharopov, F., Namiesnik, J., Roointan, A., Kamle, M., Kumar, P., Martins, N., Sharifi-Rad, J., 2019. Beneficial effects and potential risks of tomato

consumption for human health: An overview. Nutrition 62, 201–208.

Sallam, Y.I., Aly, M.H., Nassar, A.F., Mohamed, E.A., 2015. Solar drying of whole mint plant under natural and forced convection. Journal of Advanced Research 6, 171–178.

Samimi-Akhijahani, H., Arabhosseini, A., 2018. Accelerating drying process of tomato slices in a PV-assisted solar dryer using a sun tracking system. Renewable Energy 123, 428–438.

Sandali, M., Boubekri, A., Mennouche, D., 2018. Thermal behavior modeling of a cabinet direct solar dryer as influenced by sensible heat storage in a fractured porous medium, in: AIP Conference Proceedings. AIP Publishing LLC, p. 20014.

Sandali, M., Boubekri, A., Mennouche, D., Gherraf, N., 2019. Improvement of a direct solar dryer performance using a geothermal water heat exchanger as supplementary energetic supply. An experimental investigation and simulation study. Renewable energy 135, 186–196.

Seerangurayar, T., Al-Ismaili, A.M., Jeewantha, L.H.J., Al-Habsi, N.A., 2019. Effect of solar drying methods on color kinetics and texture of dates. Food and Bioproducts Processing 116, 227–239.

Selvanayaki, S., Sampathkumar, K., 2017. Techno-economic Analysis of Solar Dryers, in: Solar Drying Technology. Springer, pp. 463–493.

Shalaby, S.M., Bek, M.A., 2014. Experimental investigation of a novel indirect solar dryer implementing PCM as energy storage medium. Energy conversion and management 83, 1–8.

Sharma, A., Sharma, N., 2012. Construction and performance analysis of an indirect solar dryer integrated with solar air heater. Procedia engineering 38, 3260–3269.

Sharma, G.P., Prasad, S., 2004. Effective moisture diffusivity of garlic cloves undergoing microwave-convective drying. Journal of Food engineering 65, 609–617.

Shen, C., Yang, L., Wang, X., Jiang, Y., Yao, Y., 2014. An experimental and numerical study of a de-fouling evaporator used in a wastewater source heat pump. Applied thermal engineering 70, 501–509.

Shivhare, U.S., Arora, S., Ahmed, J., Raghavan, G.S. V, 2004. Moisture adsorption isotherms for mushroom. LWT-Food Science and Technology 37, 133–137.

Singh Chauhan, P., Kumar, A., Nuntadusit, C., Mishra, S.S., 2018. Drying kinetics, quality assessment, and economic analysis of bitter gourd flakes drying inside forced convection greenhouse dryer. Journal of Solar Energy Engineering 140.

Singh, P.P., Singh, S., Dhaliwal, S.S., 2006. Multi-shelf domestic solar dryer. Energy Conversion and Management 47, 1799–1815.

Ssemwanga, M., Makule, E., Kayondo, S.I., 2020. Performance analysis of an improved solar dryer integrated with multiple metallic solar concentrators for drying fruits. Solar Energy 204, 419–428.

Tagnamas, Z., Lamseyah, H., Moussaoui, H., Bahammou, Y., Kouhila, M., Idlimam, A., Lamharrar, A., 2020. Energy and exergy analyses of carob pulp drying system based on a solar collector. Renewable Energy.

Tarik, H., Abdelghani, B., Djamel, M., Soufien, A., Abderrahim, B., Abdelmadjid, H., 2020. EXPERIMENTAL INVESTIGATION AND MATHEMATICAL MODELING OF HOT AIR CONVECTIVE DRYING OF TOMATO PASTE UNDER NEAR SOLAR DRYING OPERATING CONDITIONS. Algerian Journal of Arid Environment “AJAE” 10.

Téllez-Pérez, C., Alonzo-Macías, M., Mounir, S., Besombes, C., Allaf, T., Amami, E., Allaf, K., 2019. Instant Controlled Pressure-Drop DIC as a Strategic Technology for Different Types of Natural Functional Foods, in: Functional Foods. IntechOpen.

Téllez-Pérez, C., Sobolik, V., Montejano-Gaitán, J.G., Abdulla, G., Allaf, K., 2015. Impact of swell-drying process on water activity and drying kinetics of Moroccan pepper (Capsicum annum). Drying Technology 33, 131–142.

Tiwari, S., Tiwari, G.N., 2016. Exergoeconomic analysis of photovoltaic-thermal (PVT) mixed mode greenhouse solar dryer. Energy 114, 155–164.

Toğrul, İ.T., Pehlivan, D., 2002. Mathematical modelling of solar drying of apricots in thin layers. Journal of Food Engineering 55, 209–216.

Toor, R.K., Lister, C.E., Savage, G.P., 2005. Antioxidant activities of New Zealand-grown

tomatoes. International journal of food sciences and nutrition 56, 597–605.

Tunde-Akintunde, T.Y., 2011. Mathematical modeling of sun and solar drying of chilli pepper. Renewable energy 36, 2139–2145.

Tütüncü, M.A., Labuza, T.P., 1996. Effect of geometry on the effective moisture transfer diffusion coefficient. Journal of Food Engineering 30, 433–447.

VACCAREZZA, L.M., LOMBARDI, J.L., CHIRIFE, J., 1974. Kinetics of moisture movement during air drying of sugar beet root. International Journal of Food Science & Technology 9, 317–327.

Van Meel, D.A., 1958. Adiabatic convection batch drying with recirculation of air. Chemical Engineering Science 9, 36–44.

Vega-Gálvez, A., Ah-Hen, K., Chacana, M., Vergara, J., Martínez-Monzó, J., García-Segovia, P., Lemus-Mondaca, R., Di Scala, K., 2012. Effect of temperature and air velocity on drying kinetics, antioxidant capacity, total phenolic content, colour, texture and microstructure of apple (var. Granny Smith) slices. Food Chemistry 132, 51–59.

Verma, L.R., Bucklin, R.A., Endan, J.B., Wratten, F.T., 1985. Effects of drying air parameters on rice drying models. Transactions of the ASAE 28, 296–301.

Vijayan, S., Arjunan, T. V, Kumar, A., 2020. Exergo-environmental analysis of an indirect forced convection solar dryer for drying bitter gourd slices. Renewable Energy 146, 2210–2223.

Wang, C.Y., Singh, R.P., 1978. Use of variable equilibrium moisture content in modeling rice drying. Transactions of American Society of Agricultural Engineers 11, 668–672.

Wang, W., Li, M., Hassanien, R.H.E., Wang, Y., Yang, L., 2018. Thermal performance of indirect forced convection solar dryer and kinetics analysis of mango. Applied Thermal Engineering 134, 310–321.

www.radioalgerie.dz/news/ar/article/20190521/170361.2019.

Xiao, H.-W., Pang, C.-L., Wang, L.-H., Bai, J.-W., Yang, W.-X., Gao, Z.-J., 2010. Drying kinetics and quality of Monukka seedless grapes dried in an air-impingement jet dryer.

Biosystems Engineering 105, 233–240.

Yagcioglu, A., 1999. Drying characteristic of laurel leaves under different conditions, in: Proceedings of the 7^< Th> International Congress on Agricultural Mechanization and Energy, 1999. Faculty of Agriculture, Cukurova University, pp. 565–569.

Yaldiz, O., Ertekin, C., Uzun, H.I., 2001. Mathematical modeling of thin layer solar drying of sultana grapes. Energy 26, 457–465.

Younis, M., Abdelkarim, D., El-Abdein, A.Z., 2018. Kinetics and mathematical modeling of infrared thin-layer drying of garlic slices. Saudi journal of biological sciences 25, 332–338.

Zhang, Q., Litchfield, J.B., 1991. An optimization of intermittent corn drying in a laboratory scale thin layer dryer. Drying technology 9, 383–395.

Zhong, H., Li, Z.M., Wu, T., Yu, M.J., Tang, R.S., 2012. Performance of a Solar Drying System Driven by a Hybrid Power System, in: Advanced Materials Research. Trans Tech Publ, pp. 139–146.

Zogzas, N.P., Maroulis, Z.B., Marinos-Kouris, D., 1996. Moisture diffusivity data compilation in foodstuffs. Drying technology 14, 2225–2253.

Zoukit, A., El Ferouali, H., Salhi, I., Doubabi, S., Abdenouri, N., 2019. Takagi Sugeno fuzzy modeling applied to an indirect solar dryer operated in both natural and forced convection. Renewable energy 133, 849–860.